The Dissertation Committee for Gayathri Nattar Ranganathan Certifies that this is the approved version of the following dissertation:

Signal propagation in recurrent networks of mouse barrel cortex

Committee:

Helmut Koester, Supervisor

Daniel Johnston

Wilson Geisler, III

Ila Fiete

Andrew Dunn

Signal propagation in recurrent networks of mouse barrel cortex

by

Gayathri Nattar Ranganathan, B.Tech.

Dissertation

Presented to the Faculty of the Graduate School of

The University of Texas at Austin

in Partial Fulfillment

of the Requirements

for the Degree of

Doctor of Philosophy

The University of Texas at Austin

December 2011

Dedication

To my parents and husband.

Acknowledgements

My learning experience as a graduate student here at the University of Texas has irreversibly changed me as a person and I'm very grateful for this.

I would like to thank my advisor Prof. Helmut Koester for his guidance and for providing me with a great learning environment. He led by example and inspired a 'can-do' attitude in us. I thank the members on my dissertation committee, Professors Daniel Johnston, Wilson Geisler, Ila Fiete and Andrew Dunn for their timely guidance, feedback and encouragement. I also want to thank Professors Eyal Seidemann, Nicholas Priebe, Jonathan Pillow, Lawrence Cormack and Dr. Thomas Middendorf for their input at various stages of this work, and Prof. Hiroshi Nishiyama for his advice.

I also extend my thanks to past members of my lab. Thanks to Dr. Juan Diego Pita-Almenar for his wonderful company and his help with the plasticity experiments; and thanks to Brett Johnson for his assistance with programming the acquisition software and for many fun discussions. It's my pleasure to have known you guys.

I cannot thank Dr. Johnston and all the members of his laboratory enough for all that I have gained from 'being next door'. I especially am grateful to Dr. Richard Gray for his support and guidance, scientific and otherwise. He turned from someone I was too scared to talk to, into a great friend and philosopher. I also thank Dr. Rishikesh Narayanan for the many scientific and non-scientific arguments over coffee. I certainly learnt a great deal from all of them. I extend my sincere thanks to Drs. Raymond Chitwood and Jennifer Siegel for their

encouragement, kind feedback and for the many bubbly Friday evenings at the Local. I would also like to thank Drs. Darrin Brager, Nikolai Dembrow, Kevin Dougherty, Payne Chang and Brian Kalmbach for their critical input. I was fortunate to have wonderful friends in Yul Young Park, Ann Clemens, Sachin Vaidya, Chung Sub Kim and Brenda Houck. Thank you very much! My thanks to Krystal Phu and Jason Goltz at the Institute for Neuroscience, Charles Thonig and Terry Watts at the Welch Machine shop (for the home-made optomechanics that I designed in metric units!) and John Lekavich at Intraaction Corp. I am deeply grateful to my past mentors Dr. Preston Devasia and Prof. Obaid Siddiqi for getting me hooked onto Neurobiology.

Finally, and most importantly I thank my parents for their constant support behind all my actions and their incredible acts of selflessness that got me here. I thank my beloved husband, Karthik Kumar, who's been my voice of reason even during unreasonable times. There will certainly be many more crazy, neuroscience discussions/arguments!

Signal propagation in recurrent networks of mouse barrel cortex

Gayathri Nattar Ranganathan, Ph.D.

The University of Texas at Austin, 2011

Supervisor: Helmut Koester

Sensory signals are represented and propagated as spiking activity in multiple neuronal populations to lead to cognitive or motor behavior in organisms. Neural processing underlying sensory-motor behavior is understood by uncovering the governing computational principles and the biophysical mechanisms that implement the principles. While these mechanisms have been studied extensively at the single-neuron and system levels, activity within neuronal networks significantly impact neural processing. For example, there are spatiotemporal interactions (neural correlations) between responses of neurons within populations that could potentially impact signal representation and propagation. Furthermore, the effects of associative plasticity are also expected to alter network activity and its propagation. The effects of plasticity on network activity cannot be predicted from individual neuronal responses due to the complex, non-linear interactions within neuronal networks. Thus examining neural correlations in network activity and the propagation of network activity, requires recording spiking activity from large, heterogeneous, populations of spatially distributed neurons simultaneously. Studies addressing the propagation of network activity have been limited to theoretical approaches. Empirical studies have been limited by the technical difficulties in recording from a large number of neurons simultaneously. To overcome this challenge we developed a novel technique, dithered random-access functional calcium imaging. This imaging

technique records and extracts suprathreshold activity from a large number of neurons. This technique also has a high spike detection efficiency and millisecond temporal precision. We applied this technique to measure the propagation of activity and neural correlations in activity evoked by afferent, thalamocortical inputs in the recurrent cortical networks of the mouse barrel cortex. We found that the cortical activity evoked by novel (naïve), thalamocortical inputs showed limited propagation of activity and decrease in propagation of neural correlations (measured from neuronal pairs within each population) from L4 to L2/3 network of the responding column. However, associative cortical plasticity was induced from pairing thalamocortical inputs with intracortical inputs. This pairing resulted in increased propagation of activity. The pairing also modified the propagation of neural correlations. Our results suggest that synaptic plasticity in intracortical circuits contributes to the modified propagation of activity and neural correlations. The modified propagation of neural correlations could in turn contribute to behavioral performance in *vivo* following perceptual learning.

Table of Contents

List of Figures

Chapter 1: Introduction

In almost all multicellular organisms, interactions with the surrounding environment are mediated by processing in the nervous systems. Sensory stimuli are transduced by peripheral receptors into neural signals. These signals are processed and propagated through multiple brain areas leading to motor or cognitive behaviors. The various contributing neural populations within a neural system commonly use trains of suprathreshold action potentials, fired in subsets of neurons (spatiotemporal patterns of spiking activity), to represent information (encode) and to propagate their output to target populations. Downstream neural populations receiving this spiking activity extract the information contained (decode) leading to further processing. Different brain areas may use different strategies or rules to decode, process, encode and propagate signals in the form of spatiotemporal patterns of spiking activity. In order to understand the neural processing behind sensory-motor behavior thus requires understanding the biophysical mechanisms that carryout and/or regulate these neural computations.

Multiple neural coding schemes have been proposed to account for neural activity recorded from various brain areas. The requirements of a candidate neural code are (i) representation of inputs (encoding); (ii) interpretation by downstream targets (decoding); (iii) propagation of information with minimal loss in signal; and (iv) adaptability with plasticity (DA and TH, 1968). These aspects of neural coding have been studied extensively at the single neuronal level and at the large scale, system level. However, responses of neurons within local populations (i.e., at the mesoscale) often interact non-linearly with each other. These interactions have been shown to significantly impact processing and

propagation of signals (Averbeck et al., 2006b). For example, while individual neurons within the vertebrate nervous system respond selectively to inputs, their responses are often variable and ambiguous. The activity of neural populations, on the other hand, was found to better represent inputs by reducing the associated noise (Georgopoulos et al., 1986). Additionally, temporal interactions between neuronal responses were found to contribute to signaling of neuronal populations (Pillow et al., 2008a). Furthermore, propagation of signals is an important step in neural processing, because interactions in population signals may be altered significantly during propagation, depending on the rules of propagation (Kumar et al., 2010). Thus, the properties of neural signaling through population activity and its propagation are important aspects of neural coding. However, the precise properties of activity, representation, propagation, and effect of plasticity within local microcircuits of neurons at the mesoscale are largely unknown. The goal of this dissertation was to examine the properties of signal propagation in the cerebral cortex. Further, we aimed to investigate the impact of cortical plasticity on the properties of signal propagation.

Examining propagation of population spiking activity requires simultaneous recording of activity from multiple neurons. This is because of the importance of non-linear, spatiotemporal interactions between neuronal responses. Studies addressing representation, propagation and adaptation with plasticity in population activity have been limited due to technical challenges in recording precise spiking activity with a large sample from local neuronal populations (microcircuits). This is especially true for studying propagation of population activity, as this requires simultaneously recording from multiple neurons in multiple neural populations. To address the goals of this study we developed

novel methods to record spiking activity with high spatial and temporal resolution. This method records from spatially distributed heterogeneous populations of 40-100 neurons with high detection efficiency and millisecond precision. This dissertation outlines the development of these methods, followed by their application towards addressing signal propagation in recurrent networks, as mentioned above. The results presented here report on the properties of propagation of neuronal population activity in a mammalian primary sensory cortex. Activity was evoked by afferent thalamocortical inputs. The results further report the impact of associative, cortical plasticity on this propagation.

1.1 STRUCTURE AND FUNCTION OF THE MAMMALIAN NEOCORTEX

The neocortex in mammals is phylogenically the youngest part of the cerebral cortex and is implicated in the neural processing underlying higher order sensory, motor and cognitive tasks. In the coarse scale, the neocortex is thought to be organized into functional modules of areas. Each of these areas is predominantly involved in particular aspects of processing, for example sensory, motor and association areas of the cortex. Additionally, anatomical and physiological data show that cortical areas also appear to follow a functional hierarchy (Felleman and Van Essen, 1991). Primary sensory areas that correspond to processing simple stimulus features of various sensory modalities (for example, vision, audition and somatosensation) in turn send outputs to areas that correspond with processing complex features. On a finer scale, the neocortex is organized into vertical columns of neurons that are further segregated into typically 6 distinct layers (Mountcastle, 1997). The cortical

columns were found to be functional modules themselves as neurons within a cortical column often shared features of their receptive fields (for example, orientation columns and barrel columns etc.

1.1 Organization in primary sensory cortices

In this work, we focused on signal propagation within a primary sensory, the rodent barrel cortex. Incoming sensory (visual, auditory and somatosensory) information enters the cerebral cortex through these areas. Sensory information is relayed through the corresponding thalamic nuclei (except olfactory information). Primary sensory areas are topographically mapped and the organization of neural populations (columns) on the cortical reflects the organization of sensory receptors in the periphery. Within primary sensory cortices thalamic projections were found to predominantly target neurons in the granular layer 4 (L4) (Koralek et al., 1988). This was also shown physiologically through L4 receptive fields (in visual cortex) that could be constructed from the superposition of thalamic receptive fields (Hubel and Wiesel, 1968). In addition to receiving thalamocortical inputs, cortical neurons also receive intracortical inputs from local and long distance sources. In fact, more than 80% of connections received by cortical neurons are from local and distant intracortcial sources (Benshalom and White, 1986). Intracortical connections lead to propagation of responses across layers, across columns as well as across cortical areas (Armstrong-James et al., 1992). These are mediated through vertical and horizontal projections. Cortical neuronal populations are distinct in their extensively recurrent local synaptic architecture. Neuronal populations, both

within and across individual layers and columns, form recurrently connected networks. However, the extent of inter-columnar recurrent connections is different across layers. Inter-columnar recurrent connections were found to be extensive in supra and subgranular cortical layers, but sparse in the granular L4 (Laaris and Keller, 2002). From anatomical and physiological studies it was proposed that thalamocortically evoked activity in L4 follows a preferred path of L4 to L2/3 to L5 (Armstrong-James et al., 1992). However, this might be a first approximation as anatomically there are extensive thalamic inputs targeting cortical layers other than L4 (Meyer et al., 2010). In addition, cortical neurons also make long-range horizontal projections originating predominantly from layers 2/3 and 5. These carry information to intracortical targets and sub-cortical targets respectively (Anderson et al., 2010).

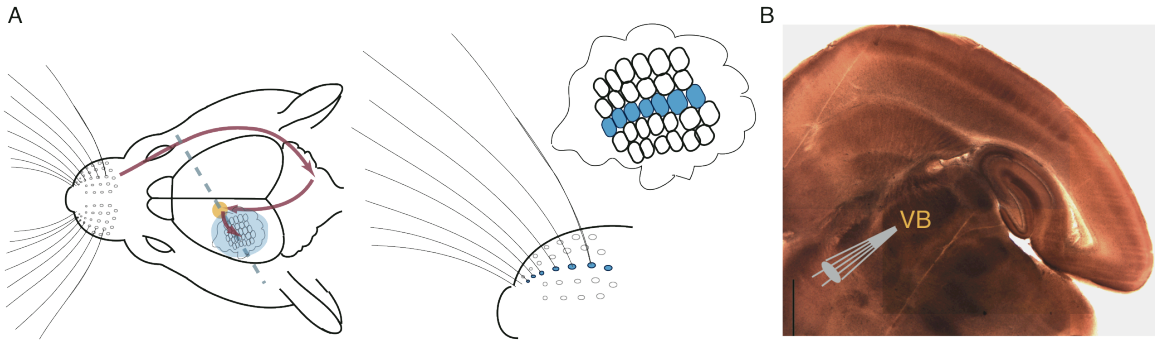

Figure 1.1: The mouse whisker sensory system.

A: Illustration of the whisker sensory pathway tracing the flow of information from peripheral receptors to the trigeminal nucleus in the brainstem, the venterobasal nucleus of the thalamus (VB)and to the posteromedial barrel subfield of the primary somatosensory cortex. The dotted line indicates the angle of cut to obtain thalamcortical slices with intact synaptic inputs from VB thalamus. The images to the right illustrate the one-to-one correspondence between individual whiskers and barrel columns as seen on the cortical surface. B: Shows image of an acute, thalamocortical slice preparation fixed with cytochrome oxidase showing the barrel column borders demarcated by the high cell density of L4 barrels. Overlaid is a pictogram of a stimulation electrode representing the afferent inputs provided from the thalamic neuronal populations in VB. (Fig. 1.1A adapted from (Petersen, 2007)).

A majority of neurons within cortical networks were found to be excitatory. However, the minority inhibitory neurons control the evoked excitation through di- or poly-synaptic inhibition (Cruikshank et al., 2007; Sun et al., 2006). Recent work has shown that excitatory and inhibitory intracortical synaptic connections within and across populations are highly non-random (Song et al., 2005; Yoshimura and Callaway, 2005).

1.2 RODENT WHISKER SENSORY SYSTEM

Many nocturnal animals including rodents use their whiskers (vibrissae) as an active sensing system. These animals use their whiskers to sense their immediate environment and to guide their movements. The large whiskers (macro vibrissae) are arranged on the snout of the animal into discreet rows and columns that are identical across animals. Tasks such as object perception and distance estimation are carried out by actively sweeping whiskers longitudinally at around 10-20 Hz, called whisking (Petersen, 2003; Brecht, 2007).

Mechanosensory receptors in follicles that form the attachment to the whisker pad transduce mechanical information from whisker deflection into neural signals. These neural signals are processed and propagated by the circuitry in the whisker sensory pathway. Signals from the neurons in trigeminal ganglion in the periphery are relayed to the trigeminal nucleus in the brainstem. From there neural signals are relayed to neuronal populations in the venterobasal nucleus of the thalamus before reaching the barrel subfield in the primary somatosensory cortex also called the barrel cortex. Notably, the brain stem, thalamus and the barrel cortex contain neuronal populations that show preferentially strong

response to the stimulation of an individual whisker. This correspondence is especially evident in the barrel cortex in which individual columns primarily receive input from individual macrovibrissae (Petersen, 2003). Although the receptive fields of neurons may be larger than a single whisker, the response evoked by the primary whisker is known to be largest and arriving the earliest in the L4 populations of the barrel columns (de Kock et al., 2007). Previous work has established a preparation of acute slices that retain synaptic connections between the thalamus and the barrel cortex (Agmon and Connors, 1991). Using this preparation, sensory evoked thalamic activity can be evoked by focal stimulation of the thalamocortical fibers that can be seen traversing the striatum (Fig. 1.1). There is a marked segregation of barrel cortical columns, arising from localization of neuronal populations in adjacent columns. We visualized these with light microscopy. Afferent input was shown has been shown to evoke suprathreshold cortical responses that are almost entirely restricted within a barrel column (Petersen and Sakmann, 2001). Thalamic inputs predominantly target the L4 neurons giving rise to the earliest sensory evoked response in L4. The L4 population in turn consists further of star pyramidal cells. These cells send projections to layers 2/3 as well as 5 in addition to local recurrent connections (Staiger et al., 2004).

The thalamocortical pathway in the rodent whisker sensory system represents a model system to examine signal propagation in primary sensory cortices, because it offers the advantages of extensively documented neuronal physiology and synaptic circuitry (between neuronal pairs), the ability to make

thalamocortical slices that allowed isolated study of the pathway from VB to L4 to L2/3, and the visualization of individual cortical columns.

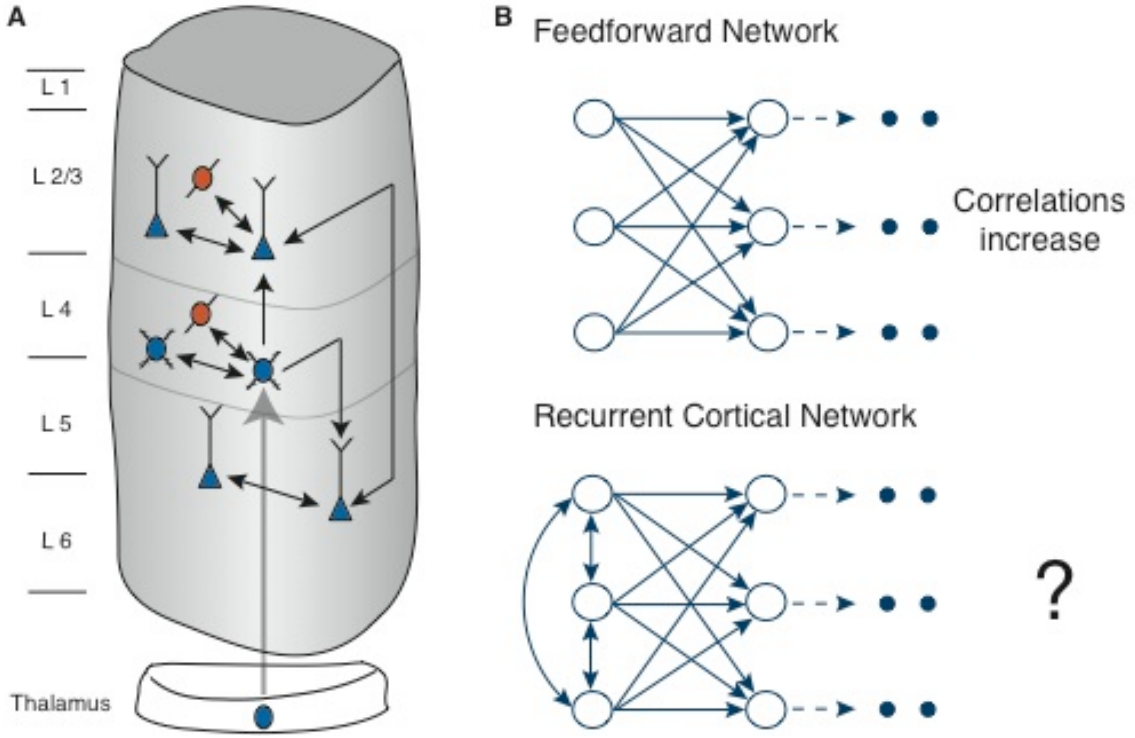

Figure 1.2: Signal propagation between recurrent networks of barrel cortex.

A: Illustration of the major synaptic connections within and across neuronal populations in a barrel column. B: Illustrates the primary question addressed in this dissertation. Namely, how do neural correlations in population activity propagate between recurrent networks in the barrel cortex. (Fig. 1.2A adapted from (Feldmeyer et al., 2006)).

1.4 POPULATION SPIKING ACTIVITY AND PROPAGATION

Neuronal responses in the CNS, including cortical populations, are variable and often show temporal interactions that lead to covariations in responses (neural correlations). Correlations between neurons may occur due to lateral synaptic connections between them, or from receiving common synaptic

inputs (divergent synaptic architecture), or receiving inputs that are themselves correlated. These correlations may occur over a wide range of timescales (e.g. sharp temporal regulation of correlations over few milliseconds or firing rate correlations over tens of milliseconds). While these response covariations may depend on stimulus conditions (signal correlations) they are also observed irrespective of the incoming stimulus (noise correlations)(Averbeck et al., 2006a). Results show that noise correlations are expected to significantly impact signal representation (Averbeck and Lee, 2006). However, the correlations present in neural population activity are also expected to undergo significant changes during the propagation of activity between populations (Kumar et al., 2008). Thus the propagation of neural correlations impacts both the downstream representation as well as the further propagation of activity in that pathway. Studies examining propagation of activity have been mostly restricted to analytical simulations due to technical challenges in obtaining empirical data from multiple populations simultaneously. The empirical studies conducted in locust auditory system as well as the analytical studies indicate that neural correlations cumulatively increase with the propagation of population spiking activity through networks connected with feedforward architecture (Vogel and Ronacher, 2007; Kumar et al., 2010). However, cortical networks, as mentioned above, contain extensive recurrently connected neuronal networks. Biological neural networks with recurrent architecture have biophysical mechanisms that may increase neural correlations as well as those that may decorrelate activity (de la Rocha et al., 2007; Padmanabhan and Urban, 2010; Renart et al., 2010; Wiechert et al., 2010). The complex, highly non-linear interactions between recurrently connected neurons make it difficult to predict the effects of competing correlating

and decorrelating mechanisms on neural correlations and their propagation from existing data.

1.4 CORTICAL PLASTICITY

Neural systems, not only in developing organisms, but also in developed adults, constantly undergo changes in response properties depending on external stimulus conditions as well as internal state of the organism. Experience-dependent changes in neural processing, called neural plasticity, are thought to underlie behavioral forms of learning and memory. Cortical areas contribute to higher order processing in the brain and thus have been observed to undergo changes in their response properties with behavioral learning (Buonomano and Merzenich, 1998). The extensive capacity for cortical plasticity, at the systems level, was observed through studies where focal lesions induced in peripheral receptors lead to rapid and massive restructuring in the cortical representation of the sensory inputs from these receptors (map plasticity). The areas corresponding to the lesioned receptors were rapidly taken over to represent the adjacent healthy receptors. Changes to the cortical representational maps were also observed through associative plasticity. In these studies responses to individual inputs were altered through repeated associations between the tested inputs, to reflect the associations presented. Associative plasticity in cortical responses has also been observed at the single neuronal level from pairing inputs in intact animals as well as in isolated cortical tissue under *in vitro* conditions. Changes in cortical responses have been attributed to plasticity in synaptic as well as intrinsic biophysical properties of neurons (Bekisz et al.,

2010; Feldman, 2009; Frégnac et al., 1996; Urban-Ciecko et al., 2005). Changes induced by plasticity both at synaptic and intrinsic neuronal levels are expected to critically impact the activity of neuronal populations as well as the propagation of activity through multiple populations. However, the impact of cortical plasticity on population activity and the propagation of this activity is largely unknown.

1.6 Overview of Dissertation

This dissertation examines neural correlations and the propagation of suprathreshold spiking activity between recurrent cortical networks. In this study, we aim to examine the effects of associative cortical plasticity on propagation of evoked activity between cortical networks. The specific aims of this study are to : (i) measure the change in neural correlations as signals propagate from one population to the next; and (ii) measure the impact of associative plasticity on the change in neural correlations with propagation of activity. To address these questions, we developed novel optical and analytical methods to record precise spiking activity from large, spatially distributed, populations of neurons. This dissertation also outlines the development of these methods.

Chapter 2 describes the development of the dithered random-access functional calcium imaging technique and demonstrates its performance in terms of spike detection efficiency. Chapter 3 describes experiments examining the propagation of afferent evoked cortical activity and the neural correlations in activity. These experiments use the thalamocortical slice preparation, providing afferent inputs by the focal stimulation of thalamocortical fibers from the venteroposteromedial nucleus of the thalamus (VB). Chapter 4 describes

experiments in which the afferent thalamocortical inputs were associated with lateral cortical inputs to induce cortical plasticity. The observed changes in propagation of afferent evoked activity and the correlations are presented. Briefly, we observed that neural correlations decreased with the propagation of spiking activity from L4 to L2/3 of the mouse barrel cortex. However, the induction of associative plasticity resulted in increased propagation of population spiking activity as well as increased propagation of neural correlations. Chapter 5 concludes the dissertation with discussing the functional implications of the findings outlined here and future directions based on predictions from the results presented.

Chapter 2: Recording precise spiking activity from neuronal populations

Information is represented and propagated in neural systems mainly through the spiking activity of populations of neurons. In many brain regions, while individual neurons respond selectively to incoming stimuli, there is significant overlap in the selectivity of neurons and there is also high variability in neuronal responses to the same stimulus. Given that the task of the neural system is to estimate the stimulus in the presence of these limitations, often the combined activity of a population of neurons better represents the stimulus than the responses of individual neurons. Thus in order to understand the computations carried out requires recording activity from a large, local population of neurons simultaneously. Several methods have been developed to meet this requirement but have technical and analytical limitations in recording precise spiking activity from a local neuronal population. To achieve this we developed an optical imaging technique, dithered random-access functional calcium imaging, to record spike associated somatic calcium signals from up to 100 neurons and a maximum-likelihood deconvolution algorithm to extract spikes and spike timings from the recorded calcium fluorescence signals. Here we show that using these methods in conjunction resulted in high spike detection efficiency and low errors in spike timing detection from a large neuronal population deep within brain tissue.

2.1 Recording activity from neuronal populations

Activity in a neuronal population can be recorded using several electrical and optical methods, each suited for a specific purpose. Each consists of a

method to record activity and a method to extractspiking activity from individual neurons from the recorded data.

2.1.1 Electrical methods

Electrical methods used to record population activity include those that employ individual bundles of wire electrodes (e.g. tetrodes) and methods that use multielectrode arrays. These consist of a collection of electrodes placed with a known, fixed spacing between them. When embedded within brain tissue they record extracellular voltage fluctuations in the immediately surrounding tissue. Activity of individual neurons, called units, can be discerned by triangulation using signals picked up by multiple electrodes that can be traced back to the same source through analytical spike sorting algorithms. While these methods have contributed to significant advances in our understanding of various neural systems, they are limited in their application as they are biased towards recording from neurons with high spiking probability. They are also best for recording from spatially well separated neurons and are thus not suitable for recording activity from within local neuronal circuits(Buzsáki, 2004).

2.1.2 Optical methods

Optical methods for recording population activity are similarly a combination of optical recording and analytical activity detection techniques. In comparison, optical recording methods are less invasive, can sample locally and also retain information about relative spatial locations. Prominent optical methods for recording neuronal population activity include voltage sensitive dye (VSD) imaging and functional calcium imaging. VSD imaging employs voltage sensitive

fluorescent dye molecules that are infused and bind to the external membrane surface. VS dyes report cellular membrane voltage though relative changes in their spectral emissive properties in response to voltage changes. VSD signals are rapid in time and report supra and subthreshold activity. However, only methods using two-photon excitation can be used to image deep within brain tissue with high spatial resolution and commonly used VS dyes cannot be illuminated with two-photon excitation. Thus they lack the ability to resolve signals from single cells in the lateral and especially in the axial dimension. (Although see (Kuhn et al., 2008) for two-photon excitation of VSD molecules). Functional calcium imaging, on the other hand, uses fluorescent indicator dyes that bind to intracellular calcium and reports activity dependent changes in calcium concentration. There are several calcium indicator dyes varying in their calcium affinity that can be excited with two-photon cross-section thus allowing imaging deep within scattering tissue. In this study we used functional calcium imaging to record population activity due to these advantages.

2.1.2.1 Functional calcium imaging of population spiking activity

Functional calcium imaging exploits the strong association between the occurrence of somatic action potentials and the transient increase in intracellular calcium concentration to report somatic spikes in neurons. Like other methods mentioned above it is a combination of the imaging technique to record somatic calcium signals and a detection algorithm that extracts spike information from the fluorescence signals. Previous techniques that have been used to record somatic calcium fluorescence signals include CCD cameras (Sasaki et al., 2008), Nipkow

disc confocal imaging (Ikegaya et al., 2005), photodiode arrays (Mao et al., 2001), acousto-optical devices in conjunction with two-photon imaging (Otsu et al., 2008), two-photon imaging using galvanometric scanners (Greenberg et al., 2008; Kerr et al., 2007; Sato et al., 2007), and targeted-path scanners using two-photon excitation (Lillis et al., 2008). As mentioned, only the methods using two-photon excitation can be used to image activity from deep within brain tissue and to sufficiently reject background signal from the neuropil surrounding neuron somata that carries other information (Kerr et al., 2005). Two-photon imaging using galvanometric scanning, however, results in a tradeoff between temporal resolution, duration of signal collection per cycle (duty cycle), and field of view (FOV). Even at low temporal resolution, the number of neurons sampled when targeting a sufficient signal-to-noise ratio (S/N) for single spike detection is limited using galvanometer based scanning. Further, the low temporal resolution can lead to errors in spike detection as spike associated calcium signals have a transient rising phase. For example, two spikes with a very small inter-spike interval in a neuron with a small spike-evoked calcium signal and one spike in a neuron with a larger spike-evoked calcium signal are indistinguishable in recordings with low temporal resolution.

The extraction of precise number of spikes and spike timings from florescence recordings involves an objective method of spike detection and rigorous hypothesis testing (Sjulson and Miesenböck, 2007). Thus, detection of spikes from fluorescence traces is accompanied by errors of type I (false positives) and type II (undetected spikes). A high spike detection efficiency (low errors of both types) is required when using functional calcium imaging for indirect recording of spikes and spike timings. Prior methods of spike inference

from calcium fluorescence signals include template-matching algorithms used in combination with thresholding (Holekamp et al., 2008; Kerr et al., 2005; Sato et al., 2007), inverse filtering (Mukamel et al., 2009; Yaksi and Friedrich, 2006) clustering using principal component analysis (Sasaki et al., 2008), and using sequential Monte Carlo methods with calcium transients defined by a particle filter (Vogelstein et al., 2009), and others (Greenberg et al., 2008). Many of these methods have been developed for a specific purpose. The majority of these methods rely on fixed kernels to detect the rise in calcium signal associated with a spike. However, spike inference methods that rely on detecting templates (fixed kernels) are expected to lead to large errors in spike detection when used to detect activity in a cell population with heterogeneous spike-evoked calcium signals. Because of the tradeoff between temporal resolution and number of recorded neurons, and the limitations of spike detection methods, using functional calcium imaging to detect neuronal spiking activity with single-cell, single-spike resolution and with known detection error rates has been restricted to limited experimental conditions (Greenberg et al., 2008; Kerr et al., 2005; Sasaki et al., 2008; Sato et al., 2007).

2.1.2.2 Dithered random-access imaging and Maximum-likelihood spike detection

In this study, we chose to overcome these limitations of functional calcium imaging by developing a random-access scanning method ("dithered random access scanning") that collects traces with increased signal-to-noise ratio (S/N) and by developing a spike detection algorithm that takes into account the heterogeneity in calcium signals from a neuronal population. Dithered random-

access scanning collects multiple samples from each recorded neuron somata and records signals with millisecond temporal resolution. Two-photon imaging using random-access scanning has been used to record calcium fluorescence signals from neuronal compartments with high temporal resolution, high duty cycle, and high S/N (Grewe et al., 2010; Iyer et al., 2006; Lechleiter et al., 2002; Otsu et al., 2008). Using random-access scanning with AODs for detecting spikes from somatic calcium transients can potentially remedy many of the limitations of current implementations of functional somatic calcium imaging for precise spike detection. As we show, however, using single-point random-access scanning to record somatic calcium fluorescence signals resulted in problems in spike detection that arose from the inhomogeneous distribution of fluorescence within a soma. We present a simple solution to this problem by implementing a dithered random-access scanning method.

We further developed a new spike detection method that takes advantage of the high S/N ratio and temporal resolution obtained from dithered random-access scanning and utilizes prior information about single spike-evoked calcium fluorescence signals from a particular neuronal population. The algorithm infers spikes and spike timings by determining the maximum likelihood model. It is useful for detecting spontaneous and/or evoked activity in a population of neurons. We also determined the limitations of excitation intensity in terms of photodamage. Here, we show that the combination of dithered random-access imaging, and the maximum-likelihood detection algorithm resulted in a high efficiency of spike detection (>97%) low rates of false positives (0.0023 spikes/s), and low errors in spike timing detection when recording from L2/3 neurons in acute brain slices.

2.2 Design and implementation of Dithered random-access scaning

2.2.1 Optical setup

An upright microscope (BX50WI, Olympus) was coupled with the scanning module consisting of two AODs (ATD-655CD2/6510CD2, IntraAction Corp.) to deflect the laser beam in two dimensions. The Ti:sapphire laser source (Chameleon Ultra II, Coherent) was operated at 840 or 880 nm and had a modelocked average power output of 2-2.5 W. The scanning module consisted of acousto optical deflectors (AODs) used to deflect the beam in two dimensions. Fig. 2.1A shows the beam path traced upon deflection forming the scan pattern. To record from individual neurons a x40 water immersion objective (UMPlanFl, 40 x, NA 0.8, Olympus) was used. The pivot point of the scan pattern generated was relayed to the back focal aperture of the objective lens using afocal coupling telescopes. AODs with large apertures (10 mm) were used for imaging large field of views of 300 μm x 300 μm. We also tested AODs with apertures of 5 mm, resulting in a field of view of 120 μm x 120 μm.

Modelocked pulsed laser output has a significant line width of wavelengths (~8nm) and thus is non-monochromatic. Due to wavelength dependent dispersive properties of the material used AODs impart significant temporal (variable group velocity) and spatial (variable deflection angle) dispersion to the incident light. Spatial and temporal dispersion in turn reduce the excitation intensity, degrade spatial resolution and impact the S/N of recordings. To compensate for the temporal dispersion we expanded and relayed the laser output through a prism-pair pre-chirper, prior to the scanning module, to impart a net negative GVD to

opposite to the positive GVD caused by the AODs (Fork et al., 1984). To compensate for the spatial dispersion introduced by the AODs a single reflective diffraction grating (53-011R, Newport Corp.) was placed at a 45° angle immediately after the AODs (Iyer et al., 2003). Fig. 2.1B illustrates the relative positions of the various elements in the dithered random-access scanner set-up.

Bright field images were obtained using Differential interference contrast (DIC) microscopy. Scanning and DIC optics were aligned for parfocality. Fluorescence was collected by detection modules with photomultiplier tubes (PMT) (H-9305, R-6357, Hamamatsu). Two detection units were used to detect both epifluorescence and transfluorescence (Koester et al., 1999) in acute slice recordings. For *in vivo* recordings, only epifluorescence was detected.

2.2.2 Scanner control and signal acquisition

The AOD beam deflection angles were controlled by voltage controlled oscillators connected to the output of a DAC board (PCI-6115, National Instruments). The DAC board was operated at a rate of 156.25 KHz when using the large AODs and at 125 kHz when using the small aperture AODs. The sample was initially imaged in raster format to obtain locations of neuron somata. Coordinates for cell-to-cell scan were selected manually from fluorescence raster images. Temporal resolution (time required for one cycle to record from all neurons once) in cell-to-cell scan was 0.4 – 4 ms. In the majority of recordings, temporal resolution was 0.998-1.536 ms. Random-access scanning is a sequential recording technique that records from a single location at any given time. To record from many neurons, the focal point was moved in a rapid manner

from neuron to neuron during one cycle. This cycle was repeated for total recording times of 1- 35 s.

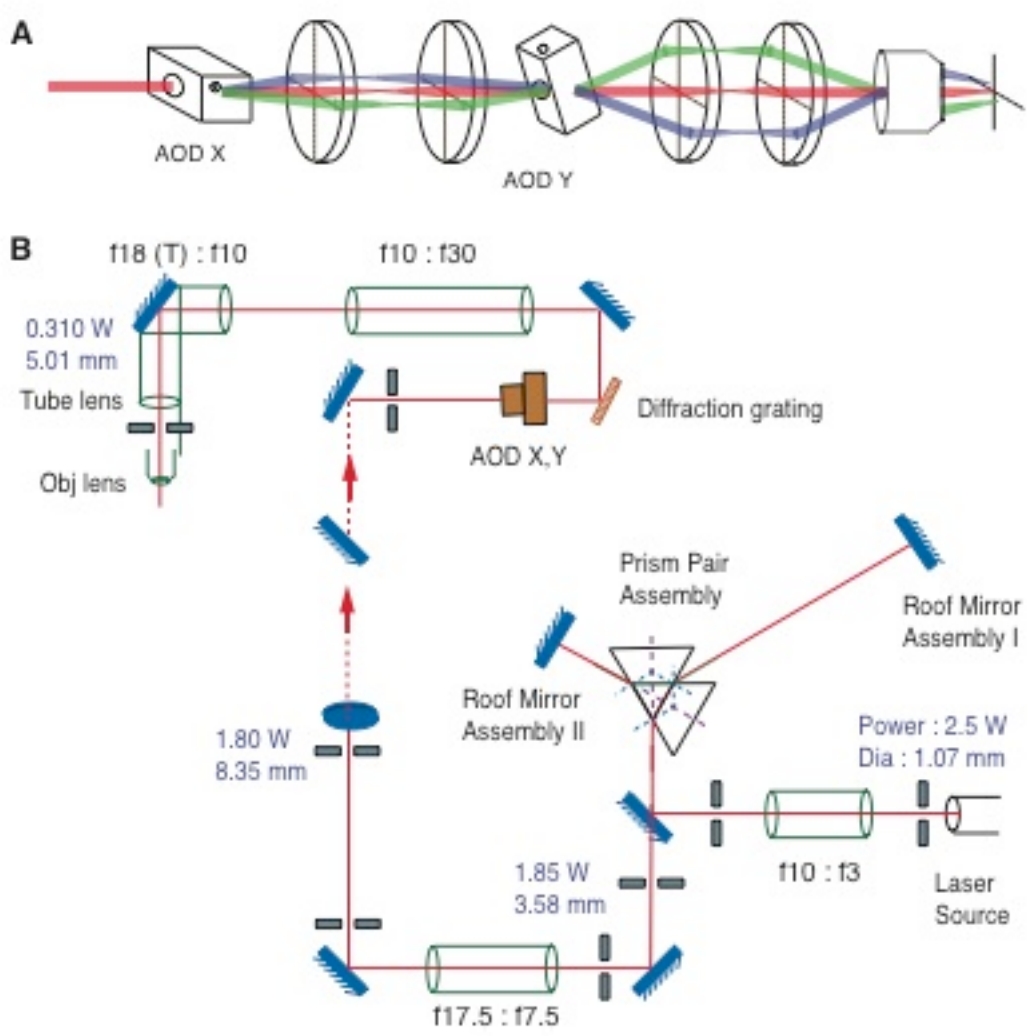

Figure 2.1: Principle and design of the Dithered random-access scanner.

A: Ray diagram tracing the path followed by the laser beam deflected by AODs B: Layout of the optical setup. Shows the relative positions of the various dispersion compensation elements (pre-chirper, diffraction grating), the scanning elements (AODs) and the scan-angle translocation and modification elements (telescopes) with the beam specifications along the path taken. Numbers alongside telescopes indicate the focal lentgth of lens pairs used.

While the beam was moved from neuron to neuron (access time), no signal was collected. Access time was 12.8 μs for the large aperture AODs and 8 μs for the small aperture AODs. In each neuron 3-5 spots were sampled before moving to the next neuron (dithering). Recordings were discarded from analysis only if the baseline was unstable or if the AP timing could not be distinctly ascertained from the electrophysiological recording.

2.3 RECORDING SOMATIC ACTION POTENTIALS FROM NEURONS

Recording calcium signals from a single spot from each neuron resulted in major problems in spike detection. The reason for this may be the inhomogeneous distribution of the amplitude of the spike-evoked relative fluorescence signals ($\Delta F/F$) within somata. To examine this problem we evoked single spikes in cells in loose-patch configuration and obtained single spike-evoked fluorescence responses from multiple locations across the area of neuron soma using a galvanometric scanner as well as the random-access scanner (n = 7 cells galvanometric scanner, n = 5 cells random-access scanner). We determined the spatial distribution of the amplitude of the fluorescence signal from single-exponential fits to the fluorescence transients.

In the recordings from the galvanometric scanner (Fig. 2.2A) sampling from individual locations resulted in very low S/N. We therefore averaged 4-31 recordings in each cell. Despite this averaging over multiple trials the low S/N was not sufficient to fit each recorded location with a single exponential with variable amplitude and variable decay time constant. We therefore first analyzed the decay time constant by averaging across all recorded locations in one soma

(184-225 pixels). The decay of the averaged fluorescence signal was fitted with a single exponential function to obtain the decay time constant. This decay time constant was then used for fitting the fluorescence signals from all locations with a single exponential to obtain the amplitude of the AP-evoked fluorescence signal in each location. In recordings using random-access scanning we sampled 9 different spots distributed over the soma. Each of 9 points placed in a single soma was recorded using the same dwell time as if recorded in dithered mode (96 μs in this set of experiments). In recordings from galvanometric scanning, amplitudes ($\Delta F/F$) of single spike-evoked calcium transients displayed large variations between different locations across the soma. In some neurons the range of $\Delta F/F$ amplitudes was as large as [-0.22 to 0.43], (average 0.11 $\pm$ 0.07, n = 7) across different locations. Similarly, amplitudes recorded using random-access scanning also had a wide range (Fig. 2.2B). With such a large range of response amplitudes, not surprisingly, single-point random-access scanning resulted in many recordings that lead to failures in spike detection.

2.3.1 Dithered random access scanning

As sampling from multiple locations strongly reduced the probability of recording only from locations with low spike-evoked calcium transients we developed a dithered scanning technique of sampling 3-5 points within each neuron soma (Fig. 2.2C). Somata locations and outlines were determined by obtaining a full x-y raster image. For dithering, 5 points were positioned in a star pattern in each neuron soma, with a point centered in the middle of the soma and 4 points at a distance of 1.8 – 2.5 μm from the central point (Fig. 2.2C).

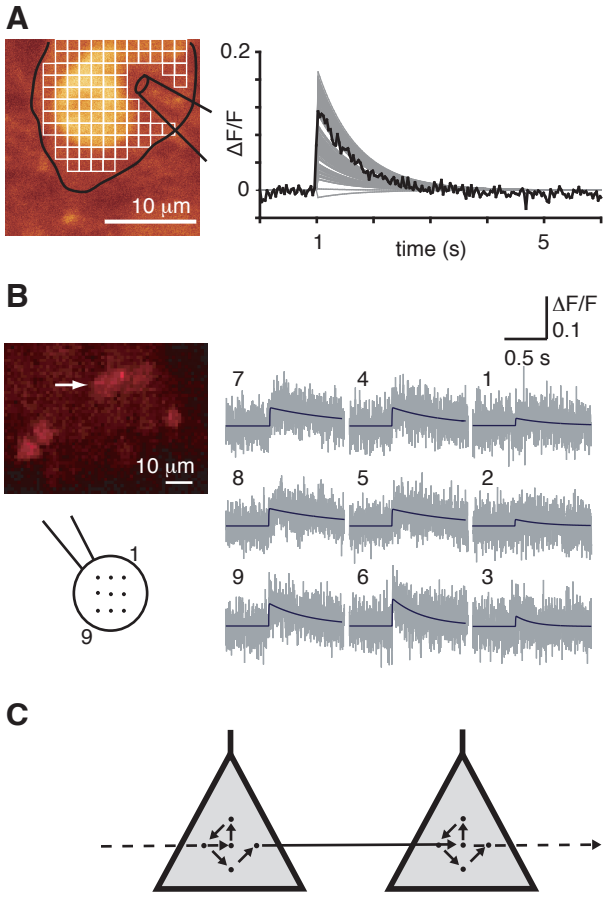

Figure 2.2: Inhomogeneous fluorescence signal distribution in L2/3 neuron.

A: Image (left) of a neuron obtained with a galvanometric scanner. Black lines delineate the soma, divided into a grid of 1.3 x 1.3 μm, and the patch pipette. Traces (right) show single-exponential fits to the relative fluorescence responses evoked by an AP from each of the grid squares averaged over 19 recordings (gray traces). Bold trace shows averaged signal all grid squares. B: Illustration of dithered random-access scanning principle. C: Fluorescence image of a neuron, obtained with the random-access scanner. The schematic below indicates the 9 different recording locations. Gray traces show fluorescence responses ($\Delta F/F$, single trial from each of the 9 sampled locations) evoked by a single AP and fits (black lines) to the fluorescence traces.

When using a low dwell time of 25.6 μs we reduced the number of dithered points to 3. As described below, dithering significantly increased the fraction of spikes detected compared to single-point imaging. Note that in this

comparison the total time spent on each neuron was the same. Dithered scanning presumably also decreased the cumulative photodamage in each sampled spot by distributing excitation over multiple locations. In comparison to galvanometric scanners that are currently used for functional calcium imaging of neuronal populations, dithered random-access scanning achieved a high temporal resolution, high duty cycle, and hence a high S/N (Fig. 2.3 A-C). As a result, dithered random-access scanning can also be used to record activity from neurons that are spatially distributed while maintaining a high duty cycle.

2.3.2 Single spike evoked calcium signals in cortical neurons

As our method of extracting the spike information from fluorescence signals required prior knowledge about the spike-evoked calcium signals, we first characterized the spike-evoked calcium signals in L2/3 neurons with high temporal resolution. We used a four-parameter to describe the single-spike evoked calcium signal h(t) (see Eq. 1). The parameters were rise time constant τ_{rise}, time between peak of action potential and start of fluorescence response t_{start}, amplitude of the calcium signal A, and decay time constant τ_{decay}. This model is based on a single compartment model for the intracellular calcium concentration (Augustine and Neher, 1992; Helmchen et al., 1996). Averages of experimentally obtained values were used for the parameters τ_{rise} and t_{start} while A and τ_{decay} were variable within an experimentally obtained range of values and were adjusted by the algorithm for each cell individually.

$$h(t) = A \times \left(1 - \exp\left(-\frac{(t - t_{start})}{\tau_{rise}}\right)\right) \times \exp\left(-\frac{(t - t_{start})}{\tau_{decay}}\right) \quad \text{for } t > 0 \qquad \text{(Eq. 2.1)}$$

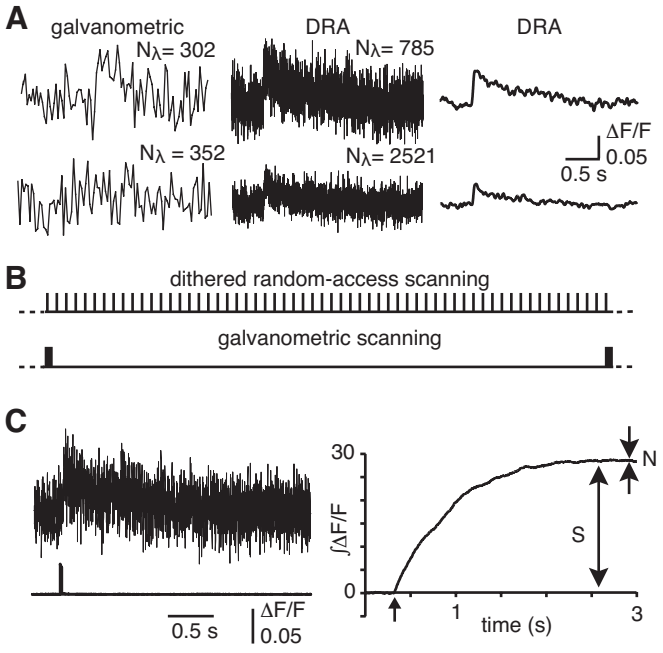

Figure 2.3: Functional dithered random-access calcium imaging.

A: Examples of fluorescence calcium transients recorded in L2/3 neurons. Left column shows recordings using a galvanometric scanner (temporal resolution 27 ms). Traces in the middle show recordings using dithered random-access scanning (temporal resolution 1.28 ms) and on the right are the same traces filtered with a 30 ms Hamming window. N_λ denotes the average number of detected photons from the neuron per data point. B: Illustration compares the duty cycles of dithered random-access scanning and galvanometric scanning. Each bar represents the time during which signal was collected from one neuron (dwell time), 25.6-96 μs every 1 ms for dithered random-access scanning and 150 μs every 60-100 ms for galvanometric scanning. C: Illustration of high S/N achieved with random-access scanning. Left trace shows a recording using dithered random-access scanning in a L2/3 neuron. Trace below shows cell-attached recording, indicating one spike at 0.313 s. Right graph shows integral of the relative fluorescence change (ΔF/F). The signal of spike detection (S) is approximately given by the integral compared to the noise (N) of the baseline.

We first determined lag and rise time by optically recording somatic calcium transients at high-temporal resolution (0.4 ms), from evoking spikes with brief current injections under either whole-cell or loose-patch configuration while

simultaneously recording electrophysiological traces. We fixed the onset of the calcium fluorescence signal by the point of intersection between baseline and a linear fit to the first 2 ms of the fluorescence signal. The average lag between peak of action potential and start of rise of fluorescence was $\overline{t_{start}}$ = 485 ± 214 μs (n = 17 cells, 9 slices, Fig. 2.4A,B). To obtain the time constant of the rise in fluorescence following an AP (τ_{rise}), points in the first 7-10 ms of the calcium fluorescence signal were fit with a kernel with variable rise time constant and amplitude, while lag and decay constant were held constant. Average value for rise time constant was $\overline{\tau_{rise}}$ = 2.25 ± 1.09 ms (n = 17 cells, 9 slices, Fig. 2.4). To obtain amplitude and decay time constant, the fluorescence signals from recordings with a temporal resolution of 1.04 ms were fit with the model with constant amplitude and variable decay time constant as free parameters, while rise time and lag were held constant at their average values $\overline{\tau_{rise}}$ and $\overline{t_{start}}$ (Fig. 2.4C+D). Precise spike timing was determined from the electrophysiological data and hence was not a free parameter. The average amplitude was $\overline{A}$ = 0.057 ± 0.0207 (ΔF/F) and average decay time constant was $\overline{\tau_{decay}}$ = 0.657 ± 0.405 s (n = 218 spikes, 47 cells, 20 slices from 17 animals, Fig. 2.4D). However, our spike detection algorithm utilizes the entire spread of amplitude and decay time constants instead of just the average values for extracting spiking information.

The joint distribution of (A, τ_{decay}) was used as a prior for the detection algorithm. To reduce the impact of the fluorescence noise (photon shot noise) on this distribution, we determined the joint distribution (A, τ_{decay}) by averaging 3-5 recordings in each tested neuron (Fig. 2.4G, n = 47 cells). Before averaging, fluorescence traces were aligned by spike timing (Fig. 3F). In this distribution,

amplitudes ranged from 0.0284 to 0.1546 and decay time constants from 0.128 to 1.403 s (Fig. 2.4G).

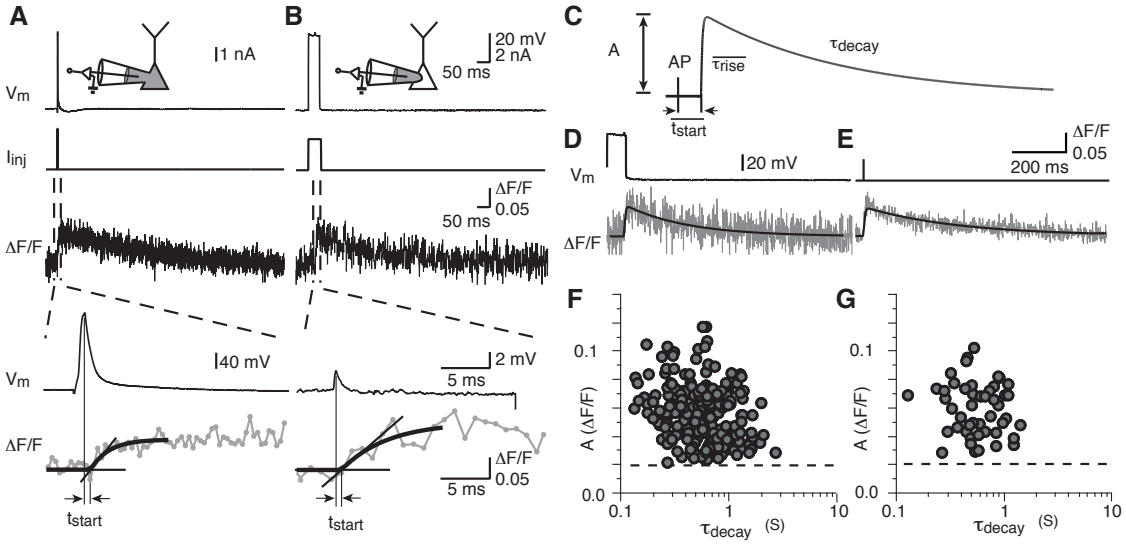

Figure 2.4: High temporal-resolution kernel and prior distribution.

A: Traces above show whole-cell current-clamp recording of a L2/3 pyramidal neuron (resting membrane potential = -76 mV). An AP was evoked by brief current injection (2.5 nA for 1 ms). Fluorescence calcium transient (ΔF/F) was recorded simultaneously with high temporal resolution (0.4 ms). Taces below show magnification of traces within the dashed lines. In this example we determined t_{start} = 508 μs and τ_{rise} = 2.499 ms. B: Lag and τ_{rise} determined from a loose patch recording. C: Illustration of the high-resolution kernel used for deconvolution described by mean lag ($\overline{t_{start}}$), mean rise time constant ($\overline{\tau_{rise}}$), variable amplitude (A), and variable decay time constant (τ_{decay}). D-E: Determination of prior distribution of kernel parameters A, τ_{decay}. D: Upper trace shows loose-patch current clamp recording of a L2/3 neuron. An AP was evoked with brief (25 ms) current injection (3.2 nA). The lower trace shows simultaneously recorded fluorescence calcium transient. E: Average of fluorescence calcium transients evoked by single AP (averaged across 5 trials), aligned by AP timing. Bold lines indicate exponential fit. F: Distribution of A and τ_{decay} derived from fits of individual fluorescence calcium transients (n = 190). G: Graph shows distribution (A, τ_{decay}) derived from fits of averaged calcium transients (n = 47). Average values were $\overline{A}$ = 0.0621 $\pm$ 0.0238 and $\overline{\tau_{decay}}$ = 0.6365 $\pm$ 0.297 ms.

2.4 EXTRACTING PRECISE SPIKES AND SPIKE TIMINGS

The task of detecting spikes from fluorescence signals from an inhomogeneous cell population is difficult as neurons can have a wide range of spike-evoked

calcium signal characteristics as seen in the distribution (A, τ_{decay}). We therefore developed a maximum-likelihood approach using a genetic algorithm to maximize likelihood. The prior distribution (A,τ_{decay}) was used by the detection algorithm to update model probability using Bayes' theorem.

2.4.1 Maximum – likelihood spike detection algorithm

The algorithm tested models M:$(\Delta F/F)_k$ with the parameters A, τ_{decay}, number of spikes S, and spike timings {$t_{spike\ (1)}$, …, $t_{spike\ (s)}$}. Note that as part of the procedure the algorithm adjusted A and τ_{decay} for each neuron. This is highly useful when detecting spikes from responses of a heterogeneous population of neurons, where spike-evoked calcium signals vary between neurons. Lag and rise time, on the other hand, were not free parameters of the model. Instead we used the average values $\overline{t_{start}}$ and $\overline{\tau_{rise}}$. Nevertheless, as shown in Fig. 2.5, the algorithm reliably detected spikes not only in recordings where only a single spike was observed (Fig. 2.5A), but also in recordings where multiple spikes occurred at low inter-spike intervals (Fig. 2.5B).

In the first step of the algorithm, for all 1 s time windows we compared the least square error of the following two functions:

$$F1(t) = F_0$$

$$F2(t) = \begin{cases} F_0 & t < 0.5s \\ F_0 \times 1.02 & t > 0.5s \end{cases} \qquad \text{(Eq. 2.2)}$$

F_0 was calculated as the average F(t) of the first 0.5 s for both functions. For all continuous intervals where the least square error of F2 was smaller than

that of F1, we determined the location of the minimum least square error t_{min}, calculating only entries F(t) < F1/F2(t). Each of these instances represented potential spikes and were thus examined in a second step by maximizing the likelihood of a model. For each instance, baseline fluorescence F_0(1...N) was calculated as the average fluorescence in the interval [t_{min}-0.5s ; t_{min}-0.08s].

Relative fluorescence increases ΔF/F were calculated by

$$\frac{\Delta F}{F} = \frac{F(t) - F_0}{F_0}. \qquad \text{(Eq. 2.3)}$$

To reduce the impact of slow baseline drifts and to reduce computational costs we determined a second time t_{max}. Model likelihood was calculated in the interval [t_{min}-0.5s, t_{max}]. To determine t_{max}, time was increased from t_{min}+0.5s until a window of 0.5s was found that had an average fluorescence F_0' that was $F_0' \leq 1.001 * F_0$, indicating that at this time (t_{max}) fluorescence had decayed back to baseline (if there was a spike). To limit computational costs associated with the maximum-likelihood deconvolution step, we limited the time interval t_{max}-t_{min} to maximal 4s. This was sufficient for the spike trains examined here as they did not contain prolonged periods of spiking activity. The interval can be increased to 10s with reasonable times to complete the algorithm. For all intervals [t_{min}-0.5 ; t_{max} s] we determined maximum likelihood by using a genetic algorithm. The only instance of user interaction was when spikes occurred within the first 0.5 s of a recording. In such a case, both the 1s time window for calculating F1 and F2 and the interval for calculating baseline fluorescence F_0 were shortened.

As described above, fluorescence calcium transients were modeled using a high-resolution kernel defined as follows:

$$h(t) = A \times \left(1 - \exp\left(-\frac{(t - t_{start})}{\tau_{rise}}\right)\right) \times \exp\left(-\frac{(t - t_{start})}{\tau_{decay}}\right) \qquad \text{for t > 0 .} \quad \text{(Eq. 2.1)}$$

The four parameters describing the model were the average lag between the peak of AP and onset of fluorescence signal ($\overline{t_{start}}$), the average time constant of the rising phase ($\overline{\tau_{rise}}$), variable peak amplitude (*A*), and variable decay time constant (τ_{decay}). Fluorescence signal was modeled by a discrete time model with *S* spikes:

$$M : (\Delta F / F)_k = \sum_{n=1}^{S} h\left(t_k - t_{spike(n)}\right) + \sigma_{shot} + \sigma_{dark} + \sigma_{electrical} \qquad \text{(Eq. 2.4)}$$

Thus the parameters of the model M:$(\Delta F/F)_k$ were *A,* τ_{decay}*, S ,* and $\{t_{spike\ (1)}, \ldots, t_{spike\ (s)}\}$.

A low-pass butterworth filter with a cut-off frequency of 100 kHz was used to minimize the noise contribution from electrical sources ($\sigma_{electrical}$) and PMT dark current (σ_{dark}), and were hence neglected. As the number of photons per data point N_λ was >> 100 for most recordings, we did not use a Poisson-distribution for shot-noise. Instead, σ_{shot} was approximated by:

$$\sigma_{shot}(\Delta F / F) = \sqrt{\frac{N_\lambda}{2\pi}} \exp\left(-\frac{(\Delta F / F)^2 N_\lambda}{2}\right) \qquad \text{(Eq. 2.5)}$$

For *in vivo* recordings, additional sources of noise such as tissue movement may contribute. To compare *in vitro* to *in vivo* recordings, we approximated all noise by a simple Gaussian distribution where:

$$\sigma_{noise}\left(\Delta F/F\right)=\sqrt{\frac{1}{2\pi s^2}}\exp\left(-\frac{\left(\Delta F/F\right)^2}{2s^2}\right) \quad \text{(Eq. 2.6)}$$

$$s^2=\frac{1}{N_\lambda} \quad \text{(Eq. 2.7)}$$

The signal in rate of detected photons is denoted by r, and was calculated as:

$$r=\frac{N_\lambda}{\Delta t} \quad \text{(Eq. 2.8)}$$

Even for calcium transients described by kernels with very small amplitudes the number of photons contributing to spike detection was > 2^3.

The deconvolution maximized the log-likelihood using a genetic algorithm (Holland JH, 1992). Likelihood p of the fluorescence data p of the fluorescence data (**y**) was calculated as:

$$p\left(\mathbf{y}\right)=\left(\sqrt{\frac{N_\lambda}{2\pi}}\right)^N\exp\left(-\frac{\sum\left(\mathbf{y}-\left(\Delta F/F\right)_k\right)^2N_\lambda}{2}\right) \quad \text{(Eq. 2.9)}$$

The prior kernel distribution was used to update the likelihood p(y) using Bayes theorem. As the correct determination of the prior distribution from data would require a very large amount of data, we instead smoothed (Gauss filter, 0.1125 s x 0.0125 ΔF/F) the binned prior distribution and used a threshold to reduce the widening of the distribution introduced by the smoothing.

The algorithm was initialized using values drawn at random from the prior distribution (A, τ_{decay}) and random spikes inserted with a probability of 0.001. In

each iteration, the likelihood for all models was calculated and ranked. Up to $4x10^6$ models were tested for each interval that potentially contained spikes. A new generation of models for the next iteration was generated by crossover, using models with a probability according to their likelihood. The genetic operators were specifically designed to utilize the topography of the log-likelihood as a function of the kernel, and the monotonic increase in likelihood for decreasing timing error. Each operator was used with a certain probability <<1. Genetic operators included the standard operator crossover, displacement of spike timings by a random Δt = -10, …,+10 ms with a probability of 0.05-0.2, simultaneous small random change (-0.05 ... +0.05) in A and τ_{decay} such that (A x τ_{decay}) remained constant (probability 0.02), and standard mutation operators (insertion and deletion of spikes with a probability of 0.005-0.02). The population of models consisted of 200 - 400 models, grouped into 20 - 40 families that had similar values of A, $\tau_{decay.}$ The genetic operator crossover was only applied within a family. The genetic algorithm was implemented in C++ as a plugin for a statistical software (IGOR pro, Wavemetrics). Kernels were pre-calculated by the algorithm for all combinations of (A,τ_{decay}) present in the population of models. This pre-calculation greatly decreased computational costs associated with calculating likelihood for 400 models in each iteration. The algorithm was terminated when no improvement in likelihood for the best model was found for 2000 iterations. Fig. 2.5A shows the progressive convergence onto the model with maximum likelihood. To account for the fact that two models, one with half the amplitude and double the number of spikes, have the same likelihood, inter-spike intervals were limited to ≥ 9ms and the model with the lowest number of spikes with likelihood $\geq$ 99% of the maximum likelihood was chosen as the best

fit. As shown in Fig. 2.5B, the algorithm successfully detected spike numbers and spike timings accurately for single as well as multiple spike conditions.

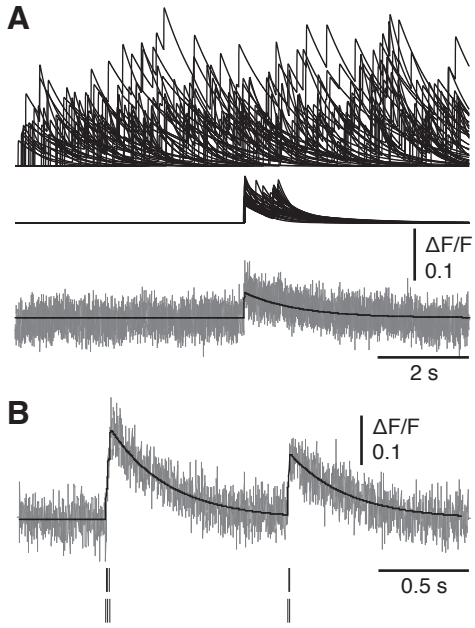

Figure 2.5: Deconvolution of spiking activity from fluorescence signals

A: Example of a cell with a single spike at t = 5.0466 s (determined from electrophysiological data). Upper graph shows a random sample of 40 models at the initialization of the deconvolution algorithm. Middle graph shows these 40 models after just 200 iterations of the algorithm. Lower graph shows the fluorescence recording (gray trace) and the final maximum likelihood model (black line). In this example the algorithm found 1 spike with a spike timing of t = 5.04712 s. Thus it extracted the correct number of spikes and the spike timing with an error of only 0.6 ms, upon adjusting amplitude and decay time constant for this particular neuron. Note that the appearance of the fluorescence trace is dominated by the large outliers (≥3 S.D. because of the large amount of data points). B: Example of the algorithm extracting spike information from a recording with multiple spikes at short inter-spike intervals. Bold line indicates best model determined by algorithm. The algorithm detected 5 spikes at t_1 ... t_5 = {0.9995, 1.0053, 1.0176, 1.9945, 2.0045}. Analysis of the simultaneously collected electrophysiological data revealed 5 spikes with spike timings (peak of action potential) t_1 ... t_5 = {0.9996, 1.004, 1.0151, 2.0001, 2.004}. The vertical bars below the trace illustrate actual spike timings (upper row of bars) and deconvolved spike timings (lower row of bars).

2.4.2 Testing for detection errors

Using AODs with an aperture of 10 mm, a large FOV of 300 μm x 300 μm was achieved, resulting in recordings of high temporal resolution (0.4 – 4 ms) from up to 103 neurons that were distributed within the entire width of a cortical column (Fig. 2.6). The detection of spikes from noisy fluorescence recordings involves hypothesis-testing (Sjulson and Miesenböck, 2007). As our approach of recording calcium fluorescence signals and extracting spike and spike timings using our detection algorithm did not allow us to determine the reliability of spike detection analytically, we determined spike detection errors empirically. Error type II was defined as the fraction of undetected spikes, error type I as the rate of false positives. These errors and the error in spike timing detection were determined from data with simultaneous optical and electrophysiological recordings, using a temporal resolution of 1.04 ms for all optical recordings. As the S/N had a large impact on these errors, we calculated signal as the rate of detected photons from the baseline fluorescence distribution for each recorded cell using Eq. (2.8).

Our combined data set consisted of data collected at signal rates of 0.16 $x10^6$ to 5.4 $x10^6$ photons/s. On testing spike detection in this data set, the error type II was low (2.5%, 9 of 362 spikes undetected in n = 43 cells). The error type I was also low (0.0023 spikes/s, 5 false positives, n = 43 cells, 575 recordings, 2,192 s total time). Similarly, the error in spike timing, calculated from the successfully detected spikes, was small, (average absolute error = 3.47 ms, Gaussian fit σ = 2.07 ms, S.D. = 8.3 ms, SEM = 0.44 ms, n = 352 recordings in

43 cells). The analytical limits of spike detection using our maximum-likelihood method were determined by simulating fluorescence responses. As shown in Fig. 2.6 (E-H), our method resulted in detection rates and errors that were close to these analytical limits.

When limiting the data set to those recordings where photon rates were maximal before the onset of photodamage (optimized condition, mean 2.3 $\pm$ 1.01 $x10^6$ photons/s, n = 192 recordings from 36 cells, second data point in Fig. 2.6E) the error type II was 3.1% (6 in 192 spikes undetected), error type I was 0.0025/s (3 false positives in 1195.6 s) and timing error was (average absolute error = 2.81 ms, Gaussian fit σ = 2.1 ms, S.D = 6.1 ms, SEM = 0.45 ms, n = 185 spikes in 36 neurons).

We also tested spike detection on data obtained with single-point random-access scanning (no dithering). In these experiments we recorded data from single locations on neuron soma. Dwell time and duty cycle were the same as in the dithered data set. The error type II was significantly higher ($p = 4.2 x10^{-09}$, Fisher's Exact Probability Test) at 41.2% (42 of 102 spikes undetected, 4 cells) compared to a error type II of 1.8% for that data recorded with dithering at a comparable signal rate (lower data point in Fig. 2.6E, mean 0.71 $\pm$ 0.35 $x10^6$ photons/s compared to 0.66 $\pm$ 0.21 $x10^6$ photons/s for dithered data). The results demonstrate that recording from multiple locations on a neuron is required for high spike detection efficiency.

As the data set used to determine the prior kernel distribution and the test data partially overlapped, we tested the performance of the algorithm after separating the training data set (used to determine the prior distribution of the kernel) and the test data set (used to determine errors of our method) for dithered scanning. There were 5 errors of type 1 (error type I of 0.0029 spikes/s, n = 415 traces in 35 neurons, total time = 1679.6 s) when testing our data in this way.

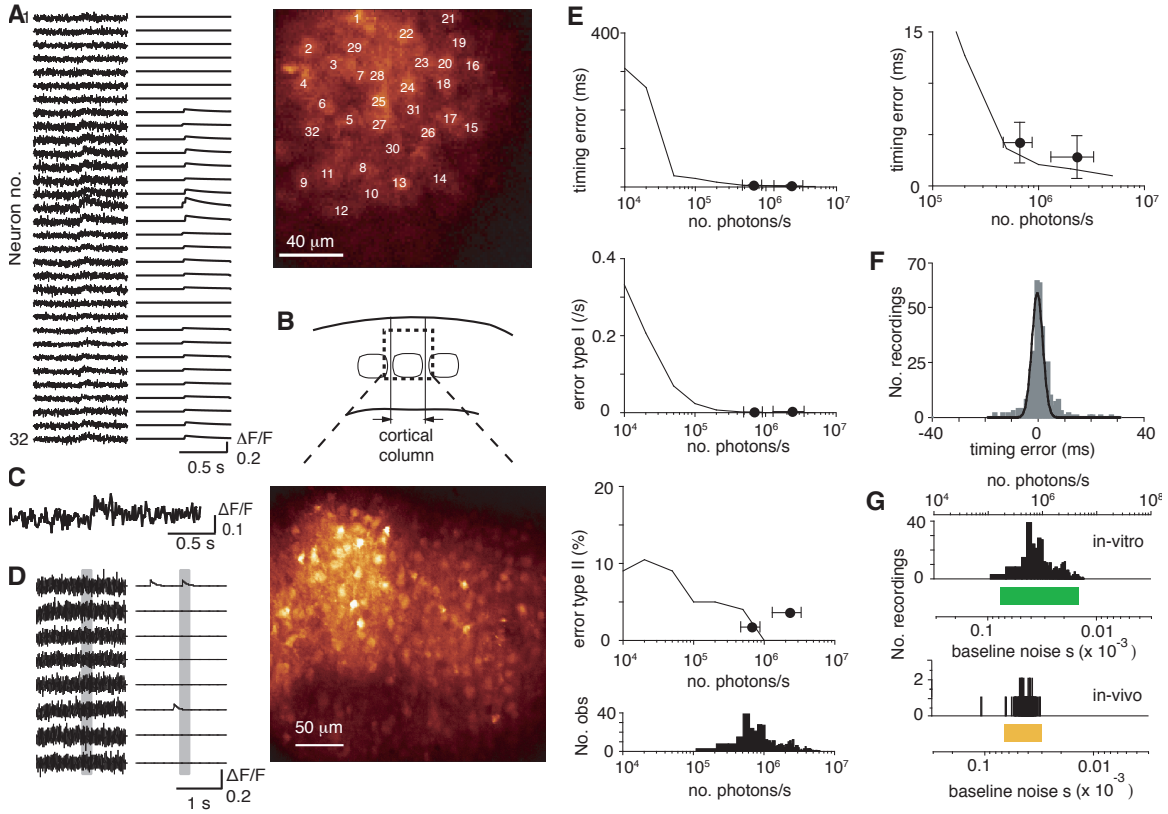

Figure 2.6: High spike detection efficiency in distributed neuronal populations.

A: Simultaneous recording of 32 neurons in L2/3 of a thalamocortical slice, using dithered random-access scanning. Responses were evoked by focal extracellular stimulation in L4. Right panel shows the spatial positions of the neurons. B: Schematic of a thalamocortical slice illustrating L4 barrel column borders. Dotted region represents the FOV (lower image) of 300 x 300 μm achieved. C: Example of fluorescent calcium transient recorded *in vivo* in mouse barrel cortex, evoked by whisker input. D: Spiking activity recorded in 8 cells *in vivo*. Colored bar illustrates onset and offset of whisker deflection. Cell 1 and cell 6 displayed spontaneous / evoked spikes. E: Graphs show the average error in spike timing detection (top), and errors type I (middle) and type II (bottom graph), respectively, as a function of rate of detected photons. Top

right graph shows magnification of the timing error. Continuous lines indicate analytical limitation determined from simulations, and markers (black circles) indicate experimentally determined errors (Error bars indicate S.D.). Bottom histogram shows the photon rates of recorded neurons. F: Histogram of the error in spike timing detection. Line indicates Gaussian fit (σ = 1.95 ms). G: Illustration showing range of signals recorded *in vitro* (green), *in vivo* (yellow), as a function of baseline noise parameter s (determined using Eq. 4).

There were also only 4 failures of spike detection (error rate type 2 = 1.8%, n = 218 spikes in 35 neurons). The timing error tested in the successfully detected spikes was also small (average absolute error = 3.95 ms, Gaussian fit σ = 1.71 ms, S.D. = 10.07 ms, SEM = 0.24 ms, n = 213 spikes in 35 neurons).

As illustrated in Fig. 2.6C and D, dithered random-access scanning can be used to record somatic calcium signals *in vivo*. Fig. 2.6.C and D show fluorescence traces of calcium transients evoked by both spontaneous activity and by whisker deflection in L2/3 neurons in mouse barrel cortex *in vivo* (Fig 2.6C and D). As expected, signals recorded *in vivo* had a larger baseline noise compared to *in vitro* recordings (Fig. 2.6G). The largest contribution to this difference was presumably the higher photon shot noise because of a lower rate of detected photons. Furthermore, tissue movements due to heartbeat and background signal from the surrounding neuropil are also likely to contribute to the recorded baseline noise *in vivo*. We did not quantify spike detection *in vivo* by simultaneous electrophysiological and fluorescence recordings.

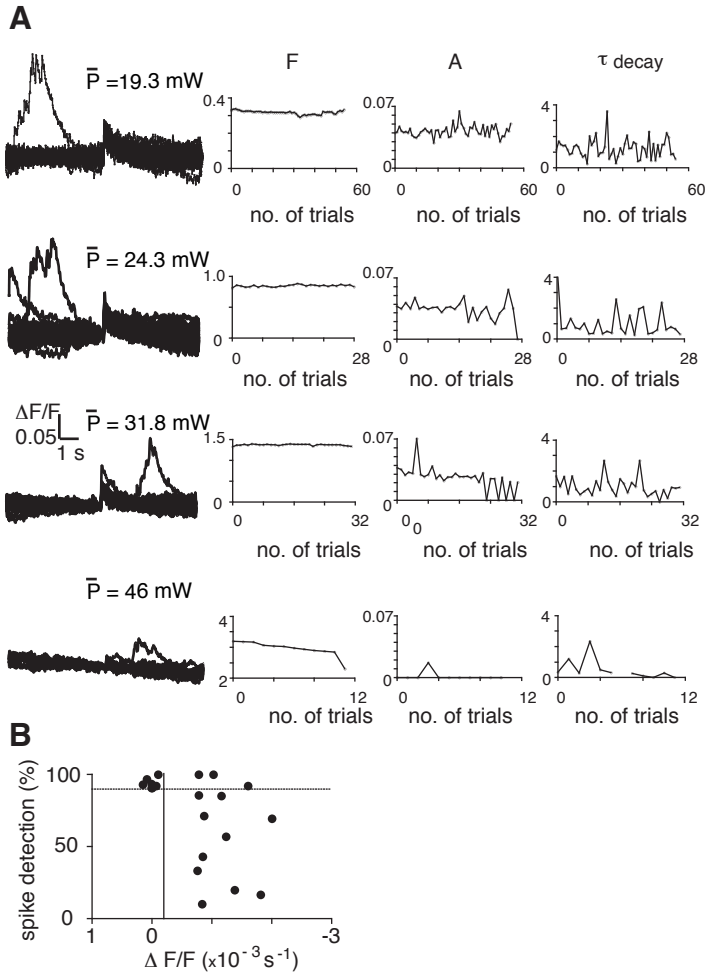

Figure 2.7: Photodamage and signal

A: Traces and graphs show 8 s recordings from a L2/3 neuron in a slice at increasing excitation intensities as given by $\overline{P}$ in each row. Laser intensity was measured at the sample. Traces on the left show overlay of all recordings for a certain excitation intensity (traces were filtered with a 30 ms Hamming window for illustration purposes. Left graphs show the baseline fluorescence F_o, middle graphs show the deconvolved amplitude A, right graphs show the decay time constant $\overline{\tau_{decay}}$. At higher excitation intensities ($\overline{P}$ = 31.8 and $\overline{P}$ = 46 mW) fluorescence baseline had a negative slope and spike detection failed consistently. Failure in spike detection is illustrated by an A = 0. B: Plot shows the relationship between detection efficiency and normalized slope of baseline fluorescence. The vertical line indicates the criterion of change in baseline fluorescence for photodamage (0.0002/s) and the horizontal line indicates 90% spike detection efficiency.

2.4 MAXIMIZING SIGNAL

The largest limiting factor in dithered random-access scanning as well as two-photon calcium imaging in general is given by the photodamage effects that alter neurons structurally as well as impact functional dynamics (Koester et al., 1999). To characterize the impact of photodamage on spike detection and to establish an indicator of onset of photodamage for our imaging method we recorded for prolonged periods of time from individual neurons. At a given laser intensity 20-75 trials (9.5 s each, 20 – 60 s between trials) were recorded. A single spike was elicited by brief current injection. From these recordings we calculated average baseline fluorescence, baseline slope across trials, amplitude and decay time constant of the spike evoked calcium signal, and spike detection rate. Average baseline fluorescence of each trace was calculated from all data points before and 3 s after the spike. The average baseline fluorescence values from consecutive runs were fit with a straight line to obtain baseline slope. This slope was normalized. As shown in Fig. 2.7, at high laser intensities changes in baseline fluorescence were observed along with a decrease in the amplitude of spike-evoked calcium transient. This decrease in amplitude eventually resulted in failures of spike detection (Fig. 2.7A, third set of traces). We therefore used the decrease in normalized baseline fluorescence as an indicator for onset of photodamage. Furthermore, as shown in Fig. 2.7B, at higher negative baseline slopes, spike detection decreased rapidly. We used a conservative criterion of -0.0002/s for the normalized baseline slope as an indicator of photodamage (see Fig. 2.7B). Spike detection efficiency was high only in recordings where normalized baseline decline was below our criterion. At higher laser intensities baseline slope exceeded our criterion and spike detection rapidly decreased (Fig.

2.7B). At very high laser intensities, dramatic structural changes were observed (data not shown) such that neurons were no longer visible after brief (<10 s) exposure.When limiting laser power according to our criterion, the signal we obtained from neurons ranged from 0.16 - 5.2x106 photons/s. Not surprisingly, dwell time did not affect the photon rate obtained before onset of photodamage. Average signal rate across all neurons recorded at below photodamage threshold was 1.54x106 photons/s (n = 43 neurons, dwell time = 96 ms, temporal resolution = 1.04 ms) and 1.35x106 (n = 88 neurons, dwell time = 25.6 ms, temporal resolution = 0.998 ms). 2.5 DiscussionThe sum of the methods presented in this study represent the significant achievement of recording spiking activity from unbiased, spatially distributed populations of neurons with low errors from a large sample of neurons. The combination of dithered random-access scanning with the deconvolution algorithm detected spikes with high efficiency, and spike timings with millisecond precision. The low errors in spike detection were a result of the combination of the high duty cycle of random-access scanning, high temporal resolution (typically 1 ms), dithering, determining the prior kernel distribution, maximizing excitation intensity by determining photodamage threshold, and optimal use of information from fluorescence signals. Although we do not test spike detection efficiency in vivo, the imaging method can be used to record somatic calcium signals in vivo.2.5.1 In comparison to other techniques for recording network activityDithered random-access functional calcium imaging is an optical technique that can record spiking activity from large populations of neurons. In contrast to techniques using microelectrodes or tetrodes it is less invasive, can record from a larger local sample including neurons with very low spiking probabilities, and the spatial

positions of neurons are known. Thus, dithered random-access scanning can be combined with other techniques that record from or manipulate individual neurons. The larger local sample is particular important in order to unravel the local computations carried out by highly recurrently connected neurons, for example within a cortical column.Probing of the somatic calcium signal can be used to extract quantities related to neuronal activity other than precise spike timings, for example firing rate (Yaksi and Friedrich, 2006) or simply discern between responding and non-responding neurons (Ohki et al., 2005). To use functional calcium imaging for detection of precise number of spikes and spike timings in individual neurons requires rigorous empirical determination of spike detection efficiency, given by errors type I and type II (Sjulson and Miesenböck, 2007). Only few studies have characterized this error systematically (Sato et al., 2007). Other studies have reported error rates from smaller test samples ($\leq$ 14 cells, (Greenberg et al., 2008; Grewe et al., 2010; Kerr et al., 2005; Kerr et al., 2007; Sasaki et al., 2008). As functional calcium imaging *in vivo* faces additional obstacles, we distinguish here between functional calcium imaging in acute brain slices (*in vitro)* and *in vivo*. The only study that characterized detection efficiency *in vitro* used Nipkow disk confocal scanning to record from slice cultures stained with the calcium indicator Oregon Green 488 Bapta-1 AM with a temporal resolution of 20-100 ms(Sasaki et al., 2008). Spike detection was high, but because of a low temporal resolution of the imaging method this study could not determine spike timings.

As mentioned above, functional calcium imaging for spike detection is a combination of an imaging method with a detection algorithm to extract precise spike timings from the noisy fluorescence signals. The aim of this study was to

refine existing imaging methods to obtain fluorescence signals from many neuron somata with low noise, high temporal resolution, and multiple samples from each neuron soma to avoid spike detection errors. In contrast to other calcium imaging methods that do not use two-photon excitation, dithered random-access scanning as well as galvanometric scanning can be used for imaging deep within opaque brain tissue and reject background signal from neuropil surrounding the recorded somata that carries other information (Kerr et al., 2005). In contrast to galvanometric scanners that do use two-photon excitation, dithered random-access scanning has a much higher duty cycle. It thus results in a higher temporal resolution and/or much larger sample size. A high temporal resolution can be achieved when using galvanometric scanners in line-scan mode instead of recording full frames. In line-scan mode, however, only very few neurons can be recorded from. Two-photon imaging using galvanometric scanner as well as AODs are scanning techniques that record from a single spot at any given time. Thus, there is a tradeoff between the number of recorded locations, the time spent to record from a location, and temporal resolution. The advantage of dithered random-access scanning over galvanometric scanning is the much smaller fraction of the duty cycle that is not used to record useful signal from neuron somata. In comparison to targeted path scanners (Lillis et al., 2008), the temporal resolution achieved using dithered random-access scanning is at least 10 times higher. Because spike detection efficiency has not been tested for data obtained with targeted-path scanning it is unclear if targeted-path scanners have an advantage over other techniques when used for functional calcium imaging to detect neuronal spiking activity.

As we show, implementing AODs to collect fluorescence signals from a single-point scanning resulted in large problems of spike detection because of inhomogeneous distributions of fluorescence and calcium transient amplitudes within a soma. As a solution to this problem, we have implemented star-patterned dithering that samples from several points within the soma. This approach reduced the probability of sampling from a location with low spike-evoked calcium transient. Dithering presumably also reduced photodamage by distributing excitation over multiple locations. Averaging over multiple samples potentially may reduce the sensitivity to small movements of the specimen as encountered for example during *in vivo* recordings. Independently from this study, another group has developed a very similar approach of using AODs in conjunction with two-photon excitation to record multiple samples from tens to hundreds of neuron somata *in vivo* with high temporal resolution (Grewe et al., 2010). The optical design was similar to our approach, except that only one prism was used for spatial and temporal dispersion compensation, resulting in higher throughput of laser intensity.

2.5.2 Acousto-optical deflectors

For ultra-short laser pulses AODs introduce spatial dispersion because of the wavelength-dependence of beam deflection. Despite dispersion compensation the spatial resolution of AOD scanning is usually lower compared to galvanometric scanning. This spatial dispersion increases with angle of deflection. Because dispersion compensation achieved using a diffraction grating is best at the center of the field of view, the spatial resolution deteriorates slightly

towards the corners of the field of view (Iyer et al., 2003). AODs also result in a temporal dispersion of short laser pulses. Temporal dispersion was compensated using a two-prism pre-chirper, as otherwise laser power would have limited excitation and thus limited signal. Two-photon imaging *in vivo* is limited to superficial layers; thus the technique presented here is also limited to superficial layers.

2.5.3 Comparison of spike detection to other methods

There are a number of methods that have been suggested for extracting spikes from fluorescence signals (Holekamp et al., 2008; Mukamel et al., 2009; Vogelstein et al., 2009). However, as these studies have not determined spike detection efficiency, we could not compare their performance to our algorithm. Our algorithm does not rely on a fixed kernel to extract spike information (Grewe et al., 2010; Kerr et al., 2005; Sato et al., 2007; Yaksi and Friedrich, 2006) but instead uses a prior distribution. The spike-evoked calcium response (kernel) is adapted to each neuron during the deconvolution process. This is paramount for spike detection efficiency in a heterogeneous population of neurons as shown by high errors of type I and type II, when using a fixed kernel on our dataset (error type 1 = 0.019/s and error type 2 = 19.8%, $p = 1.17*10^{-14}$ Fisher's Exact Probability Test). Our combined imaging/detection method is thus useful to detect precise spike timings in a population of neurons with inhomogeneous spike-evoked calcium signals. The algorithm also does not require knowledge of stimulus timings to increase robustness of spike detection in contrast to (Sato et al., 2007). Once the prior distribution used has been characterized from

simultaneous electrophysiological and optical recordings it can be used for any data set obtained under similar conditions. It is thus similar to other algorithms like (Greenberg et al., 2008; Sasaki et al., 2008). Our algorithm achieves high spike detection efficiency even when there is only a single spike in the observed neuron, and it also decodes the correct number of spikes in short bursts.

For detecting individual spikes in data containing high-frequency spike trains, a high temporal resolution is advantageous. Correct spike decoding from data containing many spikes at short inter-spike intervals also requires incorporation of indicator saturation into the model. Indicator can also easily be incorporated into our model (Eq. 2). Detecting the precise number of spikes and spike timings in data containing persistent high-frequency spike trains, however, presumably requires higher S/N than is possible to achieve using our technique without eliciting photodamage. This problem, however, can be alleviated to a large degree by utilizing information across many spikes by recording over long time periods. We note that our algorithm can easily be modified to utilize information from many spikes. Genetic algorithms are not guaranteed to converge to global maxima. The genetic operators of the algorithm were designed to minimize convergence errors. As indicated by the high detection rate and also indicated by the analysis of simulated fluorescence data, convergence errors do not play a role in the analysis of single-spike and short burst data recorded in this study. In summary, the combination of the large number of simultaneously recorded neurons, the high S/N, the high temporal resolution, and the flexible deconvolution algorithm is highly useful to detect spiking activity and spike timings in heterogeneous populations of neurons.

2.5.4 Functional calcium imaging and spike detection in vivo

Calcium imaging under *in vivo* conditions faces obstacles that are usually not encountered in *in vitro* recordings. These obstacles include tissue movement, for example because of heartbeat or muscle movements and image degradation when recording from neurons deep within tissue. Some of these problems are often more pronounced in recordings in awake animals (Dombeck et al., 2007; Greenberg et al., 2008). To determine spike detection efficiency for a particular combination of imaging/detection method requires simultaneous optical probing and recording of action potentials with another technique. Testing spike detection efficiency for *in vivo* recordings requires simultaneous electrophysiological and optical recording, which we did not achieve here. We note, that baseline noise for *in vivo* recordings was similar to the first data point (at lower photon rates) in Fig. 2.7E. As spike detection efficiency is determined by signal and kernel distribution, we estimate that our technique can record from many neurons *in vivo* with low errors in detection. This prediction is supported by a study that was published during revision of this manuscript (Grewe et al., 2010). In populations of neurons with large spike-evoked calcium signals, for example as has been reported for *in vivo* recordings in rats (amplitude $\Delta F/F > 0.1$,

(Grewe et al., 2010)) spike detection using our approach will be even more robust. When recording from such populations, one could reduce the dwell time per neuron further to increase the number of simultaneously recorded neurons.Many combinations of calcium imaging techniques and detection methods have been developed for specific experimental circumstances. For example,(Sato et al., 2007) developed a method to detect stimulus-evoked

activity *in vivo* from neurons in mice in somatosensory cortex using two-photon galvanometric scanning. This recording method in conjunction with a thresholding/clustering spike detection algorithm resulted in reliable (>95%) spike detection in 60% of neurons. By limiting the field of view of galvanometric scanner (Kerr et al., 2007)detected spiking activity *in vivo* from 10 to 14 neurons at temporal resolutions of 62.5 ms, using a template-matching algorithm. Greenberg et al developed a method based on two-photon galvanometric imaging and a detection algorithm (Greenberg et al., 2008). The detection algorithm was designed to detect both, spontaneous and stimulus-evoked activity *in vivo*, and also to decode the correct number of action potentials. Finally, as discussed above, (Grewe et al., 2010)developed a random-access scanning technique with a peeling algorithm and reported high spike detection efficiency.

2.5.5 Signal and limitations of dithered random-access scanning

As with other optical methods of detecting neuronal activity dithered-random access functional calcium imaging has limited access in depth of tissue. Using two-photon microscopy using longer wavelength excitation light increases the accessible depth but it is limited to few hundreds of microns by the scattering of light and loss of signal. While it may be challenging to record neuronal activity using two-photon microscopy from freely behaving animals, recent studies have achieved recording conditions that allow for free behavior. However, recent studies have adapted designed recording conditions that allow for free behavior of animals (Dombeck et al., 2007; Dombeck et al., 2009; O'Connor et al., 2010). The surprising finding of this study is that very high fluorescence signal rates can

be achieved in recordings from neurons before the onset of detectable impact of photodamage. There is, however, only a very small window of excitation intensity where high detection efficiency can be achieved consistently. This “high-efficiency window” is limited by the impact of photodamage on calcium signals for high intensities and the low S/N for low intensities. This “high-efficiency window” is presumably even smaller for *in vivo* recordings. As this window is rather small, we regard it as important to precisely determine baseline noise and detection efficiency in experimental studies using functional calcium imaging to detect precise spiking activity. In particular the decline in detection efficiency with increasing exposure time can introduce systematic errors in studies that rely on quantifying changes in neuronal activity. A high S/N is required to detect spikes and precise spike timings in unbiased populations of cortical neurons. Such populations include neurons that have very low amplitude spike-evoked calcium transients, such as interneurons (Fierro and Llano, 1996). The combination of dithered random-access scanning with our deconvolution algorithm was able to detect spike-evoked calcium fluorescence signals that have amplitudes as low as 0.025 ($\Delta F/F$) and thus has a much higher sensitivity and precision than previous implementations of functional calcium imaging and spike detection methods. Dithered random-access scanning has a duty cycle that is about 9-10 times higher compared to galvanometric scanning. A 10 fold higher duty cycle is expected to amount to gain in signal by the same factor. However, we find that the signal using dithered random-access scanner was more than 10 times higher compared to a galvanometer-based implementation. Excitation intensity is not limited by available laser power but by rate of photodamage for both methods. Photodamage in turn depends on peak intensity, which can be quite high for

femtosecond laser pulses. In contrast to two-photon calcium imaging in dendrites and axons of neurons, photodamage in dithered random-access imaging for somatic calcium signals manifests as reduction in amplitude and baseline decline, not increases in baseline(Koester et al., 1999). The reason for this difference is not known. A possible contribution to this difference may be that bleached fluorescence molecules in a dendrite can be replaced from a large pool (the soma). We speculate that the higher than expected advantage of dithered random-access scanning arises from the highly nonlinear dependence of photodamage on excitation intensity in two-photon imaging (exponent $n > 2$, indicating contribution of three-photon effects to photodamage, (Hopt and Neher, 2001; Koester et al., 1999) the high energy deposit of radiation-less transitions of excited molecules throughout the neuropil, ground state depletion, or a combination of these factors. A simple calculation based on the signal collection efficiency, detection rate and number of excited dye molecules (Koester et al., 1999) shows that ground-state depletion may occur when using a low duty cycle and high excitation intensity. Another limitation to excitation intensity may be given by dielectric breakdown. In fact, as a simple calculation shows, the peak intensity required ($\sim 10^{12}$ W/cm^2) to match the signal of a galvanometric scanner to our implementation would approach the dielectric breakdown of water ($\sim 10^{13}$ W/cm^2) (Xu et al., 1996).

We conclude that the combination of dithered random-access scanning and the maximum-likelihood detection algorithm result in a high spike and spike timing detection efficiency for recording from populations of neurons when operating within the “high-efficiency window” of excitation intensity. Detection of spikes from neuronal populations using functional calcium imaging is not useful

for brain areas where somatic calcium transients and spiking activity are not highly correlated (Lin et al., 2007).

2.5.6 Functional significance

The result of our technique refinement and tool development is a method to record from up to 100 neurons that are spatially distributed with known and low errors of spike and spike timing detection. It further allows sampling from an unbiased population of neurons, not only those with large spike-evoked calcium transients. Our method thus presents the tool to address central questions in neuroscience that require recordings from large populations of neurons. For example, theoretical studies predict that the detection of synfire chains or the detection of “neuronal groups” requires data from 50 and more neurons (Izhikevich et al., 2004; Schrader et al., 2008b).

2.5.7 Further improvements

As a scanning technique, dithered random-access scanning requires a certain access time to move the focal point between spatial positions. Access time is given by the aperture of the AODs and the speed of the acoustic wave propagating through the crystals. The aperture determines field of view and spatial resolution (as it determines the beam diameter at the back aperture of the objective). For larger AOD apertures the access time constitutes a significant fraction of the dwell time required to collect sufficient signal for single spike detection. In our recordings, the access time was 8-12.8 μs, compared to the dwell time of 25.6 – 96 μs. Thus, access time contributed significantly to the cycle

time, reducing duty cycle. A reduction in access time thus would lead to further increase in the number of neurons that can be recorded. Another increase in sample size could be gained by adapting dwell time for each neuron depending on signal (photon rate) and spike-evoked calcium signal. Furthermore, one could also increase spike detection efficiency by assigning different weights to the 5 samples recorded in a neuron. This, however, would require incorporation of the weights parameters into the model and increase the complexity of the deconvolution algorithm. Further gain in signal, without increase in photodamage, could be obtained from increasing pulse rate (Ji et al., 2008) reducing peak intensities and thus reducing the contribution of higher order excitation processes to photodamage. The deconvolution method can be improved by using information across many spikes, reducing uncertainty about the kernel. The method presented in this paper can also be combined with light-sensitive ion-channels to selectively induce or prevent spiking activity in individual neurons. The combination of recording of neuronal spiking activity with the ability to change spiking activity will be highly useful to test models of neuronal processing and plasticity on the mesoscale in the central nervous system.

2.6 SUMMARY

Recording suprathreshold activity of large, distributed neuronal populations simultaneously is required for understanding neural processing at the network level. Here, we have presented a novel technique, dithered random-access functional calcium imaging, to optically record suprathreshold activity of a spatially widespread, heterogeneous population of neurons. Fluorescence

changes associated with spiking activity in individual neuronal somata are recorded with high spatial and temporal resolution and a high signal-to-noise ratio. This technique also includes a novel spike-detection method that extracts precise spiking activity from the high-resolution fluorescence recordings. The combination of these methods resulted in the detection of spiking activity with single cell, single spike resolution, low errors of spike detection and millisecond precision in spike timing detection. This technique can be used to investigate network activity in various neural systems deep within neuronal tissue, under *in vitro* and *in vivo* conditions. We used this technique to examine the properties of propagation of suprathreshold population activity and the impact of plasticity on the propagation of activity between recurrent networks of the mouse barrel cortex.

Chapter 3: Signaling in the mammalian primary sensory cortex

External inputs are processed by the spiking activity of multiple neuronal populations to lead to cognitive or motor behavior. Thus signaling of information in a neural system includes the local representation of inputs through population activity as well as the faithful propagation of activity to appropriate downstream target areas.

Previous studies have examined putative neural codes for signaling in the cellular and systems level (Luna et al., 2005). However, activity at the microcircuit (mesoscale) level has a significant impact on processing of information. There have been few empirical studies investigating signaling in the mesoscale owing to the technical challenges in recording from a large, spatially distributed population of neurons. This limitation is particularly applicable for studying signal propagation, which requires recording from multiple neurons from multiple populations simultaneously.

Here we utilized the dithered random-access functional calcium imaging technique to record from sufficiently large neuronal population(s) to address signal representation and propagation between recurrent neuronal networks in the mammalian primary sensory cortex. Specifically, we recorded the propagation of evoked population activity from layer 4 (L4) to layer 2/3 (L2/3) in acute, thalamocortical slices of the mouse barrel cortex. We found that inputs were represented by evoked sparse evoked activity containing small ensembles of neurons with significant spiking probability. The observed activity evoked by naïve inputs had limited propagation from L4 to L2/3. Furthermore, neural

correlations measured within population activity decreased with the propagation of activity from L4 to L2/3.

3.1 SIGNALING IN NEURAL POPULATIONS

While signal processing occurs through multiple brain areas the task of a neural system is outlined to be extraction of relevant information at each stage of processing, the stable local representation of this information (encoding) and the propagation of this information so that a downstream receiving brain area may extract this information (decoding) and carry out further processing. Thus neural system may use any coding scheme that satisfies the following criteria: stable encoding, efficient decoding, transformation with plasticity and transmission with high fidelity (Kumar et al., 2010). Studies having evaluated the performance of several putative neural code suggest that neural codes relying on population activity better represent inputs than those that consider individual neuronal responses (Petersen et al., 2001; Pillow et al., 2008a; Pouget et al., 2000).

3.1.1 Neural correlations in population activity

Responses of individual neurons are often not independent and temporal interactions between neuronal responses impact the properties of the neural coding scheme. For example, neuronal responses are seldom independent of each other and the temporal interactions between spiking activity of neurons (neural correlations) within local microcircuits have an impact on both the representation and propagation of signals (Averbeck et al., 2006b). While neural correlations have been examined for their impact on representation (Petersen et

al., 2001; Pillow et al., 2008a) the changes in neural correlations from propagation of activity between multiple neuronal populations are largely relatively less known.

3.1.2 Propagation of neural correlations

Measuring propagation of population activity requires recording spiking activity from a large population of neurons from multiple populations simultaneously. Until recently, such measurements were impracticable. Thus, except for a few studies in the locust auditory system (Vogel and Ronacher, 2007) propagation of population activity has been mostly examined using analytical methods. Results from the empirical studies suggest that correlated neural population activity is preserved and may even increase with propagation through multiple levels of the circuitry. Similarly, the analytical studies conducted in network simulations or in networks iteratively constructed with experimentally obtained neural activity predict that cross correlations in population spiking activity increases with the propagation of the activity from one layer of neurons to the next. However, both the analytical studies and the empirical studies were carried out in networks with feed-forward connectivity. Neural networks in mammalian cerebral cortex on the other hand have extensive, recurrently connected synaptic architecture. In recurrent networks, there are mechanisms that contribute to decorrelation of neuronal spiking activity(de la Rocha et al., 2007; Renart et al., 2010; Wiechert et al., 2010).

3.2 EXPERIMENTAL METHODS

We used dithered random-access functional calcium imaging in conjunction with maximum-likelihood spike detection to record spiking activity from up to 40 neurons as activity propagated from L4 to L2/3 in acute slices of the mouse barrel cortex.

3.2.1 Slice preparation and imaging

C57Bl6 mice (P14 – P20) were anesthetized by intraperitoneal injection of ketamine/xylazine (80 and 20 mg/ml), decapitated, and the brain was quickly removed. All experimental procedures were approved by The Institutional Animal Care and Use Committee of The University of Texas at Austin. Acute thalamocortical brain slices (300-350 μm thick) were prepared in cold slicing solution (containing in mM: 2.5 KCl, 1.25 NaH_2PO_4, 25 $NaHCO_3$, 1 $CaCl_2$, 7 $MgCl_2$, 7 dextrose, 240 sucrose, 1 ascorbic acid and 3 sodium pyruvate) as described previously(Agmon and Connors, 1991). Slices were transferred to a chamber with extracellular solution (containing in mM: 125 NaCl, 2.5 KCl, 1.25 NaH_2PO_4, 25 $NaHCO_3$, 1.7 $CaCl_2$, 1 $MgCl_2$, 10 dextrose, 1 ascorbic acid and 3 sodium pyruvate). Both solutions were bubbled with 95% O_2 and 5% CO_2. Slices were incubated at 35°C for 30 mins, and stored at room temperature prior to experiments. Neurons within 1-2 mm^2 of cortex were stained by multiple bolus injections of the cell permeant ester form of a Ca^{2+} indicator (50 mg Oregon Green 488 Bapta-1 (OGB-1) AM dissolved in 5 μl DMSO, diluted with 34 μl extracellular solution containing pluronic (20%), final concentration of OGB-1 AM was 1 mM). Neurons were visualized by differential interference contrast

microscopy (DIC). Neurons were allowed to take up the indicator for at least 1 hr. All experiments were carried out at ~35°C bath temperature

To detect suprathreshold neuronal activity we used dithered random-access scanning in conjunction with maximum-likelihood detection(Ranganathan and Koester, 2010b). Briefly, an upright microscope (BX50WI, Olympus) was coupled with the scanning module consisting of two AODs (ATD-6510CD2, IntraAction Corp.) with 10 mm apertures to deflect the laser beam in two dimensions. The Ti:Sapphire laser source (Chameleon Ultra II, Coherent) was operated at 840 nm. To record from individual neurons a x 40 water immersion objective (UMPlanFI, NA 0.8, Olympus) was used. Somatic calcium fluorescence signals were recorded at 651 Hz. In each cycle, fluorescence signals were recorded for 25.6 μs from 3 locations in the somata of each neuron. No recording was done while switching between neuron somata (access time, 12.8 μs). We recorded exclusively from neuronal somata and avoided astrocytes as distinguished by their distinct morphology and higher resting fluorescence (Hirase et al., 2004; Stosiek et al., 2003). Neurons were further easily distinguished from astrocytes by the calcium dynamics (Gobel and Helmchen, 2007). Fluorescence was collected by detection modules with photomultiplier tubes (PMT) (H-9305, R-6357, Hamamatsu). Two detection units were used to detect both epifluorescence and transfluorescence (Koester et al., 1999).

3.2.2 Measuring signal propagation between populations

We used thalamocortical slices where borders of the L4 barrels could be visually delineated under low magnification through DIC microscopy (Fig. 3.1).

We used an additional marker of spatial location, a pipette whose tip was placed along the L4-L3 border of the column of interest as a reference for neuron somata location in terms of layer and column (L4 or L2/3). To evoke cortical suprathreshold activity a theta glass stimulation electrode was placed in the thalamocortical fibers (Fig. 3.1A). Brief electrical stimuli (3-7 at 40-100 Hz, 1 ms duration) were applied using stimulus isolators. Population responses in cortical columns were recorded first by imaging under low magnification (x10 objective) to coarsely locate the responding column after which population activity with cellular resolution was recorded higher higher magnification (x40 objective). Under higher magnification the imaging field of view was placed such that neurons in both layers could be simultaneously visualized and recorded from. Spike timings were extracted from fluorescence signals using a maximum-likelihood deconvolution algorithm. Laser excitation intensity was adjusted to optimize spike detection efficiency, which is bounded by photon shot noise on the lower end and photodamage on the higher (Ranganathan and Koester, 2010b). As shown previously, spike detection efficiency using these optical methods was high (>97% spike detection; 0.0023 spikes/s false positives, and average spike timing error of ~ 3 ms) (Ranganathan and Koester, 2010b).

Cortical activity evoked by thalamocortical inputs showed adaptation with repeated stimulation as shown previously (Middleton et al., 2010). Experimental conditions were chosen such that adapted cortical suprathreshold responses were largely restricted to a single column. Experiments where the amplitude of spiking activity in the adjacent columns was not significantly lower than the column under consideration were discarded. At the end of all experiments glutamate receptor antagonists (10 mM NQBX, 2 mM MK-801 and 50 mM AP-5)

were bath applied. Experiments with phasic activity in any neuron following electrical stimulation after blocking glutamatergic synaptic transmission (n = 3) were discarded as they suggested antidromic stimulation of cortical neurons. In 9 out of 25 experiments, the amplitude of spiking activity (spike count) in L2/3 was too low to measure correlations (< 0.05 spikes/neuron/trial). Furthermore, there was no neuron that had a significantly distinct spiking probability from any other neuron (Fisher's exact probability test, a = 0.05). These experiments were also excluded from analysis. Occasionally, we observed responses that manifested as unadapted, propagating waves of activity, which were not analyzed.

3.2.3 Measuring neural correlations

To measure correlations in activity spike timings were binned into spike trains *s(t)*. As the timescales on which correlations may be important are unknown, we used bin sizes in multiples of 1.536 ms (the temporal resolution of the fluorescence signals) up to a maximal bin size of 99.83 ms. From the binned discrete spike trains *s(t)* we calculated cross-covariance and complex coherence for pairs of neurons as described previously (Aertsen et al., 1989; Kimpo et al., 2003a; Tetzlaff et al., 2008; Vogel and Ronacher, 2007). Cross-covariance (cov(τ)) was calculated as:

$$cov_{ij}(\tau) = \left\langle \frac{1}{T} \sum_{t=1}^{T} \left(s_i(t) - \langle s_i(t) \rangle \right) \left(s_j(t+\tau) - \langle s_j(t+\tau) \rangle \right) \right\rangle \qquad \text{(Eq. 3.1)}$$

where $\langle\ \rangle$ denotes expected values (average over all trials), and *T* denotes the length of the spike trains (number of discrete time points). For each neuron pair *(i,j)* the cross-covariance function was calculated over a time period

restricted to 0.5 s before and after the stimulus. The cross-covariance function was normalized by auto-variance of neurons (at $\tau = 0$) to derive the cross-correlation coefficient r (at $\tau = 0$):

$$r_{ij} = \frac{cov_{ij}}{\sqrt{cov_{ii} \times cov_{jj}}} \qquad \text{(Eq. 3.2)}$$

Coherence was calculated by normalizing the Fourier transform of the cross-covariance function by the Fourier transforms of the auto-covariance functions to obtain complex coherence γ (at $\tau = 0$) (Kimpo et al., 2003a; Rosenberg et al., 1989; Tetzlaff et al., 2008; Vogel and Ronacher, 2007):

$$\gamma_{ij}(\omega) = \frac{cov_{ij}(\omega)}{\sqrt{cov_{ii}(\omega) \times cov_{jj}(\omega)}} \qquad \text{(Eq. 3.3)}$$

We obtained the complex coherence (γ (τ)) in the time domain by calculating the inverse Fourier Transform of $\gamma(\omega)$. We refer to the normalized γ at $\tau = 0$, as the complex coherence.

Data are expressed as Mean ± S.D. unless stated otherwise. For correlations measured in each experiment we tested if the average values measured were > 2 S.D calculated from jackknife resampling (Kimpo et al., 2003b**UNRESOLVED**). As calculating variance from resampling was computationally intensive we tested only for the selected bin sizes of 10, 25 and 50 ms. For average correlations measured across experiments and the decrease in correlations both within and across experiments we tested for significance using the Student's t-test with a significance level $\alpha = 0.05$.

3.3 Propagation of activity from L4 to L2/3

To measure the propagation of suprathreshold spiking activity between cortical networks we recorded activity from 20 neurons in L4 and 20 neurons in L2/3 simultaneously in acute slices of rodent barrel cortex. Activity was evoked by focal electrical stimulation using a stimulation electrode placed on the thalamocortical fibers in the striatum (Fig. 1).

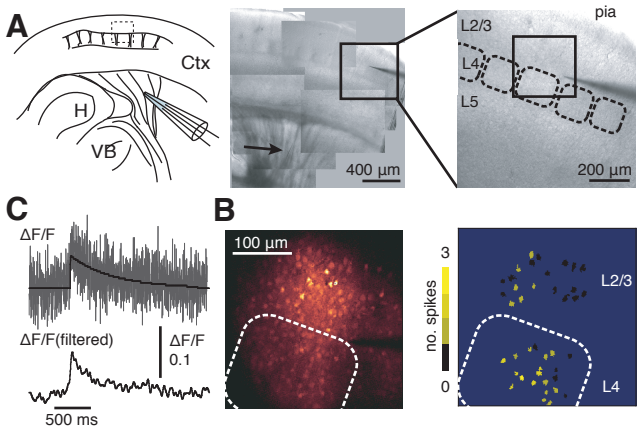

Figure 3.1**:** Recording activity propagation between cortical populations.

A: Left: Illustration of experimental design. H: Hippocampus, VB: ventrobasal nucleus of the Thalamus, Ctx: Cerebral cortex. Center image shows patchwork of photomicrographs showing striatum and barrel cortex in an acute thalamocortical slice. Arrow indicates position of stimulation pipette. Right image shows photomicrograph of the barrel cortex; dashed boxes illustrate L4 barrels. Image shows region indicated by box in center image. The dark shadow visible on the right is a pipette that was positioned at the border between L4 and L2/3 as a marker. B: Left image shows fluorescence image of the region indicated by box in right image in A. Rounded box illustrates barrel borders. Right image illustrates locations of recoded neurons, with their activity in one trial encoded in pseudocolors. C: Magnification of fluorescence trace of one neuron for illustration. Bottom trace shows fluorescence signal (above) filtered with a 30 ms Hamming filter.

Suprathreshold activity was recorded with single-cell, single-spike and high temporal resolution using dithered random-access functional calcium imaging (Grewe et al., 2010; Ranganathan and Koester, 2010b). The location of recorded neuron somata in terms of cortical layer and column was inferred from

the overlay of infrared DIC and fluorescence images (Fig. 3.1 A, B). In each trial of 2-3 seconds of fluorescence imaging, neuronal responses to one set of 3-7 electrical stimuli at 40-100 Hz were recorded (Fig. 3.1C,D). We refer to one set of electrical stimuli in one trial as an input stimulus.

3.3.1 Cortical activity evoked by naïve stimuli

Following an input stimulus, suprathreshold spiking activity was observed in L4 and L2/3 neurons. To calculate the amplitude of the suprathreshold spiking response for a population, we measured the average spikes per neuron per trial. In most trials the input stimulus elicited only one or a few spikes and response was restricted to < 200 ms following the input stimulus (Fig.3.1B,C and 3.2). The average response in L4 was 0.92 ± 0.45 spikes/cell/trial and the average response in L2/3 was 0.19 ± 0.09 spikes/cell/trial (n = 15 experiments, 1188 trials). The spiking response in L2/3 was significantly correlated with that in L4 (r = 0.67 ± 0.16, n = 15 experiments, $p = 8.6 \times 10^{-11}$) indicating dependence of L2/3 responses on activity in L4. We mapped the spiking activity in all three dimensions. The activity was largely restricted to the observed column. The average response in the adjacent columns was 0.039 ± 0.061 spikes/cell/trial compared to 1.02 ± 0.52 spikes/cell/trial for the observed column (n = 15 experiments). This indicated that we sampled from those neuronal populations that participated in propagating the evoked activity. Blocking glutamatergic synaptic transmission reduced responses to an average of 0.0098 ± 0.02 spikes/cell/trial (L4). This strong reduction indicated that evoked activity was not a result of antidromic stimulation of corticofugal axons.

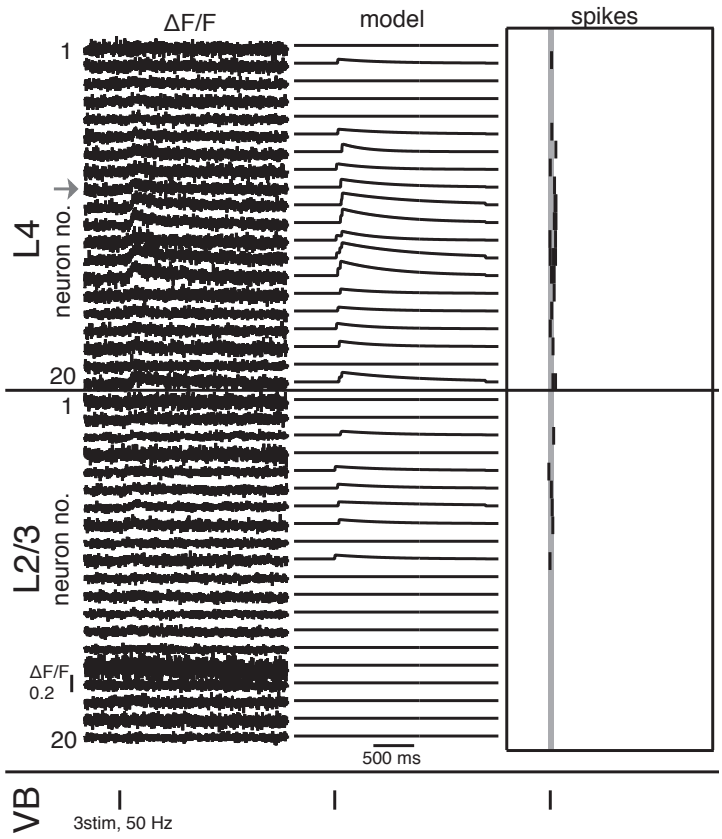

Figure 3.2**:** Propagation of spiking activity from L4 to L2/3.

Supra threshold activity recorded from 40 neurons using dithered random-access scanning, 20 neurons in L4 and 20 neurons in L2/3. Left traces show fluorescence signals (arrow marks the example neuron in C), center traces show model with maximum likelihood, right traces detected spike timings. Gray line indicates the time window of the fiber stimulus provided. Stimulus timings are also illustrated by vertical bars below each set of traces.

Suprathreshold responses were binned to measure neural correlations between pairs of neurons. As the timescales on which correlations are important are unknown we used different bin sizes at multiples of the temporal resolution of the fluorescence recordings, ranging from 1.536 to 99.83 ms. One example

experiment is shown in Fig. 3.3 with correlations calculated over a sample bin size of 6.14 ms for illustration. In each experiment, we calculated cross-correlation functions ($cc(\tau)$) from the binned responses in a pair-wise manner for each of the 190 pairs of L4 neurons and 190 pairs of L2/3 neurons recorded simultaneously. To account for expected correlations ($E[cc(\tau)]$) that result from co-varying firing rates of neurons we calculated cross-covariance ($cov(\tau)$).We also calculated the complex coherence ($coh(\tau)$) to account for any temporal structure of spiking activity within a neuron. Both the cross-covariance and coherence functions of each neuron pair were normalized by the auto-covariance. Normalization was required to compare correlations between neurons and to average over all pairs. We derived the average cross-correlation coefficient (r) and the complex coherence (γ) from the values of average $cov(\tau)$ and $coh(\tau)$ at $\tau = 0$, across all neuron pairs.

Even after correcting for expected correlations we found significant temporal interactions between neurons. Fig. 3.3A shows the cross-correlation, expected cross-correlation, cross-covariance and complex coherence functions for an example pair of neurons. Fig. 3.3C and D show the cross-correlation coefficients (r), $cov(\tau)$ and $coh(\tau)$ functions for an example experiment. The average covariance across all experiments was 0.092 ± 0.033 for L4 and 0.037 ± 0.019 for L2/3 (bin size of 10.75 ms, n = 2850 pairs). The average coherence was 0.103 ± 0.038 for L4 and 0.036 ± 0.019 for L2/3 (bin size of 10.75 ms, n = 2850 pairs, n = 15 experiments). In all experiments r and γ were statistically significant (> 2 S.D. jackknife estimate, 15 experiments, bin sizes 10, 25 and 50).

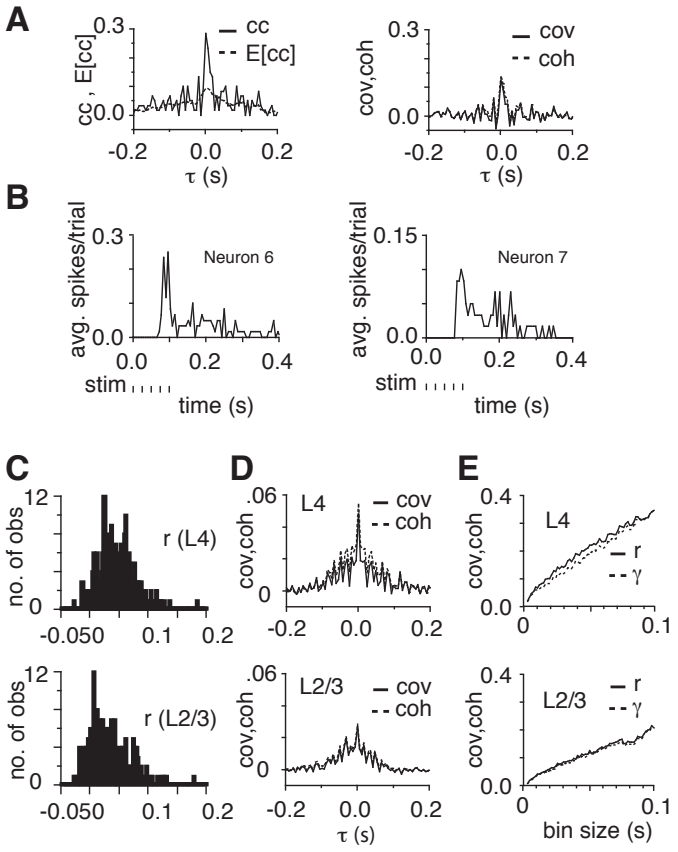

Figure 3.3**:** Signal propagation and change in correlations with propagation from L4 to L2/3.

A: Graphs show the cross-correlation, (cc(τ)) and expected cross-correlation, (E[cc(τ)]) functions (left) and the covariance, (cov(τ)) and coherence, (coh(τ)) functions (right) for an example pair of neurons. (cov(τ) and coh(τ) denote normalized cross-covariance and complex coherence, respectively). In the illustrated example responses were binned with a bin size of 6.14 ms. B: Peristimulus time histograms of the two neurons. C: Histogram of cross-correlation coefficient (r) for all 190 neuron pairs in L4 (top) and all 190 pairs in L2/3 (bottom). D: Average covariance and coherence for all pairs of neurons in L4 (top graph) and all pairs in L2/3 (bottom graph, bin size = 6.14 ms). E: Cross-correlation coefficient (r) and complex coherence (γ) of L4 (top) and L2/3 (bottom) neurons for bin sizes from 1.536 to 99.83 ms in steps of 1.536 ms.

Recent studies have reported a dependence of correlations on the rate of neuronal spiking activity (de la Rocha et al., 2007). Although the covariance and response amplitudes in each population, both L4 and L2/3, were weakly

correlated (r = 0.367 for L4 and r = 0.084 for L2/3) the correlation was not statistically significant in both cases (p = 0.089 for L4 and p = 0.38 for L2/3, n = 15 experiments). In summary, these results indicate the presence of neural correlations within the L4 and L2/3.

3.3.1.2 Correlations decrease with propagation from L4 to L2/3

To measure how correlations change as activity propagated from L4 to L2/3 we compared the cross-correlation coefficient (r) and the complex coherence (γ) in L2/3 to that in L4. The average correlations measured in L23 were significantly smaller than that measured in L4 both within experiments (10, 25 and 50 ms bin sizes tested using jackknife estimates) as well as across all experiments (for all bin sizes, $p < 0.05$, Student's t-test, Fig. 3.4A,B). For example, the average difference in covariance (r(L2/3) – r (L4)) was -0.055 ± 0.032 (bin size of 10.75 ms, $p = 4.9 \times 10^{-6}$, Student's t-test) and average difference in coherence (γ (L2/3) – γ (L4)) was -0.067 ± 0.034 (bin size of 10.75 ms, $p = 1.5 \times 10^{-6}$, Student's t-test).

As suprathreshold spiking activity propagated from L4 to L2/3, the change in correlations can also be viewed as a conversion of the correlations in L4 to the correlations in L2/3. We therefore also calculated the ratio of the average correlations in L2/3 and L4. As shown in Fig. 3.4C, the average ratio of the two correlations was significantly below 1, indicating that L2/3 correlations were bounded by the correlations in L4 (for all bin sizes, $p < 0.05$, Student's t-test). On average the ratio for cross-correlation coefficient was 0.42 ± 0.19 and the ratio for

complex coherence was 0.38 ± 0.16 (bin size of 10.75 ms, n = 15 experiments). To illustrate the relationship between correlations measured in L2/3 and L4 neurons across all experiments we chose two representative bin sizes, 10.75 ms (Fig. 3.4D, left column) and 24.58 ms (Fig. 3.4D, right column).

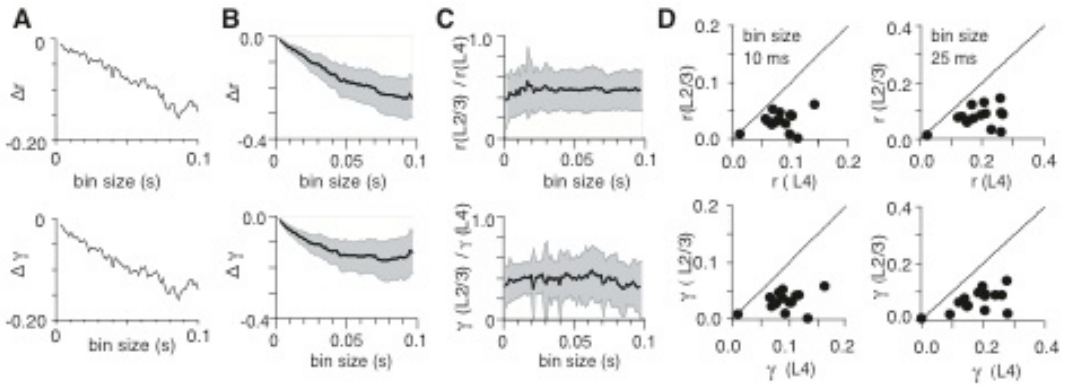

Figure 3.4: Correlations decrease as spiking activity propagates from L4 to L2/3.
A: Graphs show difference in cross-correlation coefficient (Δr, top) and complex coherence (Δγ, bottom) of L2/3 and L4, as a function of time bin size, in an example experiment. B: The average difference in (r) and (γ) across all experiments. Shaded area denotes 95% confidence intervals. C: Graphs shows average ratio of (r) and (γ) measured in L2/3 to that measured in L4 neurons, as a function of time bin size. Shaded area denotes S.D. D: Plot of the cross-correlation coefficient (r, top graph) and complex coherence (γ, bottom graph) measured in L2/3 as a function of (r) and (γ) in L4, at bin sizes of 10 ms (left) and 25 ms (right). Data points represent experiments.

In two experiments we determined the impact of the $GABA_A$ receptor antagonist Bicuculline methiodide (5 μM) on the change in correlations with propagation. In these experiments, correlations decreased in control conditions but increased in the presence of Bicuculline as activity propagated from L4 to L2/3. On average, the difference in covariance (r (L2/3) – r (L4)) was -0.024 ± 0.018 under control conditions and 0.036 ± 0.009 in the presence of Bicuculline (bin size of 10.75 ms, n = 2 experiments). These results indicate that under our

experimental conditions spike correlations decrease with propagation of activity from L4 to L2/3.

3.4 Discussion

In this study we measured the changes in neuronal spike correlations as suprathreshold activity propagated between recurrent networks in the mammalian cerebral cortex. Using functional calcium imaging in acute slices of rodent barrel cortex, we recorded suprathreshold spiking activity from a large sample of neurons in L4 and L2/3 simultaneously. Our results indicate a significant decrease in correlations, measured as covariance and complex coherence, over timescales ranging from 1.5 to 100 ms as activity propagated from L4 to L2/3.

We examined the propagation of evoked spiking activity from L4 to L2/3 because this vertical propagation of activity is an important step in the cortical processing of sensory inputs. In the rodent whisker system, thalamocortical afferents largely terminate in L4 (Koralek et al., 1988; Lu and Lin, 1993) and rarely innervate neurons in L2/3 directly (Bureau et al., 2006). L4 neurons in turn predominantly project to L2/3 neurons of the same cortical column (Bureau et al., 2006; Feldmeyer et al., 2002). The flow of excitation in this system thus follows the cortical architecture (Lübke and Feldmeyer, 2007). In agreement with the propagation of activity from L4 to L2/3 we found that suprathreshold activity in L2/3 was dependent on activity in L4.

Directly measuring the change in correlations with propagation requires simultaneous recordings of activity of multiple neurons from multiple neuronal populations. Until recently (Kimpo et al., 2003b) such measurements were technically impracticable. Here we utilized a novel optical approach to detect spikes from many neurons. Dithered random-access functional calcium imaging records suprathreshold spiking activity with single-cell, single-spike and millisecond temporal resolution (Grewe et al., 2010; Ranganathan and Koester, 2010a). In conjunction with maximum-likelihood deconvolution this method has a high spike detection efficiency (>97% of spikes detected with low false positives 0.0023 spikes/s) and temporal precision (Ranganathan and Koester, 2010a). The error in spike timing detection may have resulted in an underestimation of correlations measured for small time bins, but presumably did not affect results for time bins >> 3 ms. The focal extracellular electrical stimulation used here represents a highly coherent input to L4. In this regard it is noteworthy that the high correlations in thalamic neurons resulting from focal extracellular stimulation are not detrimental to testing change in correlations with propagation of activity from L4 to L2/3.

Under our experimental conditions spiking activity did not propagate beyond L2/3 of the responding column. Activity presumably failed to propagate beyond L2/3 of the observed column due to the absence of long-distance target neurons in the slice. We sampled neurons far away from the slice surface to avoid recording from neurons that were severely affected by the slicing procedure. Indeed, when blocking $GABA_A$ receptors we found that the evoked activity propagated from L4 to L2/3 and laterally. The effect of the $GABA_A$

receptor antagonist indicated that our observations were not a result of a lack of synaptic connections from L4 to L2/3 in the acute slice.

3.4.1 Change in correlations with propagation in comparison to other studies

The decrease in correlations with propagation of activity that we observed here is different from the results of previous empirical studies (Vogel and Ronacher, 2007) and many studies using simulations (Diesmann et al., 1999; Kumar et al., 2010; Mehring et al., 2003; Reyes, 2003a; van Rossum et al., 2002; Vogels and Abbott, 2005). The increase in correlations (synchronization of activity) observed in simulations is expected for feed-forward convergent network architectures as these simply pool inputs (Rosenbaum et al., 2010). Some simulation studies have reported stable propagation of uncorrelated (asynchronous) activity through layers of neurons. However, the mechanisms implemented on those simulations to prevent synchronization of activity, for example uncorrelated background activity, sparse convergence or divergence of connections or selectively strengthened feedforward connections (van Rossum et al., 2002; Vogels and Abbott, 2005), do not apply to the network architecture (Feldmeyer et al., 2002) and recording conditions (low background activity) of this study. The experimental studies conducted in the locust auditory system did not observe a decrease in with propagation of activity through neuronal populations. One reason for the difference to this study may be the different functional architecture compared to the cortical networks studied here. Indeed, recent studies have reported mechanisms that contribute to decorrelation of spiking activity. These include inputs from recurrently connected excitatory and inhibitory

neurons (Renart et al., 2010) the non-linearity of spike generation (de la Rocha et al., 2007), the heterogeneity of intrinsic biophysical properties of neurons (Padmanabhan and Urban, 2010) and synaptic unreliability (Rosenbaum and Josić, 2011). A combination of these mechanisms may have contributed to the decrease in correlations observed here. One can also speculate that the stimuli presented here to the L4 neurons were naïve, limiting propagation and in turn also affecting how correlations propagate. Our results show that under our experimental conditions correlations in neuronal spiking activity significantly decreased as population activity evoked by naïve inputs propagated between the recurrent cortical networks. This indicates that correlations do not necessarily increase with propagation between recurrent networks of mammalian cerebral cortex as suggested for networks with feed-forward topology. Our recording conditions were limited to those found in acute slices. These conditions include absence of spontaneous background activity, absence of top-down inputs, and absence of neuromodulation. The unexpected finding that contrary to simulations and previous empirical studies correlations decrease thus indicate that increase in correlations with propagation is not universal and may depend on the conditions and the systems studied. Thus further studies are required to dissect the impact of synaptic architecture and other factors on signal propagation and correlations in the cerebral cortex.

3.5 SUMMARY

Neural correlations in spiking activity impact information signaling. Correlations in population activity change with the propagation of activity from

one neuronal population to the next. Previous theoretical studies have predicted increase in correlations with propagation of activity between networks with feed-forward architecture. Empirical study in the locust peripheral nervous system with feed-forward architecture also showed increase in correlations with propagation. However, networks in the cerebral cortex are extensively recurrent in their connectivity. In this study we examined the propagation of population activity and the change in neural correlations with propagation between the recurrent networks in the mammalian cerebral cortex. We found that under our experimental conditions neural correlations decreased with the propagation of evoked population activity between the L4 and L2/3 networks of the mouse barrel cortex.

Our results show that the change in correlations with propagation of activity is different in recurrent networks compared that expected in networks with feed-forward topology. They also indicate that the change in correlations with propagation was dependent on the state of inhibition. These results were obtained under controlled conditions devoid of parameters like top-down regulation and spontaneous activity and for activity evoked by novel afferent inputs. Measuring signal propagation and correlations under controlled conditions in a biological system is an important step in testing predictions from theoretical studies.

This study interfaces between theoretical, experimental studies in non-mammalian systems, and *in vivo* conditions. It thus extends the results from simulations and studies of the locust auditory system to mammalian recurrent cortical networks. In contrast to *in vivo* conditions we were able to locate and record from those neurons that are part of the signal propagation chain. In

contrast to simulations, including those that experimentally determined the input/output functions of neurons (de la Rocha et al., 2007; Reyes, 2003a; Shea-Brown et al., 2008); we measured propagation in a biological system and in a cortical network.

Our finding here, that correlations do not increase with propagation, is consistent with a high fidelity of a rate code for propagation of activity through networks of the cerebral cortex. The prediction of a high performance of a rate code in the rodent somatosensory cortex is in agreement with a low contribution of correlations to encoding of stimulus location (Panzeri et al., 2001) as well as a disturbance analysis that also predicted a rate code (London et al., 2010).

Chapter 4: Plasticity induced changes in propagation of neural correlations

Experience dependent plasticity of responses is a fundamental neural mechanism that sustains behavioral adaptability (learning) to a changing environment. While experience dependent plasticity is most pronounced during early stages of development of an organism, studies have showed that even the developed adult brain constantly undergoes plastic changes in its response properties. Plasticity may occur through multiple functional mechanisms and at a variety of locations in a neural system. One of the main forms of plasticity is through activity dependent changes in the structural and functional synaptic architecture of brain areas, also known as synaptic plasticity (Abbott and Nelson, 2000). The induction of synaptic plasticity may impact both the local representation as well as the propagation of neural signals. While the effects of synaptic plasticity have been extensively studied in the single-neuron level and at the system level (map plasticity), the occurrence of structural and functional plasticity in neuronal circuits and the impact of plasticity on properties of signal propagation in the microcircuit level are largely unexamined due to challenges in recording precise spiking activity from large, local neuronal populations.

Here we utilized the dithered random-access functional calcium imaging technique to record from sufficiently large neuronal population(s) to address the impact of plasticity on the properties of evoked population activity and its propagation between recurrent neuronal networks in the mammalian primary sensory cortex, using the mouse barrel cortex as a model system. Specifically, we induced associative cortical plasticity by pairing afferent thalamocortical inputs with lateral intracortical inputs and we investigated the impact of plasticity

on the vertical propagation of activity and neural correlations from L4 to L2/3, evoked by afferent thalamocortical inputs. We found that induction of cortical network plasticity resulted in increased propagation of activity and increased propagation of neural correlations over a large range of timescales, from L4 to L2/3 in the barrel cortex.

4.1 PLASTICITY IN NEURAL POPULATION ACTIVITY

Learning is defined as the experience-dependent, conditioned change in behavioral performance (sensory perception or cognitive/motor action) in response to repeated presentation of the same input. The neural correlate of learning is believed to be the input-specific, induction of activity-dependent change (increase or decrease) in response properties of one or many neural systems that contribute to processing of the learned inputs and the resulting behavior.

4.1.1 Forms of neural plasticity

The goal of all forms of plasticity is to alter the input – output transformation of neurons, i.e alter the amount of activity evoked in a neuron for a given synaptic input. Various forms of plasticity have been proposed to account for the change in cortical neuronal responses. Synaptic plasticity is one of the main mechanisms in which rapid changes in neuronal responses are achieved through long-lasting increase or decrease in synaptic strength between specific neurons following Hebbian learning rules. Input-specific, long-term potentiation and depression involving glutamatergic and GABAergic synapses between

neurons in various cortical and sub-cortical areas of the mammalian central nervous system have been shown to be responsible for plasticity at the cellular level (Kirkwood and Bear, 1994; Kirkwood and Bear, 1995; Aroniadou-Anderjaska and Keller, 1995; Zilberter et al., 2009; Sale et al., 2011). In the larger scale, synaptic plasticity is also believed to contribute to extensive changes in the macroscopic distribution (mapping) of responsive elements in the cortex, also known as “map plasticity” (Buonomano and Merzenich, 1998; Karl et al., 2001; Feldman and Brecht, 2005; Pienkowski and Eggermont, 2011). Other forms of plasticity include changes in the excitability of a neuron from altering its biophysical properties (intrinsic plasticity), and global compensatory changes in intrinsic or synaptic mechanisms to regulate neuronal excitability in the event of input-specific plasticity thus maintaining stability (homeostatic plasticity) (Turrigiano and Nelson, 2000; Kim and Linden, 2007).

4.1.2 Cortical network plasticity

Many studies have examined changes in cortical responses as a result of experience(Hubel and Wiesel, 1963), at the cellular level and at the level of representational maps. For example, studies have characterized the changes in the response properties of individual neurons (Cruikshank and Weinberger, 1996; Eyding et al., 2002; Eysel et al., 1998; Frégnac et al., 1988; Jacob et al., 2007; Meliza and Dan, 2006; Weinberger et al., 1984), and changes in spatial cortical representations (Feldman and Brecht, 2005; Fox, 2002; Merzenich et al., 1983; Recanzone et al., 1992; Simons and Land, 1987) with plasticity. [or by utilizing techniques that record population-averaged activity (Schuett et al., 2001).]

However, a significant component of neural computation, including signal representation, transformation, and propagation, occurs at the microcircuit level of networks of neurons. For example, the precise patterns of activity in a network of neurons encode information about sensory attributes (Pillow et al., 2008b) or motor output (Georgopoulos et al., 1986). How plasticity changes local, suprathreshold, population activity dynamics and modifies the propagation of population activity is not readily inferred from synaptic or cellular learning rules, as – particularly in recurrent networks – network dynamics can be complex and highly non-linear. Additionally, as mentioned above, while individual neurons show slight changes in response properties with learning the changes may be more apparent at the microcircuit level. Thus here we induced cortical plasticity by pairing two inputs, afferent and lateral, provided to a cortical neural network under controlled conditions and examined the changes in the properties of activity evoked by afferent input and its propagation between recurrent cortical networks.

4.2 Experimental and analytical methods

Similar to experiments examining signal propagation (Chapter 3), here we used dithered random-access functional calcium imaging in conjunction with maximum-likelihood spike detection to record spiking activity from up to 40 neurons as activity propagated from L4 to L2/3 in acute slices of the mouse barrel cortex. We induced cortical network plasticity by pairing afferent thalamocortical inputs with nearly coincident, local, lateral cortical inputs from L2/3 of the neighboring column (with relative temporal delay in onset of 65 -100

ms) and examined changes in evoked activity and its propagation upon induction of plasticity.

4.2.1 Slice preparation and Imaging

We followed procedures as outlined previously (Ranganathan and Koester, 2011). Briefly, C57Bl6 mice (P14 – P20) were anesthetized by intraperitoneal injection of ketamine/xylazine (80 and 20 mg/ml). The brain was removed and acute thalamocortical brain slices (350 μm thick) were prepared in cold slicing solution (containing in mM: 2.5 KCl, 1.25 NaH_2PO_4, 25 $NaHCO_3$, 1 $CaCl_2$, 7 $MgCl_2$, 7 dextrose, 240 sucrose, 1 ascorbic acid and 3 sodium pyruvate) following methods described previously (Agmon and Connors, 1991). All experimental procedures were approved by The Institutional Animal Care and Use Committee of The University of Texas at Austin. Slices were stored in ACSF solution (containing in mM: 125 NaCl, 2.5 KCl, 1.25 NaH_2PO_4, 25 $NaHCO_3$, 1.7 $CaCl_2$, 1 $MgCl_2$, 10 dextrose, 1 ascorbic acid and 3 sodium pyruvate). Slicing and ACSF solutions were bubbled with 95% O_2 and 5% CO_2. Slices were incubated at 35°C for 30 mins, and stored at room temperature prior to experiments. Slices containing a planar projection of thalamocortical fibers were selected and the neurons within 1-2 mm^2 of cortex were stained by multiple bolus injections of the cell permeant ester form of a Ca^{2+} indicator (Oregon Green 488 Bapta-1 (OGB-1) AM, 1mM concentration). Neurons were visualized by differential interference contrast microscopy (DIC). Neurons were allowed to take up the indicator for at least 1 hr. All experiments were carried out at ~35°C bath temperature

Neuronal suprathreshold activity was recorded using dithered random-access scanning (except Fig. 4.1A which used a two-photon, resonant galvanometric scanner). Experimental conditions were set to thalamocortically evoke adapted, cortical responses that were largely restricted to a single cortical column. Evoked activity was recorded first at low magnification using a x10 water immersion objective (UMPlanFl, NA 0.3, Olympus) to initially locate the responding column and then under higher magnification with a x40 water immersion objective (UMPlanFl, NA 0.8, Olympus) to record activity with cellular resolution and high temporal precision. Using dithered random-access functional calcium imaging, somatic calcium fluorescence signals were recorded at 651 Hz. In each cycle, fluorescence signals were recorded for 25.6 μs from 3 locations in the somata of each neuron. Data collected during switching between neuron somata was discarded (access time, 12.8 μs). We recorded exclusively from neuronal somata and avoided astrocytes as distinguished by their distinct morphology and higher resting fluorescence (Hirase et al., 2004; Stosiek et al., 2003). Neurons were further easily distinguished from astrocytes by the calcium dynamics (Gobel and Helmchen, 2007). Fluorescence was collected by detection modules with photomultiplier tubes (PMT) (H-9305, R-6357, Hamamatsu). Two detection units were used to detect both epifluorescence and transfluorescence (Koester et al., 1999).

4.2.2 Recording signal propagation and induction of plasticity

Borders of individual cortical columns and layers 4 and 2/3 were localized using visual markers as described before (Chapter 3). To induce long-lasting

changes in evoked suprathreshold cortical activity we paired cortical activity evoked by two different input signals (Fig. 4.1). Spiking activity from afferent inputs (the first input) was evoked with focal electrical stimulation of afferent thalamocortical fibers. Brief electrical stimuli with 3-7 pulses at 40-100 Hz and duration 1 ms were applied using stimulus isolators. We refer to this input as the afferent thalamic input (s_A), the response evoked as the afferent response (r_A) and the column that response is evoked in as column C0. Lateral cortical input (the second input) was provided by focal stimulation of the cortical L2/3 neurons of the immediately adjacent column (Fig. 4.1) with 3 pulses at 40 Hz and 1 ms duration. We refer to this input as the lateral cortical input (s_L), the response evoked as the lateral response (r_L) and the column that response is evoked in as column C1. Stimulus intensities were adjusted such that r_L was mostly restricted to the adjacent column (C1). The plasticity induction protocol consisted of presenting the afferent input followed by the lateral input with a temporal delay in onset of 65-100 ms. 100 - 200 pairings were presented at 0.1Hz frequency (Fig. 4.1). Activity from population average (Fig. 4.1) was recorded as wide-field fluorescence changes using a two-photon, resonant, galvanometric scanner (Leica). Regions of interest (ROIs) corresponding to cortical layers and columns were identified using perimeters obtained from DIC images of the same cortical area. Each ROI spanned one layer in one column. For each ROI the fluorescence signal was averaged over a 2 s time window following a stimulus and all pixels:

$$\int \Delta F = \int^{pixels} \int_{0}^{2s} \frac{\Delta F}{F}(t) dt dx dy \Big/ \int^{pixels} dx dy \qquad \text{(Eq. 4.1)}$$

Activity with single cell, single spike resolution was recorded using the dithered random-access scanner. Spike timings were extracted from fluorescence signals using a maximum-likelihood deconvolution algorithm with high spike detection efficiency (>97% spike detection; 0.0023 spikes/s false positives, and average spike timing error of ~ 3 ms). As before, laser excitation intensity was adjusted to optimize spike detection efficiency, which is bounded by photon shot noise on the lower end and photodamage on the higher (Ranganathan and Koester, 2010b).

At the end of all experiments glutamate receptor antagonists (10 mM NQBX, 2 mM MK-801 and 50 mM AP-5) were bath applied to ensure that the responses were a result of orthodromic stimulation of thalamocortical fibers. Responses that manifested as unadapted, propagating waves of activity were isolated from analysis, as followed for the study of signal propagation for naïve inputs (Chapter 3).

4.2.3 Measuring neural correlations and change in correlations with propagation

Neural correlations in activity were measured from binning spiking activity of neurons into spike trains *s(t)*. As outlined in Chapter 3 a range of bin sizes from 1.536 to 99.83 ms were used in multiples of 1.536 ms (the temporal resolution of the fluorescence signals). From the binned discrete spike trains *s(t)* we calculated cross-covariance for pairs of neurons as described previously (Aertsen et al., 1989; Kimpo et al., 2003a; Tetzlaff et al., 2008; Vogel and

Ronacher, 2007). Cross-covariance (cov (τ=0)) was calculated as:

$$cov_{ij} = \sum_{trials}\left[\sum_{t=1}^{N}\left(s_i(t) - \langle s_i(t)\rangle\right)\left(s_j(t) - \langle s_j(t)\rangle\right)\right] \qquad \text{(Eq. 4.2)}$$

where $\langle\ \rangle$ denotes expected values (average over all trials), and *T* denotes the length of the spike trains (number of discrete time points). For each neuron pair *(i,j)* the cross-covariance (at τ=0) was calculated over a time period restricted to 0.5 s before and after the stimulus. The cross-covariance was normalized by auto-covariance of neurons (i=j; also at τ = 0) to derive the cross-correlation coefficient r (at τ = 0):

$$r_{ij} = \frac{cov_{ij}}{\sqrt{cov_{ii} \times cov_{jj}}} \qquad \text{(Eq. 4.3)}$$

Neural correlations in a given neuronal population were measured as the mean correlation coefficient across all neuronal pairs recorded from that population. Correlations measured within each population of an experiment we deemed significant if the average values measured were > 2 S.D calculated from jackknife resampling (Kimpo et al., 2003b**UNRESOLVED**). As calculating variance from resampling was computationally intensive we tested only for the selected bin sizes of 10, 25 and 50 ms.

Vertical propagation of neural correlations in cortical columns was measured as the difference between the mean correlation coefficient calculated from L2/3 neuron pairs and that calculated from L4 pairs, of the same column. Impact of plasticity on the change in correlations with propagation of activity was computed by comparing the difference values from data collected before and/or

after induction of plasticity. Data are expressed as Mean ± S.D. unless stated otherwise. The statistical significance of (i) average correlations measured across experiments, (ii) the change in correlations with propagation of activity both within and across experiments, and (iii) change in correlations with propagation before and after plasticity, was tested using the Student's t-test with a significance level $\alpha = 0.05$.

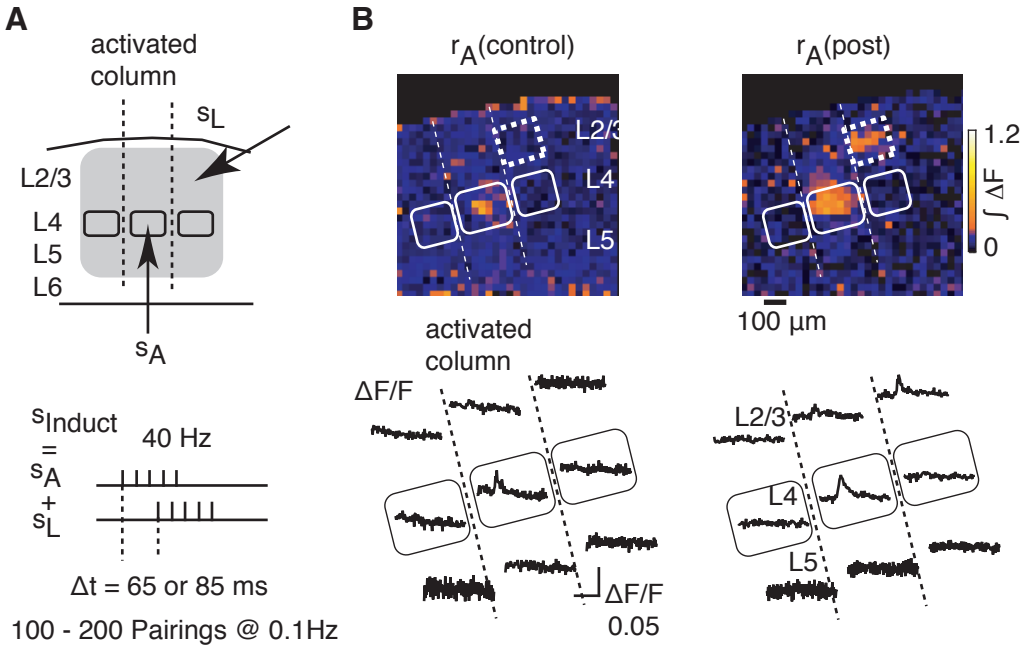

Figure 4.1: Induction of plasticity in evoked, suprathreshold network activity.

A: Schematic illustrating the experimental design for induction of local cortical network plasticity (above) and pictogram of the pairing protocol used (below). sA and sL denote the afferent and lateral stimuli used. rA and rL represent the responses evoked by each of these inputs, respectively. Afferent stimulus was provided by focal electrical stimulation of afferent thalamocortical fibers. Note that plasticity was also observed when this was replaced with local cortical stimulation of L4 neurons. Shaded region denotes the field of view imaged for activity evoked by the afferent stimulus before and after induction of plasticity using wide-field, two-photon galvanometric fluorescence microscopy, the results of which are shown in B. B: The images show the integral of the fluorescence responses over a 2 s duration after stimulus for each pixel, encoded in pseudocolor. The traces below show fluorescence responses ΔF/F (t) to the afferent input averaged over all pixels within each ROI defined by layer and column boundaries.

4.3 PLASTICITY INDUCED CHANGES IN SIGNALING

In order to measure the impact of cortical plasticity on evoked population activity we recorded neuronal population responses evoked by afferent inputs before and after the induction of plasticity, with coarse and fine scales resolution. Under both conditions, plasticity was induced by pairing afferent, thalamocortical inputs (sA) and lateral, intracortical inputs (sL) with a temporal delay, as illustrated in Fig 4.1A. Paired inputs were presented over 100 - 200 repetitions at 0.1Hz. The example experiment in Fig. 4.1B shows evoked cortical responses recorded as population averages under low magnification. Overlaying white lines demarcate the borders of the regions (layers and columns) of interest, obtained from superimposed DIC images. The recordings under low magnification showed localized changes in cortical activity with the induction of plasticity. These changes were observed from significant increase in intensity of evoked fluorescence signals over the cortical regions (layers/columns) of interest (Fig. 4.1B represented with pseudocolor scaling). Plasticity induced changes included significant increase in evoked activity within the primary cortical column (C0) as well as increase in the propagation of evoked activity to the adjacent (paired) column (C1). The traces in Fig. 4.1B show cortical activity within each layer/column obtained from pooling responses in all pixels within the outlined borders of each layer/column. Notably, this form of cortical plasticity was also induced if the afferent inputs were provided from sparse, local stimulation of L4 neurons of the responding column instead of the thalamocortical fibers. This indicated that plasticity was primarily mediated by mechanisms occurring within the intracortical networks.

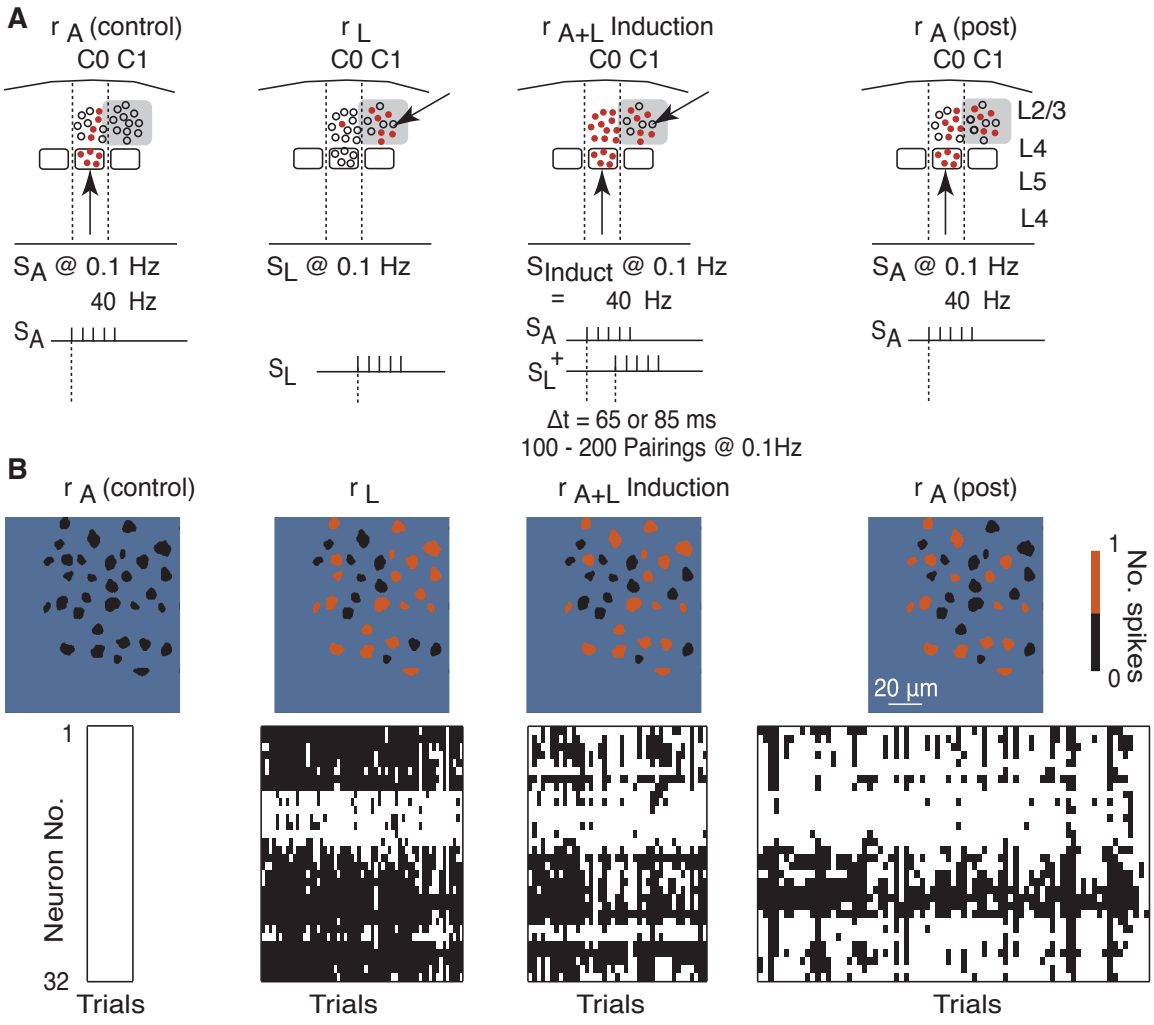

Figure 4.2**:** Plasticity resulted in increased propagation of evoked activity to C1.

A: Shows a cartoon representation of each of the four stimulus conditions presented and the responses evoked within cortical populations. Circles represent neurons and colored circles indicate evoked suprathreshold neuronal response. Below each schematic is a pictogram of the stimulus condition. B: Top row shows raster images of L2/3 neurons in C1 with their responses in a single trial indicated by the pseudocolor scale. The bottom row shows responses of the 32 neurons (shown in the raster images above) in the form of vector matrices of spiking activity collected under each stimulus condition corresponding to schematic in A. Rows represent neurons and columns trials. Each black tick indicates that the neuron fired at least one action potential in that trial. Comparing responses for all four input conditions shows that plasticity increased activity evoked by afferent stimulus (r_A) from a null response to a distinct population response that had a high spatial overlap with responses evoked by the lateral stimulus (r_L) and the induction stimulus (r_{A+L}).

On average the population averaged cortical responses to the thalamic input increased by 141.4 ± 30.1 % (measured as integral ΔF/F, n = 19 experiments). In all experiments rA (post) extended into L2/3 of adjacent column C1, where the cortical electrode was placed, following the pairing protocol (average change in $\int \Delta F$ = 189.8 ± 27.9%, $p < 0.001$, n = 19).

4.3.1 Plasticity increased propagation of evoked population activity to C1

We also examined changes in cortical activity induced by plasticity under higher magnification, with single-cell, single-spike resolution. These results showed that plasticity-induced increased spiking response and spiking probability in a distinct ensemble of neurons in the activated areas. Fine - scale changes in evoked cortical activity could also be induced with afferent input (s_A) from local L4 stimulation instead of thalamocortical stimulation, like the changes observed for population-averaged signals. Fig. 4.2 shows an example experiment in which afferent input (s_A) was provided with L4 stimulation (in C0) and plasticity-induced changes in response properties were observed in L2/3 neurons in the neighboring column (C1, shaded gray area in the schematic). We recorded responses evoked in L2/3 (C1) by individual afferent and lateral inputs prior to induction of plasticity. This was followed by recording responses during plasticity induction with 100-200 presentations of the paired inputs ($s_{Induct} = s_A+s_L$). We then recorded the responses evoked in L2/3 C1 by the afferent input alone. The results showed that the naïve, afferent input (before plasticity) evoked almost no suprathreshold response in the L2/3 neurons of C1. However, following plasticity the same afferent input evoked suprathreshold activity in a distinct ensemble of

neurons in L2/3 of C1 (Fig. 4.2). Thus induction of plasticity significantly increased the response amplitude of a specific subgroup of L2/3 neurons of the paired column (C1). The average increase in afferent evoked activity was 0.026 ± 0.06 spikes/neuron before and 0.92 ± 0.84 spikes/neuron after the induction of plasticity (n=129 neurons, 5 experiments; $p < 10^{-50}$). Additionally, as shown in Fig. 4.2, neurons that showed a supralinear increase in spiking activity when both inputs were presented during induction, over their responses for the individual inputs, had higher probability of being recruited into the post response to afferent input. In all the observed experiments, the increased responses in L2/3 neurons in C1 were long-lasting (> 1-2 hrs). As shown in a previous study (Pita-Almenar et al., 2011), this form of plasticity was observed to be input specific. That is, plasticity induced increase in responses of L2/3 neurons in C1 were observed only for the afferent input that was paired with lateral input during induction. Additionally, the increased activity from plasticity was blocked by the addition of blockers of glutamatergic synaptic transmission (10 mM NQBX, 2 mM MK-801 and 50 mM AP-5). This indicated that the increased activity was mediated through synaptic transmission and not direct stimulation of the responding neurons. We also found that the induction of this form of cortical plasticity was dependent on the relative timing of the thalamic and cortical inputs. Optimal inter-stimulus intervals ranged between 65-100 ms with the afferent input followed by the lateral input (J.D. Pita-Almenar, G.N. Ranganathan, and H.J.Koester, unpublished observations). Furthermore, induction of cortical plasticity was blocked by the application of the reversible NMDA receptor antagonist, AP-5 during the induction phase (pairing of afferent and lateral inputs) alone. This indicated that synaptic plasticity of intracortical connections was a mechanism

contributing to the plasticity-induced increase in propagation of activity (n=3, J.D. Pita-Almenar, G.N. Ranganathan, and H.J.Koester, unpublished observations). A similar form of associative synaptic plasticity, that altered responses of neuronal ensembles from activation of distinct inputs was observed in the hippocampal CA1 circuit in another independent study (Yuan et al., 2011).

4.3.2 Plasticity increased signal propagation from L4 to L2/3 of C0

The neurons in L2/3 of C1 showed significantly increased evoked activity following cortical plasticity. Under our experimental conditions, suprathreshold cortical activity evoked by naïve afferent inputs was restricted to a single cortical column. Additionally, recordings under low magnification suggested localized changes in cortical activity restricted to L4 and L2/3 populations of C0 and L2/3 population of C1 due to plasticity (see Fig. 4.1B). Furthermore, the increased activity of L2/3 neurons in C1 required glutamatergic synaptic transmission. These results implicated the increase in propagation of activity via the L4 to L2/3 pathway of the primary responding column (C0) leading to increased propagation between L2/3 neurons of C0 and C1. We therefore addressed how plasticity impacted signal propagation within the primary column (C0). For this we recorded activity evoked by afferent inputs in L4 and L2/3 neurons within C0, simultaneously, after the induction of cortical network plasticity. In some experiments (n=2), we monitored response properties and propagation before, during and after the induction of plasticity. Fig. 4.3 shows the impact of plasticity on the propagation of suprathreshold activity from L4 to L2/3 in one example experiment.

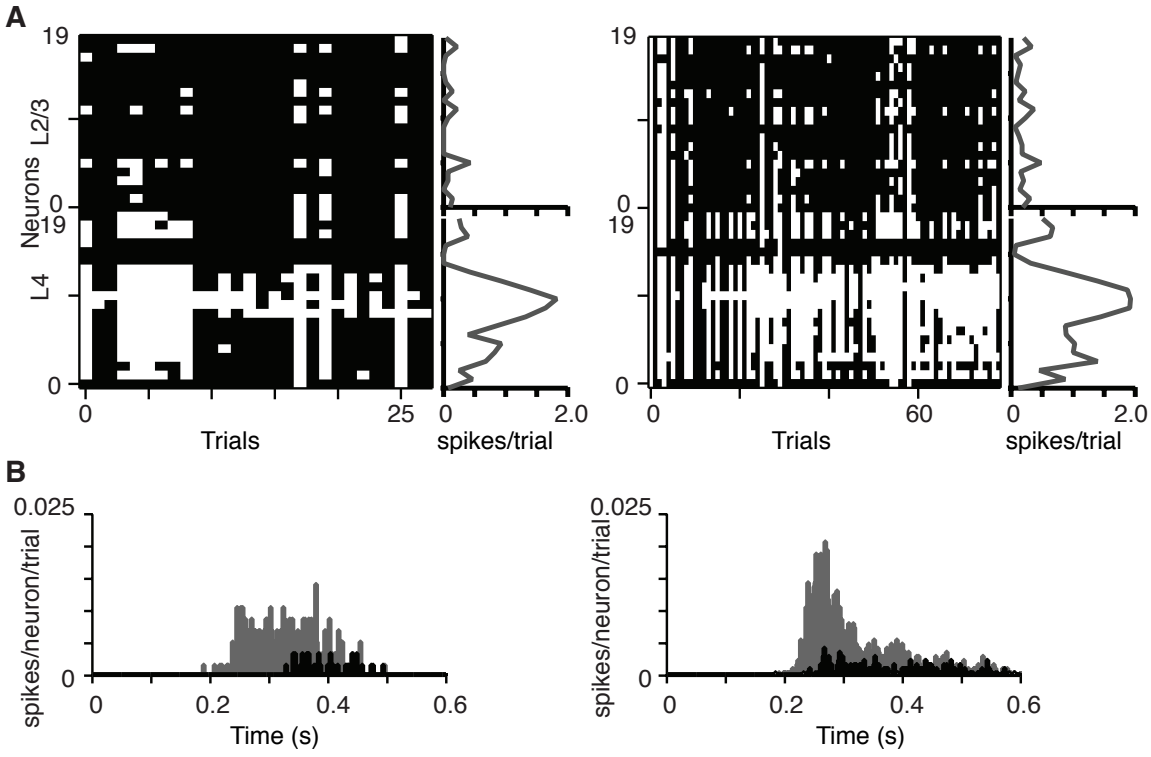

Figure 4.3**:** Plasticity increased propagation of evoked activity in C0.

A: Shows thalamcorotically evoked suprathreshold responses of L4 (n=20) and L2/3 (n=20) neurons in C0, before (left column) and after (right column) induction of cortical network plasticity. Spiking activity is represented in the form of vector matrices with rows as neurons and columns as trials where each black tick indicates that the neuron fired at least one spike in that corresponding trial. Graphs to the right of each response matrix show the average response of individual neurons (corresponding to the vector matrix) across all trials. B: Graphs show peristimulus histograms of thalamocortically-evoked activity in L4 (light gray) and L2/3 (black) neuronal populations before (left) and after (right) induction of plasticity. As indicated the responses evoked after plasticity occur earlier in time with respect to the stimulus. C: Graphs show the average cross-correlation coefficient measured across all neuronal pairs within L4 (light gray) and L2/3 (black) neuronal population, before (left) and after (right) network plasticity.

As shown, the induction of plasticity significantly increased the evoked response amplitude of neurons in L4 as well as L2/3 of column C0. The average afferent evoked response in this experiment was 0.648±0.553 spikes/neuron/trial in L4 and 0.079 ±0.109 spikes/neuron/trial in L2/3 before plasticity. Upon induction of plasticity the average evoked response increased to 0.914±0.592 spikes/neuron/trial in L4 and 0.195±0.107 spikes/neuron/trial in L2/3. This

increased was found to be significant ($p= 6x10^{-6}$ and $p= 8.3 \times 10^{-11}$ for L4 and L2/3 neurons, respectively; n = 20 neurons in each population).

Notably, while the change in activity was observed in average response amplitude, the increase in response was observed in a distinct ensemble of neurons. This was similar to the plasticity-induced changes observed in evoked suprathreshold activity in L2/3 neurons of C1. This spatially specific effect of cortical plasticity can be observed in the example experiment shown in Fig. 4.3 A. Plasticity induced a significant increase in response in a few cells while inducing a limited change in others (response remains nearly zero even after plasticity).

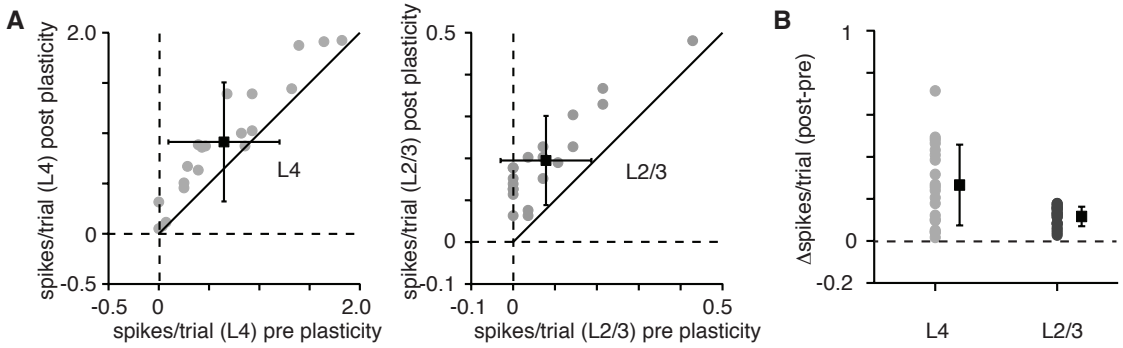

Figure 4.4**:** Plasticity increased propagation of evoked activity in specific neurons.

A: Graphs show the average evoked response of neurons in L4 (left) and L2/3 (right) before (x-axis) and after (y-axis) the induction of plasticity. The dotted lines mark the no response condition. The diagonal (slope =1) indicates the expected value for neurons that undergo no change in activity with plasticity. The markers indicate individual neurons recorded from L4 (n=20) and L2/3 (n=20) in C0, in the example experiment presented in Fig. 4.3. B: Graph shows the change in evoked activity in L4 and L2/3 neurons as the difference between average evoked response amplitude after and before the induction of plasticity.

The cell specific change in neuronal evoked activity can also be observed from the relationship between activity recorded from individual neurons before and after plasticity. This is shown in Fig.4.4. The graphs plotting average

neuronal responses after and before plasticity show that all points (representing individual neurons) on or above the diagonal indicating the condition of no change in activity with plasticity. However, the points with large positive deviations above the diagonal indicate neurons whose response significantly increased after plasticity. The points lying close to or on the diagonal represent neurons that had limited to no change in response due to plasticity. This is large range of effects on neuronal response due to plasticity is also shown by the difference in neuronal activity after and before plasticity for L4 and L2/3 neurons (Fig. 4.4B). We also found that induction of plasticity resulted in reduction of delay in onset of evoked activity in L4 as well as L2/3 neuronal populations. However, this did not result in significant change in delay between activity in L4 and the propagated activity in L2/3. This is shown by the average peristimulus time histograms plotted for activity evoked in L4 (gray) and in L2/3 (black) neurons before and after the induction of plasticity Fig. 4.3B. For activity evoked by naïve inputs, the average delay in response on L4 neurons was 0.101±0.03 s and the average delay in response evoked in L2/3 was 0.213±0.09 s. Upon induction of plasticity the delay in L4 response reduced to 0.910±0.06 s and the delay in L2/3 response was 0.265±0.12 s. The greater delay in L2/3 response was contributed by the activity of neurons whose response had been increased by plasticity. These results were reproduced across experiments. The average response amplitude of activity evoked by naïve inputs was 0.594 ±0.384 spikes/neuron/trial in L4 and 0.0971±0.112 spikes/neuron/trial in L2/3 (n=60 neurons; 3 experiments). Upon induction of plasticity the response amplitude was 0.908±0.517 spikes/neuron/trial in L4 and 0.367±0.229 spikes/neuron/trial in L2/3 (n= 80; 4 experiments). The pre-plasticity responses were comparable to the

values obtained for activity evoked by naïve afferent inputs; 0.92 ± 0.45 spikes/cell/trial in L4 and 0.19 ± 0.09 spikes/cell/trial in L2/3 (n=15 experiments) (Ranganathan and Koester, 2011).

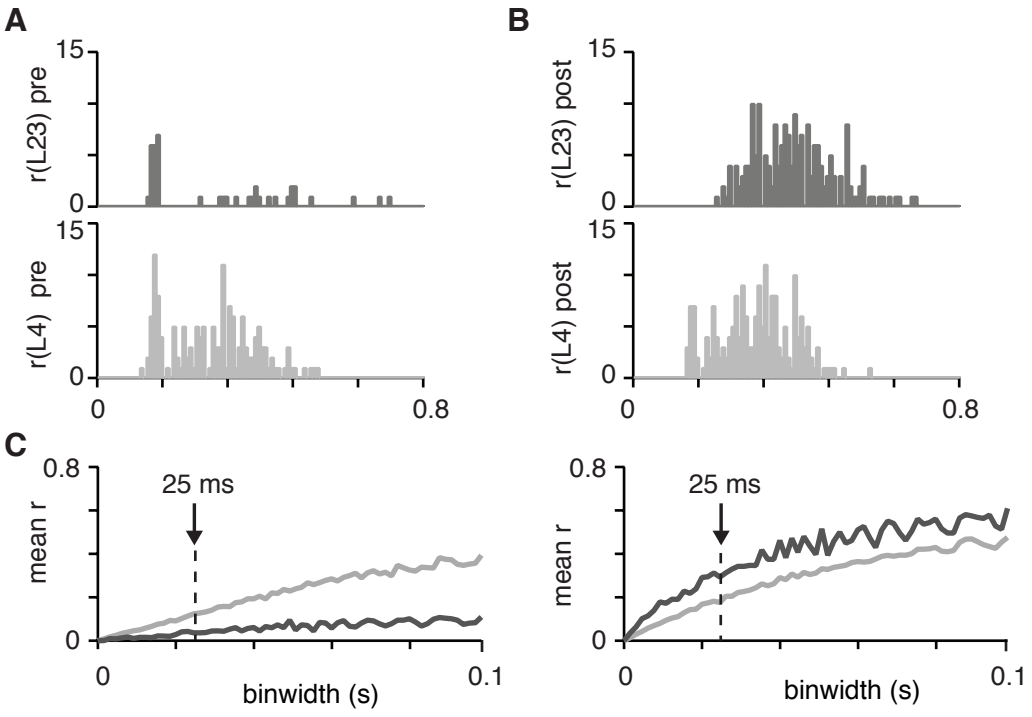

Figure 4.5**:** Plasticity induced changes in neural correlations in L4 and L2/3.

A: Graphs show histograms of the neural correlations (r) measured between neuronal pairs in L4 (below) and L2/3 (above), from activity evoked before plasticity. B: Graphs show histograms of correlations measured between the same L4 and L2/3 neuronal pairs as in A, after the induction of cortical plasticity. These correlations (A and B) were measured from activity binned at 25 ms. C: Graphs show the average neural correlations across all neuronal pairs measured over a large range of timescales. The average correlations are plotted as a function of the binwidth used to calculate the correlations. The histograms shown in A and B correspond to the average value at 25 ms indicated by the arrows.

Thus induction of plasticity increased evoked population activity and increased the vertical propagation of evoked activity in C0 by increasing response of a spatially specific subset of neurons. Furthermore, the evoked

activity was abolished upon application of blockers of glutamatergic synaptic transmission (10 mM NQBX, 2 mM MK-801 and 50 mM AP-5) thus confirming that the increase in evoked activity was due to increased synaptic transmission i.e. increased propagation of activity.

4.3.2 Plasticity altered the change in correlations with propagation of activity from L4 to L2/3

In addition to changes in neuronal response amplitude cortical plasticity is also expected to change the interactions between neuronal responses. We examined the impact of cortical plasticity on the neural correlations within L4 and L2/3 populations. We also compared the change in neural correlations with the propagation of evoked activity between L4 and L2/3 neuronal populations, before and after the induction of plasticity. We found that cortical plasticity resulted in significant positive as well as negative changes in the neural correlations measured within each population. This in turn reflected in the effect of plasticity on the change in correlations with propagation of activity from L4 to L2/3. We measured neural correlations over a large range of timescales (1.5 – 100 ms). Fig. 4.5 shows the histogram of correlations measured at 25 ms binwidth, before and after induction of plasticity. On average the correlations between neurons increased with plasticity, although there occurred neuronal pairs with negative correlations even after plasticity. The positive change in the distribution of correlations was much greater for neuronal pairs in L2/3 compared to pairs from L4.

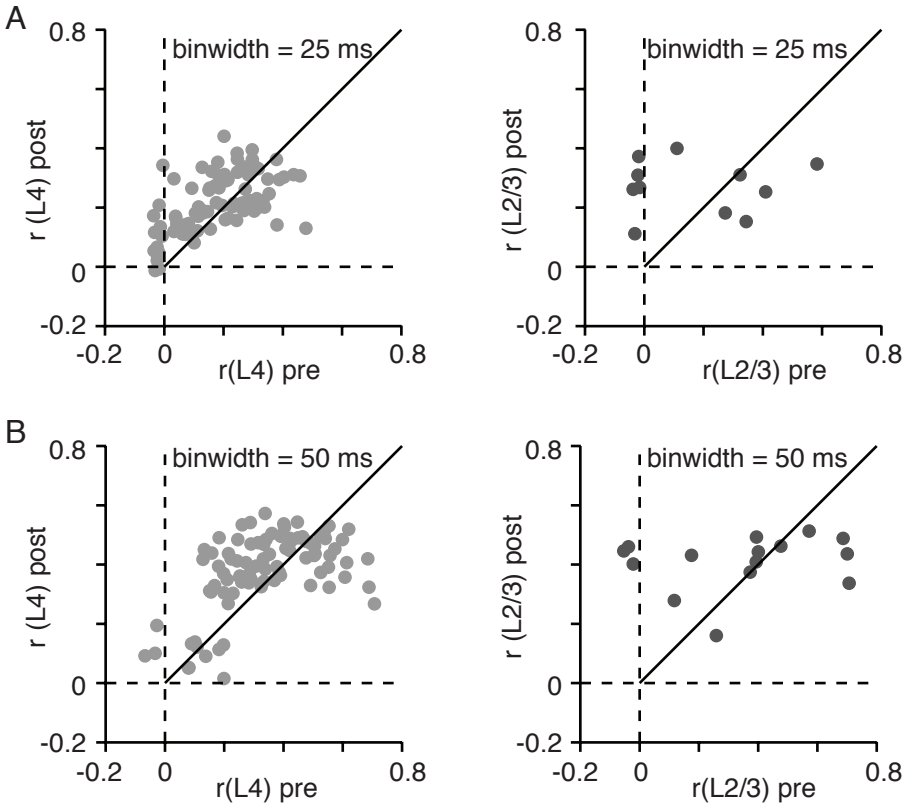

Figure 4.6**:** Plasticity induced changes in neural correlations in L4 and L2/3.

A: Graphs show correlations measured for individual neuronal pairs in L4 (left) and in L2/3 (right) from activity evoked before (x-axis, pre)) and after (y-axis, post) plasticity. The filled markers represent correlations between individual neuronal pairs. The dotted lines mark null correlations. The diagonal line marks the expected values for conditions of no change in correlations with plasticity. The correlations were measured from neuronal spiking activity binned at 25 ms. B: Graphs show the relationship between correlations before and after plasticity for the same L4 and L2/3 neuronal pairs as in A, but for activity binned at 50 ms binwidth.

To measure the change in correlations with propagation of activity we compared the average correlations of all the neuronal pairs across all timescales from L4 and fro L2/3. The results indicated that plasticity converted the decrease in correlations with propagation (for naïve inputs) to an increase in correlations with propagation of activity from L4 to L2/3. This is shown in Fig. 4.5C by the reversal of order in the lines denoting average correlations measured in L4 (light

gray) and in L2/3 (dark gray) with plasticity. We further investigated the change in correlations with plasticity in individual pairs of neurons. The results indicated that the change in correlations also occurred in a subset of neuronal pairs. Graphs in Fig. 4.6 show the relationship between correlations after and before the induction of plasticity for all the neuronal pairs recorded in the example experiment discussed above (same experiment as Fig. 4.3-4.5).

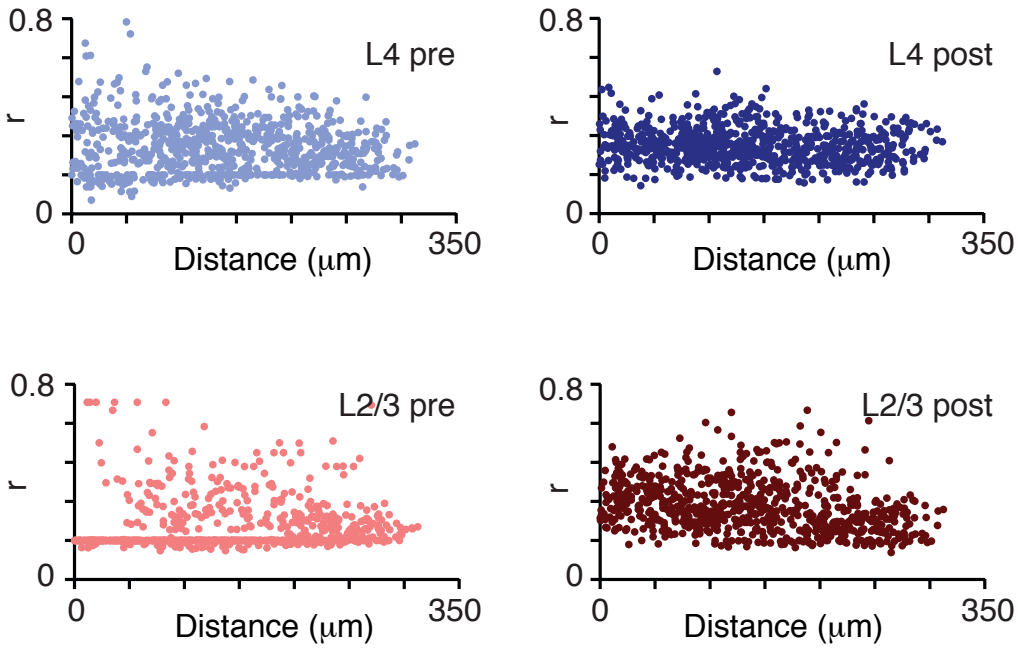

Figure 4.7**:**Distance dependent changes in correlations between neuron pairs from cortical plasticity

Graphs show the distribution of neural correlations (cross-correlation coefficients) between individual neuronal pairs as a function of distance between the pairs. Top graphs (Blue markers) show correlations measured in the same neuronal pairs in L4 before plasticity (left) and after induction of plasticity (right). Bottom graphs (Red markers) show the distribution of correlations measured between pairs in L2/3 before and after plasticity (n=4 experiments).

Correlations measured at 25 ms and 50 ms binwidth are presented for illustration over different timescales. As shown, a subset of individual neuronal

pairs underwent significant increase or decrease in correlations due to cortical plasticity. However, there also neuronal pairs that had limited to no change in their correlations due to plasticity.

We also examined the distribution of correlations as a function of distance between the neuronal pairs measured. The results are shown in Fig. 4.7. Correlations in both L4 and L2/3 populations did not show any significant distance dependent relationship and this did not change with the induction of plasticity. Both populations showed small negative dependence in correlations with increasing distance before plasticity (average slope (L4) = -0.00018±0.0005; average slope (L2/3) = -0.00017±0.0001, n= 760 pairs, 4 experiments). This was even further reduced resulting in a more uniform distribution of correlations with increasing distance up to 315 μm (slopes < 0.000017 for both populations).

We also measured the average change in correlations as the difference and ratio between the average pairwise cross-correlation coefficient calculated from all pairs of neurons within each population. The results from the example experiment along with three other similar experiments reproducing the result are shown in Fig. 4.8. As shown the difference between average correlations measured between L2/3 neuronal pairs and L4 neuronal pairs is significantly negative before plasticity and in converted to positive difference after cortical plasticity. This can also be seen as the change in ratio of output correlations in L2/3 to input correlations from L4, before (blue traces) and after (red traces) plasticity. The data from the previous study conducted with naïve inputs (Chapter 3) is also overlaid for comparison (Black line with dark gray confidence bands).

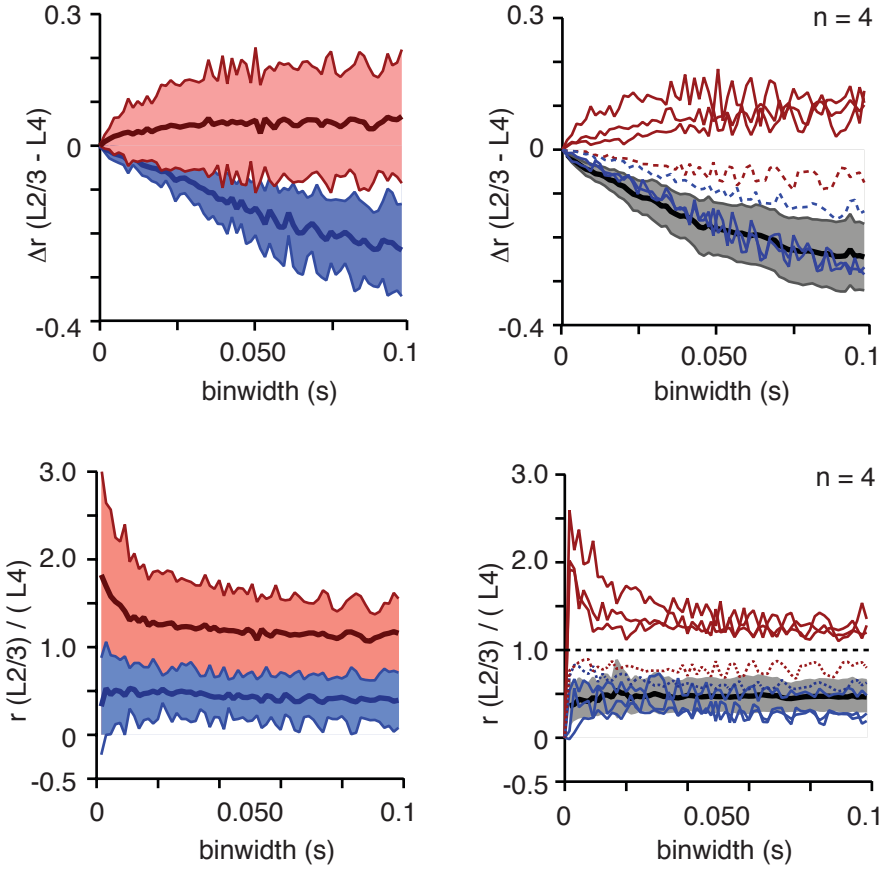

Figure 4.8**:**Plasticity induced increased neural correlations with propagation from L4 to L2/3

Graph shows the difference in neural correlations (measured as average cross-correlation coefficient) between L2/3 and L4 neuronal populations indicating change in correlations with propagation. Blue lines (n=2) represent difference in correlations measured for activity evoked by naïve thalamocortical inputs and red lines (n=3) represent correlations measured after afferent inputs were paired with lateral inputs to induce cortical network plasticity. Two sets of data presented here were obtained from the same input before and after plasticity. Black line in the background indicates the average difference in correlations measured for naïve inputs in a separate set of experiments (n=15) shown here for comparison. The bounding gray shaded area shows confidence intervals.

As shown in the previous study, for cortical activity evoked by naïve, afferent inputs, average neural correlations measured in L2/3 neuronal population were significantly less than that measured in L4 neuronal population

(Fig.4.8 (Ranganathan and Koester, 2010a). However, with the induction of plasticity, neural correlations increased with the propagation of activity between L4 and L2/3. This change with plasticity occurred for activity evoked by the same inputs, in the same neuronal population as measured before induction, indicating that the population of neurons sampled had indeed undergone synaptic plasticity that reflected in the change in correlations.

4.4 Discussion

We examined the impact of cortical network plasticity on the propagation of suprathreshold, spiking activity and the propagation of neural correlations in spiking activity evoked by afferent, thalamocortical inputs in the rodent barrel cortex. We induced cortical network plasticity by pairing afferent thalamocortical inputs with lateral intracortical inputs. The successful induction of network plasticity was identified by increased propagation of evoked activity resulting from increased evoked response of a spatially specific sub-population of neurons. Increased propagation of activity was observed both between L4 and L2/3 of the main column as well as between L2/3 neuronal populations of adjacent cortical columns. From measuring neural correlations within L4 and L2/3 populations of the main responding column we observed that cortical network plasticity also increased the propagation of neural correlations over a wide range of timescales from 1.5 to 100 ms as evoked activity propagated from L4 to L2/3.

Efficient propagation of evoked activity is an important requirement for signaling in a neural system. We studied the propagation of afferent evoked activity from L4 to L2/3 as flow of excitation through this pathway is important for

the cortical integration of sensory information. In the rodent whisker system, thalamocortical afferents predominantly terminate in L4 (Koralek et al., 1988; Lu and Lin, 1993) and rarely innervate neurons in L2/3 directly (Bureau et al., 2006). Additionally L4 neurons largely project to L2/3 neurons of the same cortical column (Bureau et al., 2006; Feldmeyer et al., 2002). Furthermore, the relay of whisker evoked sensory information in the rodent barrel cortex was showed to be initiate radially between layers 4 and 2/3 of the principle column followed by intercolumnar relay within L2/3 neuronal populations (Armstrong-James et al., 1992). In a previous study, we found that neural correlations, measured as average cross-covariance between spiking activity of neuronal pairs, decreased with the propagation of afferent evoked activity from L4 to L2/3 (Ranganathan and Koester, 2011). However, thalamcortical inputs evoked sparse, suprathreshold activity that was mostly restricted within a single cortical column with limited propagation of activity to L2/3. One reason for the decrease in propagation of activity and neural correlations may be that the thalamocortical stimulation provided naïve stimuli that were new to the system thus limiting propagation. Neural systems even in the developed brain constantly undergo changes to responses properties from structural and functional plasticity. The impact of plasticity in addition to changing response selectivity/sensitivity of neurons is also expected to alter properties of signal propagation. Indeed, our results indicate that induction of associative cortical network plasticity from pairing afferent thalamocortical inputs with lateral intracortical inputs results in significantly increased propagation of evoked activity as well increased propagation of neural correlations from L4 to L2/3 of the responding barrel cortical column. Increased correlations with the propagation of activity was

observed over timescales of 1.5 to 100 ms. We used the dithered random-access functional calcium imaging technique to record from up to 20 neurons each from L4 and L2/3 populations simultaneously to measure propagation of activity and correlations. The error in spike timing detection from this technique while minimal (< 3 ms) may have resulted in an underestimation of correlations measured for small time bins, but presumably did not affect results for time bins >> 3 ms.

4.4.1 Increased neural correlations in layer 2/3 network from cortical network plasticity

Our findings presented here, show that that associative cortical plasticity induced by time dependent pairing of afferent and lateral inputs changes evoked responses and neural correlations in cortical networks. The change in evoked responses is consistent with previous studies that have examined cortical plasticity mediated by spike timing dependent mechanisms through NMDA-R mediated synaptic transmission (Froemke and Dan, 2002; Jacob et al., 2007; Schulz et al., 2010). We found that cortical network plasticity was also induced with afferent input from local L4 stimulation instead of thalamocortical inputs. Evoked activity upon induction of plasticity was abolished with blocking glutamatergic synaptic transmission. Additionally, increased activity in L2/3 neurons was correlated with increase in L4 activity as well. These results indicated that the increased downstream activity was a result of increased propagation of spiking activity from L4 to L2/3 mediated by increased intracortical synaptic transmission.

We found increase in neural correlations with propagation of activity from L4 to L2/3 after the induction of plasticity. Previous analytical and experimental

studies of activity propagation and changes in correlations have reported increase in neural correlations with propagation through networks with feed-forward architecture (Kumar et al., 2008; Reyes, 2003b; Vogel and Ronacher, 2007). However, biological neuronal networks with recurrent connections contain mechanisms that contribute to increase in correlations as well as mechanisms that decorrelate spiking activity (de la Rocha et al., 2007; Padmanabhan and Urban, 2010; Renart et al., 2010; Rosenbaum and Josić, 2011; Wiechert et al., 2010). One way to separate the impact of local mechanisms is to compare incoming correlations to local correlations within a network of neurons. In the circuits studied here, while correlations decreased with propagation of activity evoked by naïve inputs, this was converted into increase in correlations with propagation by the induction of plasticity i.e. greater neural correlations occurred within L2/3 neuronal population compared to L4 population following plasticity.

Increase in correlations within L2/3 was blocked by NMDA receptor antagonists during the induction phase suggesting the involvement of synaptic plasticity during induction. Increased correlations in L2/3 neurons may have arisen from local mechanisms that correlate activity, or from increased neural correlations in incoming activity from L4 neuronal population. Indeed, induction of plasticity resulted in increase in correlations within L4 neuronal population in 2 of the 3 experiments examined. Increase in L2/3 correlations may also results from receiving increased number of common synaptic inputs from L4, or increased recurrent synaptic inputs from within the L2/3 neuronal population. This source of increase in correlations may be expected due to the increased activity in both L4 and L2/3 neurons in addition to the dependence on synaptic mechanism for induction of plasticity. We found that increase in neural correlations in neuronal

pairs within L2/3 were significantly higher than that within L4 or that between both populations. Furthermore, under our experimental conditions there were no external sources of activity or mechanisms inducing plasticity due to the absence of modulatory or background activity. This indicated that synaptic plasticity within the L2/3 network largely contributed to the increase in neural correlations within L2/3. Recent studies show that the effects of recurrent excitatory and inhibitory intracortical synaptic inputs have opposing impact on change in correlations in a neuronal population (Renart et al., 2010). Thus, the selective impact of network plasticity on the excitatory and inhibitory components of intracortical synaptic input may determine the overall impact of plasticity on the change in correlations with propagation. Additionally, recent studies have showed a fundamental association between spiking activity and the measured correlations in a neuronal population due to the non-linear, biophysical properties of neuronal excitability (de la Rocha et al., 2007). Thus, an increase in evoked activity in L2/3 is expected to contribute to increased neural correlations in L2/3 not only through increased recurrent synaptic excitation but also through this non-linear relationship. However, we did not observe a significant relationship between local population spiking activity and the neural correlations measured within that population. This finding further emphasizes that in recurrent cortical networks there are complex, non-linear interactions between individual mechanisms that may increase or decrease neural correlations when isolated. The increase in correlations with propagation due to plasticity observed here, thus, may be a result of a combination of plasticity-induced changes including increased common synaptic input from L4 to L2/3, increased recurrent excitation, increased synaptic reliability and decreased decorrelation from intrinsic mechanisms.

Several studies have reported measuring low neural correlations in responses evoked by sensory stimulation within single cortical neuronal populations (Ecker et al., 2010; Renart et al., 2010). This may not be necessarily be at odds with results from the present study. The low correlations observed may be due to activity evoked by presentation of naïve inputs, novel to the system studied, which is consistent with the present findings. In another independent study conducted in the dorsal medial superior temporal area (MSTd), Gu et al. have reported decrease in neural correlations, measured from pairs of simultaneously recorded neurons, with perceptual learning of a visual/vestibular discrimination task (Gu et al., 2011). The difference between this finding and the results presented here may be due to (i) difference in the cortical area under investigation, MSTd being a higher order processing compared to the primary sensory barrel cortex studied here; (ii) differences in organism being studied; or more importantly (iii) the distance between the neuronal pair recorded from and the temporal scale in which correlations were measured. Gu et al. reported that measured neural correlations increased with decrease in distance between neurons. However, the results of their study were pooled across distances < 1mm. In comparison, the neurons recorded in the present study were within a spatial separation of 200μm, laterally. Recurrent intracortical connections significantly decrease in a distance dependent manner. Furthermore, correlations in MSTd were calculated over a timescale of up to 1 sec while in the present study correlations were measured at finer temporal scales of 1.5 to 100 msec. Thus, cortical plasticity may lead to decrease in long-term, neural correlations measured between neurons across larger cortical

distances, while simultaneously resulting in increased propagation of neural correlations at smaller temporal measured at the local population level.

4.4.2 Functional significance

Cortical plasticity has been implicated in mediating perceptual learning represented by increased acuity in sensory perception with training [goldstone 1998]. Specifically, with perceptual learning, plasticity in primary sensory cortical areas has been suggested to contribute to enhanced neurometric performance that is increasingly close to the psychometric performance with perceptual learning. Perceptual learning has also been shown to be dependent on the context or attentive state of the subject, thus suggesting the importance of interplay between local network activity evoked by regulatory, top-down inputs and activity evoked by afferent sensory inputs within neuronal microcircuits in primary sensory cortices (Gilbert et al., 2000). While studies have found little to no change in the response properties of individual neurons that correlated with perceptual learning (Chowdhury and DeAngelis, 2008; Crist et al., 2001; Ghose et al., 2002; Raiguel et al., 2006; Schoups et al., 2001; Yang and Maunsell, 2004; Zohary et al., 1994) other studies have suggested the role of plasticity in the neuronal network level, for example, plasticity in horizontal synaptic connections within primary sensory cortex, altering response properties of intracortical microcircuits (Gilbert et al., 2000). The results presented here are consistent with this prediction. Our results show the relative spike timing dependent induction of network plasticity from associating afferent evoked activity with activity evoked by lateral, intracortical inputs within local neuronal populations in the primary

sensory, barrel cortex. Network plasticity resulted in selective increase in response of a subset of neurons that lead to increased propagation of signal and neural correlations. This induction of spike timing dependent, spatially specific, associative cortical network plasticity at the microcircuit level presents a candidate mechanism to mediate forms of perceptual learning at the primary sensory cortical areas. Thus it provides a predictive basis to examine the impact of input specific, associative plasticity under *in vivo* conditions, by pairing functionally relevant sensory inputs with controlled top-down, regulatory inputs. Experiments conducted *in vivo,* replicating results presented here along with improved behavioral performance will indicate the role of plasticity-induced increase in propagation of activity and neural correlations in perceptual learning.

Additionally, under our experimental conditions, thalamocortically evoked activity from naïve inputs was predominantly restricted within an individual cortical column with limited signal propagation to L2/3 of the main column. The induction of plasticity increased lateral propagation of evoked activity from the main responding column (C0) to the paired cortical column (C1). This was closely associated with plasticity-induced increase in spiking activity and neural correlations within the L2/3 neuronal network of C0. This suggests the requirement for substantial local network activity and neural correlations within L2/3 neurons of a cortical column to results in the lateral, intercolumnar propagation of cortical activity. This result is consistent with previous studies suggesting a gating role for L2/3 neuronal population to regulate the flow of excitation within the primary sensory cortex (Petersen et al., 2003). The present results suggest that neural correlations along with amplitude of evoked activity in

L2/3 of the main column may be important in regulating the spread of excitation to the adjacent columns.

4.5 SUMMARY

In the previous study (Chapter 3) we found that neural correlations in suprathreshold activity decreased with propagation between recurrent cortical networks. This result was obtained from evoking activity with afferent thalamocortical inputs that were presumably novel to the system. However, cortical plasticity from behavioral learning is expected to impact both evoked neuronal activity and the propagation of evoked activity between networks in the cortex. Therefore, in this study we addressed the impact of associative cortical plasticity on the propagation of afferent evoked activity between neuronal networks in the mouse barrel cortex. We also examined the impact of cortical plasticity on the change in neural correlations with the propagation of evoked activity between L4 and L2/3 networks. We found that pairing afferent inputs with a delayed intracortical input induced cortical plasticity. The induction of plasticity resulted in increased propagation of activity evoked by the afferent input, within the main column (C0) as well as to the paired column (C1). Additionally, we observed that plasticity led to increase in neural correlations with the propagation of activity between the L4 and L2/3 networks of the main column. Both increased propagation of activity as well as increased correlations occurred in a specific subpopulation of neurons. The induction of plasticity depended on the relative delay ion onset of the inputs. Plasticity also depended on NMDA receptor mediated synaptic transmission during induction.

The results indicated that the change in correlations with propagation of activity between mammalian cortical networks was not fixed. Rather, it was dependent on the state of the networks and the properties of the inputs (e.g. novelty). The results also showed that associative plasticity increased neural correlations in both L4 and L2/3. Due to the greater increase in correlations in L2/3 plasticity resulted in increase in correlations with vertical propagation. The dependence on NMDA receptor activation and input timing indicate that mechanisms of spike-timing dependent synaptic plasticity contributed to this effect. This suggests an increased synaptic connectivity within the L4 and L2/3 networks or between the two networks, or a combination of both. This result is consistent with the recent finding of high correlations and high connectivity between L2/3 neurons with similar response properties (Ko et al., 2011).

This study shows the impact of plasticity at the microcircuit level with single cell, single spike resolution. Thus, it connects studies describing cortical plasticity at the system wide level with studies examining plasticity from changes in response properties of individual neurons. The results from this study suggest synaptic plasticity at the network level, resulting in increased neural correlations with propagation, to contribute to behavioral learning.

Chapter 5: Conclusions

This dissertation describes our study examining the propagation of evoked suprathreshold electrical activity between recurrent networks in the primary sensory mouse barrel cortex. We examined the impact of associative cortical plasticity on the propagation of evoked suprathreshold population activity. We also measured the impact of plasticity on the change in neural correlations with the propagation of evoked activity. In order to record the propagation of spiking activity and to measure neural correlations in activity, we developed a novel method, dithered random-access functional calcium imaging. This optical technique records suprathreshold somatic responses with high spatial and temporal resolution, from large samples of spatially distributed neurons. This technique included the development of novel analytical methods to extract (deconvolve) the underlying spiking activity from the recorded fluorescence responses. This dissertation also outlines the development of these methods and reports on their performance in the examined cortical networks in the mouse barrel cortex.

We found that under our experimental conditions, cortical activity evoked by naïve, afferent, thalamocortical inputs were largely restricted within a single cortical column. The vertical propagation of activity from L4 to L2/3 was limited. Additionally, the average neural correlations measured between pairs of neurons within each population decreased with the propagation of activity from L4 to L2/3. Interestingly, associative cortical plasticity was induced with the repeated pairing of afferent thalamocortical inputs with activity evoked by other inputs (for example, lateral intracortical inputs). Induction of cortical plasticity resulted in

increased cortical activity evoked by the afferent inputs. Plasticity resulted in increased propagation of evoked activity between L4 and L2/3 neuronal populations within the primary responding column. Activity following plasticity also showed increased propagation between L2/3 neuronal populations of the main column and the paired (adjacent) column. Additionally, the increased propagation of activity within a column was accompanied by increase in neural correlations with the propagation of activity from L4 to L2/3. The induction of cortical plasticity was dependent on the relative timing of the paired inputs. Induction was also dependent on NMDA receptor mediated synaptic transmission.

5.1 Recording population activity

Previous studies show that the performance of neural codes relying on population activity better represent sensory attributes/motor activity signals than those that use activity of individual neurons (Georgopoulos et al., 1986). Interactions between neuronal responses have also been shown to contribute to representation of information (Pillow et al., 2008a). These results emphasize the importance of studying neural population activity to understand the mechanisms underlying neural signal processing (Schrader et al., 2008a; Izhikevich et al., 2004). The optical technique presented here, dithered random-access functional calcium imaging, has been demonstrated to record suprathreshold activity from multiple neurons in a heterogeneous population, under *in vitro* as well as *in vivo* conditions, with high spatial and temporal resolution. In conjunction with the maximum-likelihood spike detection method outlined here, this method can

extract spiking activity of 40-100 neurons with high detection efficiency at millisecond temporal precision. Thus it presents a significant advance in methods to examine neural population activity at the network level (mesoscale). This method allows one to quantitatively address central questions regarding mechanisms underlying signal processing at the network level in various neural systems.

5.2 Impact of associative cortical plasticity on signal propagation and changes in neural correlations with propagation between cortical layers 4 and 2/3

Results from this study show that adapted, cortical activity evoked by afferent thalamocortical inputs was mostly sparse and restricted within a single cortical column. Furthermore, the evoked activity within populations of L4 and L2/3 contained significant neural correlations, measured between pairs of neurons, over a large range of timescales. We found that neural correlations in cortical population activity changed with the propagation of activity. However, counter to predictions from experimental and analytical studies conducted on networks with feedforward architecture, neural correlations in activity evoked by naïve (novel) inputs decreased with propagation between recurrent cortical networks. Interestingly, the induction of cortical plasticity resulted in increase in neural correlations with the propagation of activity. Upon induction of plasticity, neural correlations in L2/3 were greater than correlations in L4 and thus were not limited by incoming correlations from L4.

Our results were obtained under the conditions limited to those of the acute slice preparation (i.e. restricted synaptic architecture, absence of top-down

inputs and long-distance targets, lack of neuromodulatory/regulatory inputs and lack of spontaneous background activity). However, the results presented here provide a quantitative measurement of propagation of activity and neural correlations at the population level. They also provide a measure of effects of plasticity on poulation acitivity under known and controlled conditions. Thus the presented results form a critical link between results from studies of signaling and plasticity using simulations, and from empirical studies at the single neuronal and system levels of complexity. Further studies conducted *in vivo* are required to test if these observations are carried over to awake and behaving animals.

Empirical studies conducted in the rodent somatosensory system(Petersen et al., 2001) and studies based on perturbation analysis (London et al., 2010) suggest low contribution of correlations to representation of information (signaling). Additionally, other studies have analytically predicted limiting effects of neural correlations on the fidelity of rate based neural codes (Mazurek and Shadlen, 2002). However, the effects of neural correlations on signaling depend on complex interactions between neural correlations that are dependent on stimulus conditions (signal correlations) and those that do not (noise correlations) (Averbeck et al., 2006a). Additionally, the functional impact of neural correlations can only be measured by determining their impact on the downstream population of neurons (decoding).

Firstly, our results indicate that neural correlations and their change with the propagation of population activity are not fixed and may depend on the state of the system and the properties of the inputs (e.g. novelty). Additionally, the increase in neural correlations with propagation of activity due to plasticity suggests a significant impact of neural correlations on cortical signaling of

information. Our results also suggest that mechanisms of synaptic plasticity in intracortical connections contribute to the increase in neural correlations. Specifically, neural correlations in L2/3 activity were measured to be greater than the incoming correlations from L4 following plasticity. This result suggests a significant increase in local excitatory synaptic connectivity within the L2/3 neuronal population. This is consistent with the recent findings of increased synaptic connectivity and increased neural correlations between L2/3 neurons with similar response selectivity in the visual cortex (Hofer et al., 2011; Ko et al., 2011). Thus, based on our results, we predict increase in neural correlations with propagation of cortical activity following behavioral learning; through plasticity mediated by cellular, synaptic and network mechanisms that control properties of population activity.

References

Abbott, L.F., and Nelson, S.B. (2000). Synaptic plasticity: taming the beast. Nat Neurosci 3 Suppl, 1178-1183.

Aertsen, A.M., Gerstein, G.L., Habib, M.K., and Palm, G. (1989). Dynamics of neuronal firing correlation: modulation of "effective connectivity". J Neurophysiol 61, 900-917.

Agmon, A., and Connors, B.W. (1991). Thalamocortical responses of mouse somatosensory (barrel) cortex in vitro. Neuroscience 41, 365-379.

Anderson, C.T., Sheets, P.L., Kiritani, T., and Shepherd, G.M. (2010). Sublayer-specific microcircuits of corticospinal and corticostriatal neurons in motor cortex. Nat Neurosci 13, 739-744.

Armstrong-James, M., Fox, K., and Das-Gupta, A. (1992). Flow of excitation within rat barrel cortex on striking a single vibrissa. J Neurophysiol 68, 1345-1358.

Aroniadou-Anderjaska, V., and Keller, A. (1995). LTP in the barrel cortex of adult rats. Neuroreport 6, 2297-2300.

Augustine, G.J., and Neher, E. (1992). Neuronal Ca2+ signalling takes the local route. Curr Opin Neurobiol 2, 302-307.

Averbeck, B.B., and Lee, D. (2006). Effects of noise correlations on information encoding and decoding. J Neurophysiol 95, 3633-3644.

Averbeck, B.B., Latham, P.E., and Pouget, A. (2006a). Neural correlations, population coding and computation. Nat Rev Neurosci 7, 358-366.

Averbeck, B.B., Latham, P.E., and Pouget, A. (2006b). Neural correlations, population coding and computation. Nat Rev Neurosci 7, 358-366.

Bekisz, M., Garkun, Y., Wabno, J., Hess, G., Wrobel, A., and Kossut, M. (2010). Increased excitability of cortical neurons induced by associative learning: an ex vivo study. Eur J Neurosci 32, 1715-1725.

Benshalom, G., and White, E.L. (1986). Quantification of thalamocortical synapses with spiny stellate neurons in layer IV of mouse somatosensory cortex. J Comp Neurol 253, 303-314.

Brecht, M. (2007). Barrel cortex and whisker-mediated behaviors. Curr Opin Neurobiol 17, 408-416.

Buonomano, D.V., and Merzenich, M.M. (1998). Cortical plasticity: from synapses to maps. Annu Rev Neurosci 21, 149-186.

Bureau, I., von Saint Paul, F., and Svoboda, K. (2006). Interdigitated paralemniscal and lemniscal pathways in the mouse barrel cortex. PLoS Biol 4, e382.

Buzsáki, G. (2004). Large-scale recording of neuronal ensembles. Nat Neurosci 7, 446-451.

Chowdhury, S.A., and DeAngelis, G.C. (2008). Fine discrimination training alters the causal contribution of macaque area MT to depth perception. Neuron 60, 367-377.

Crist, R.E., Li, W., and Gilbert, C.D. (2001). Learning to see: experience and attention in primary visual cortex. Nat Neurosci 4, 519-525.

Cruikshank, S.J., and Weinberger, N.M. (1996). Receptive-field plasticity in the adult auditory cortex induced by Hebbian covariance. J Neurosci 16, 861-875.

Cruikshank, S.J., Lewis, T.J., and Connors, B.W. (2007). Synaptic basis for intense thalamocortical activation of feedforward inhibitory cells in neocortex. Nat Neurosci 10, 462-468.

DA, P., and TH, B. (1968). Neural coding: a report based on an NRP work sesson. Neurosci. Res. Program Bull. 6, 219-349.

Diesmann, M., Gewaltig, M.O., and Aertsen, A. (1999). Stable propagation of synchronous spiking in cortical neural networks. Nature 402, 529-533.

Dombeck, D.A., Graziano, M.S., and Tank, D.W. (2009). Functional clustering of neurons in motor cortex determined by cellular resolution imaging in awake behaving mice. J Neurosci 29, 13751-13760.

Dombeck, D.A., Khabbaz, A.N., Collman, F., Adelman, T.L., and Tank, D.W. (2007). Imaging large-scale neural activity with cellular resolution in awake, mobile mice. Neuron 56, 43-57.

Ecker, A.S., Berens, P., Keliris, G.A., Bethge, M., Logothetis, N.K., and Tolias, A.S. (2010). Decorrelated neuronal firing in cortical microcircuits. Science 327, 584-587.

Eyding, D., Schweigart, G., and Eysel, U.T. (2002). Spatio-temporal plasticity of cortical receptive fields in response to repetitive visual stimulation in the adult cat. Neuroscience 112, 195-215.

Eysel, U.T., Eyding, D., and Schweigart, G. (1998). Repetitive optical stimulation elicits fast receptive field changes in mature visual cortex. Neuroreport 9, 949-954.

Feldman, D.E. (2009). Synaptic mechanisms for plasticity in neocortex. Annu Rev Neurosci 32, 33-55.

Feldman, D.E., and Brecht, M. (2005). Map plasticity in somatosensory cortex. Science 310, 810-815.

Feldmeyer, D., Lubke, J., and Sakmann, B. (2006). Efficacy and connectivity of intracolumnar pairs of layer 2/3 pyramidal cells in the barrel cortex of juvenile rats. J Physiol 575, 583-602.

Feldmeyer, D., Lubke, J., Silver, R.A., and Sakmann, B. (2002). Synaptic connections between layer 4 spiny neurone-layer 2/3 pyramidal cell pairs in juvenile rat barrel cortex: physiology and anatomy of interlaminar signalling within a cortical column. J Physiol 538, 803-822.

Felleman, D.J., and Van Essen, D.C. (1991). Distributed hierarchical processing in the primate cerebral cortex. Cereb Cortex 1, 1-47.

Fierro, L., and Llano, I. (1996). High endogenous calcium buffering in Purkinje cells from rat cerebellar slices. J Physiol 496 (Pt 3), 617-625.

Fork, R.L., Martinez, O.E., and Gordon, J.P. (1984). Negative dispersion using pairs of prisms. Opt Lett 9, 150-152.

Fox, K. (2002). Anatomical pathways and molecular mechanisms for plasticity in the barrel cortex. Neuroscience 111, 799-814.

Frégnac, Y., Bringuier, V., and Chavane, F. (1996). Synaptic integration fields and associative plasticity of visual cortical cells in vivo. J Physiol Paris 90, 367-372.

Frégnac, Y., Shulz, D., Thorpe, S., and Bienenstock, E. (1988). A cellular analogue of visual cortical plasticity. Nature 333, 367-370.

Froemke, R.C., and Dan, Y. (2002). Spike-timing-dependent synaptic modification induced by natural spike trains. Nature 416, 433-438.

Georgopoulos, A.P., Schwartz, A.B., and Kettner, R.E. (1986). Neuronal population coding of movement direction. Science 233, 1416-1419.

Ghose, G.M., Yang, T., and Maunsell, J.H.R. (2002). Physiological correlates of perceptual learning in monkey V1 and V2. J Neurophysiol 87, 1867-1888.

Gilbert, C., Ito, M., Kapadia, M., and Westheimer, G. (2000). Interactions between attention, context and learning in primary visual cortex. Vision Res 40, 1217-1226.

Gobel, W., and Helmchen, F. (2007). In vivo calcium imaging of neural network function. Physiology (Bethesda) 22, 358-365.

Greenberg, D.S., Houweling, A.R., and Kerr, J.N. (2008). Population imaging of ongoing neuronal activity in the visual cortex of awake rats. Nat Neurosci 11, 749-751.

Grewe, B.F., Langer, D., Kasper, H., Kampa, B.M., and Helmchen, F. (2010). High-speed in vivo calcium imaging reveals neuronal network activity with near-millisecond precision. Nat Methods 7, 399-405.

Gu, Y., Liu, S., Fetsch, C.R., Yang, Y., Fok, S., Sunkara, A., Deangelis, G.C., and Angelaki, D.E. (2011). Perceptual learning reduces interneuronal correlations in macaque visual cortex. Neuron 71, 750-761.

Helmchen, F., Imoto, K., and Sakmann, B. (1996). Ca2+ buffering and action potential-evoked Ca2+ signaling in dendrites of pyramidal neurons. Biophys J 70, 1069-1081.

Hirase, H., Qian, L., Bartho, P., and Buzsaki, G. (2004). Calcium dynamics of cortical astrocytic networks in vivo. PLoS Biol 2, E96.

Hofer, S.B., Ko, H., Pichler, B., Vogelstein, J., Ros, H., Zeng, H., Lein, E., Lesica, N.A., and Mrsic-Flogel, T.D. (2011). Differential connectivity and response dynamics of excitatory and inhibitory neurons in visual cortex. Nat Neurosci 14, 1045-1052.

Holekamp, T.F., Turaga, D., and Holy, T.E. (2008). Fast three-dimensional fluorescence imaging of activity in neural populations by objective-coupled planar illumination microscopy. Neuron 57, 661-672.

Hopt, A., and Neher, E. (2001). Highly nonlinear photodamage in two-photon fluorescence microscopy. Biophys J 80, 2029-2036.

Hubel, D.H., and Wiesel, T.N. (1963). Single-Cell Responses in Striate Cortex of Kittens Deprived of Vision in one Eye. J Neurophysiol 26, 1003-1017.

Hubel, D.H., and Wiesel, T.N. (1968). Receptive fields and functional architecture of monkey striate cortex. J Physiol 195, 215-243.

Ikegaya, Y., Le Bon-Jego, M., and Yuste, R. (2005). Large-scale imaging of cortical network activity with calcium indicators. Neurosci Res 52, 132-138.

Iyer, V., Hoogland, T.M., and Saggau, P. (2006). Fast functional imaging of single neurons using random-access multiphoton (RAMP) microscopy. J Neurophysiol 95, 535-545.

Iyer, V., Losavio, B.E., and Saggau, P. (2003). Compensation of spatial and temporal dispersion for acousto-optic multiphoton laser-scanning microscopy. J Biomed Opt 8, 460-471.

Izhikevich, E.M., Gally, J.A., and Edelman, G.M. (2004). Spike-timing dynamics of neuronal groups. Cereb Cortex 14, 933-944.

Jacob, V., Brasier, D.J., Erchova, I., Feldman, D., and Shulz, D.E. (2007). Spike timing-dependent synaptic depression in the in vivo barrel cortex of the rat. J Neurosci 27, 1271-1284.

Ji, N., Magee, J.C., and Betzig, E. (2008). High-speed, low-photodamage nonlinear imaging using passive pulse splitters. Nat Methods 5, 197-202.

Karl, A., Birbaumer, N., Lutzenberger, W., Cohen, L.G., and Flor, H. (2001). Reorganization of motor and somatosensory cortex in upper extremity amputees with phantom limb pain. J Neurosci 21, 3609-3618.

Kerr, J.N., de Kock, C.P., Greenberg, D.S., Bruno, R.M., Sakmann, B., and Helmchen, F. (2007). Spatial organization of neuronal population responses in layer 2/3 of rat barrel cortex. J Neurosci 27, 13316-13328.

Kerr, J.N., Greenberg, D., and Helmchen, F. (2005). Imaging input and output of neocortical networks in vivo. Proc Natl Acad Sci U S A 102, 14063-14068.

Kim, S.J., and Linden, D.J. (2007). Ubiquitous plasticity and memory storage. Neuron 56, 582-592.

Kimpo, R.R., Theunissen, F.E., and Doupe, A.J. (2003a). Propagation of correlated activity through multiple stages of a neural circuit. J Neurosci 23, 5750-5761.

Kimpo, R.R., Theunissen, F.E., and Doupe, A.J. (2003b). Propagation of correlated activity through multiple stages of a neural circuit. J Neurosci 23, 5750-5761.

Kirkwood, A., and Bear, M.F. (1994). Hebbian synapses in visual cortex. J Neurosci 14, 1634-1645.

Kirkwood, A., and Bear, M.F. (1995). Elementary forms of synaptic plasticity in the visual cortex. Biol Res 28, 73-80.

Ko, H., Hofer, S.B., Pichler, B., Buchanan, K.A., Sjöström, P.J., and Mrsic-Flogel, T.D. (2011). Functional specificity of local synaptic connections in neocortical networks. Nature 473, 87-91.

de Kock, C.P.J., Bruno, R.M., Spors, H., and Sakmann, B. (2007). Layer- and cell-type-specific suprathreshold stimulus representation in rat primary somatosensory cortex. J Physiol 581, 139-154.

Koester, H.J., Baur, D., Uhl, R., and Hell, S.W. (1999). Ca2+ fluorescence imaging with pico- and femtosecond two-photon excitation: signal and photodamage. Biophys J 77, 2226-2236.

Koralek, K.A., Jensen, K.F., and Killackey, H.P. (1988). Evidence for two complementary patterns of thalamic input to the rat somatosensory cortex. Brain Res 463, 346-351.

Kuhn, B., Denk, W., and Bruno, R.M. (2008). In vivo two-photon voltage-sensitive dye imaging reveals top-down control of cortical layers 1 and 2 during wakefulness. Proc Natl Acad Sci U S A 105, 7588-7593.

Kumar, A., Rotter, S., and Aertsen, A. (2008). Conditions for propagating synchronous spiking and asynchronous firing rates in a cortical network model. J Neurosci 28, 5268-5280.

Kumar, A., Rotter, S., and Aertsen, A. (2010). Spiking activity propagation in neuronal networks: reconciling different perspectives on neural coding. Nat Rev Neurosci 11, 615-627.

de la Rocha, J., Doiron, B., Shea-Brown, E., Josic, K., and Reyes, A. (2007). Correlation between neural spike trains increases with firing rate. Nature 448, 802-806.

Laaris, N., and Keller, A. (2002). Functional independence of layer IV barrels. J Neurophysiol 87, 1028-1034.

Lechleiter, J.D., Lin, D.T., and Sieneart, I. (2002). Multi-photon laser scanning microscopy using an acoustic optical deflector. Biophys J 83, 2292-2299.

Lillis, K.P., Eng, A., White, J.A., and Mertz, J. (2008). Two-photon imaging of spatially extended neuronal network dynamics with high temporal resolution. J Neurosci Methods 172, 178-184.

Lin, B.-J.J., Chen, T.-W.W., and Schild, D. (2007). Cell type-specific relationships between spiking and [Ca2+]i in neurons of the Xenopus tadpole olfactory bulb. J Physiol 582, 163-175.

London, M., Roth, A., Beeren, L., Hausser, M., and Latham, P.E. (2010). Sensitivity to perturbations in vivo implies high noise and suggests rate coding in cortex. Nature 466, 123-127.

Lu, S.M., and Lin, R.C. (1993). Thalamic afferents of the rat barrel cortex: a light- and electron-microscopic study using Phaseolus vulgaris leucoagglutinin as an anterograde tracer. Somatosens Mot Res 10, 1-16.

Luna, R., Hernandez, A., Brody, C.D., and Romo, R. (2005). Neural codes for perceptual discrimination in primary somatosensory cortex. Nat Neurosci 8, 1210-1219.

Lübke, J., and Feldmeyer, D. (2007). Excitatory signal flow and connectivity in a cortical column: focus on barrel cortex. Brain Struct Funct 212, 3-17.

Mao, B.Q., Hamzei-Sichani, F., Aronov, D., Froemke, R.C., and Yuste, R. (2001). Dynamics of spontaneous activity in neocortical slices. Neuron 32, 883-898.

Mazurek, M.E., and Shadlen, M.N. (2002). Limits to the temporal fidelity of cortical spike rate signals. Nat Neurosci 5, 463-471.

Mehring, C., Hehl, U., Kubo, M., Diesmann, M., and Aertsen, A. (2003). Activity dynamics and propagation of synchronous spiking in locally connected random networks. Biol Cybern 88, 395-408.

Meliza, C.D., and Dan, Y. (2006). Receptive-field modification in rat visual cortex induced by paired visual stimulation and single-cell spiking. Neuron 49, 183-189.

Merzenich, M.M., Kaas, J.H., Wall, J., Nelson, R.J., Sur, M., and Felleman, D. (1983). Topographic reorganization of somatosensory cortical areas 3b and 1 in adult monkeys following restricted deafferentation. Neuroscience 8, 33-55.

Meyer, H.S., Wimmer, V.C., Hemberger, M., Bruno, R.M., de Kock, C.P., Frick, A., Sakmann, B., and Helmstaedter, M. (2010). Cell type-specific thalamic innervation in a column of rat vibrissal cortex. Cereb Cortex 20, 2287-2303.

Middleton, J.W., Kinnischtzke, A., and Simons, D.J. (2010). Effects of thalamic high-frequency electrical stimulation on whisker-evoked cortical adaptation. Exp Brain Res 200, 239-250.

Mountcastle, V.B. (1997). The columnar organization of the neocortex. Brain 120 (Pt 4), 701-722.

Mukamel, E.A., Nimmerjahn, A., and Schnitzer, M.J. (2009). Automated analysis of cellular signals from large-scale calcium imaging data. Neuron 63, 747-760.

O'Connor, D.H., Peron, S.P., Huber, D., and Svoboda, K. (2010). Neural activity in barrel cortex underlying vibrissa-based object localization in mice. Neuron 67, 1048-1061.

Ohki, K., Chung, S., Ch'ng, Y.H., Kara, P., and Reid, R.C. (2005). Functional imaging with cellular resolution reveals precise micro-architecture in visual cortex. Nature 433, 597-603.

Otsu, Y., Bormuth, V., Wong, J., Mathieu, B., Dugué, G.P., Feltz, A., and Dieudonné, S. (2008). Optical monitoring of neuronal activity at high frame rate with a digital random-access multiphoton (RAMP) microscope. J Neurosci Methods 173, 259-270.

Padmanabhan, K., and Urban, N.N. (2010). Intrinsic biophysical diversity decorrelates neuronal firing while increasing information content. Nat Neurosci 13, 1276-1282.

Panzeri, S., Petersen, R.S., Schultz, S.R., Lebedev, M., and Diamond, M.E. (2001). The role of spike timing in the coding of stimulus location in rat somatosensory cortex. Neuron 29, 769-777.

Petersen, C.C., and Sakmann, B. (2001). Functionally independent columns of rat somatosensory barrel cortex revealed with voltage-sensitive dye imaging. J Neurosci 21, 8435-8446.

Petersen, C.C.H. (2003). The barrel cortex--integrating molecular, cellular and systems physiology. Pflugers Arch 447, 126-134.

Petersen, C.C.H. (2007). The functional organization of the barrel cortex. Neuron 56, 339-355.

Petersen, C.C.H., Grinvald, A., and Sakmann, B. (2003). Spatiotemporal dynamics of sensory responses in layer 2/3 of rat barrel cortex measured in vivo by voltage-sensitive dye imaging combined with whole-cell voltage recordings and neuron reconstructions. J Neurosci 23, 1298-1309.

Petersen, R.S., Panzeri, S., and Diamond, M.E. (2001). Population coding of stimulus location in rat somatosensory cortex. Neuron 32, 503-514.

Pienkowski, M., and Eggermont, J.J. (2011). Cortical tonotopic map plasticity and behavior. Neurosci Biobehav Rev

Pillow, J.W., Shlens, J., Paninski, L., Sher, A., Litke, A.M., Chichilnisky, E.J., and Simoncelli, E.P. (2008a). Spatio-temporal correlations and visual signalling in a complete neuronal population. Nature 454, 995-999.

Pillow, J.W., Shlens, J., Paninski, L., Sher, A., Litke, A.M., Chichilnisky, E.J., and Simoncelli, E.P. (2008b). Spatio-temporal correlations and visual signalling in a complete neuronal population. Nature 454, 995-999.

Pita-Almenar, J.D., Ranganathan, G.N., and Koester, H.J. (2011). Impact of cortical plasticity on information signaled by populations of neurons in the cerebral cortex. J Neurophysiol 106, 1118-1124.

Pouget, A., Dayan, P., and Zemel, R. (2000). Information processing with population codes. Nat Rev Neurosci 1, 125-132.

Raiguel, S., Vogels, R., Mysore, S.G., and Orban, G.A. (2006). Learning to see the difference specifically alters the most informative V4 neurons. J Neurosci 26, 6589-6602.

Ranganathan, G.N., and Koester, H.J. (2010a). Optical recording of neuronal spiking activity from unbiased populations of neurons with high spike detection efficiency and high temporal precision. J Neurophysiol 104, 1812-1824.

Ranganathan, G.N., and Koester, H.J. (2010b). Optical recording of neuronal spiking activity from unbiased populations of neurons with high spike detection efficiency and high temporal precision. J Neurophysiol 104, 1812-1824.

Ranganathan, G.N., and Koester, H.J. (2011). Correlations decrease with propagation of spiking activity in the mouse barrel cortex. Front Neural Circuits 5, 8.

Recanzone, G.H., Merzenich, M.M., Jenkins, W.M., Grajski, K.A., and Dinse, H.R. (1992). Topographic reorganization of the hand representation in cortical area 3b owl monkeys trained in a frequency-discrimination task. J Neurophysiol 67, 1031-1056.

Renart, A., de la Rocha, J., Bartho, P., Hollender, L., Parga, N., Reyes, A., and Harris, K.D. (2010). The asynchronous state in cortical circuits. Science 327, 587-590.

Reyes, A.D. (2003a). Synchrony-dependent propagation of firing rate in iteratively constructed networks in vitro. Nat Neurosci 6, 593-599.

Reyes, A.D. (2003b). Synchrony-dependent propagation of firing rate in iteratively constructed networks in vitro. Nat Neurosci 6, 593-599.

Rosenbaum, R., and Josić, K. (2011). Mechanisms that modulate the transfer of spiking correlations. Neural Comput 23, 1261-1305.

Rosenberg, J.R., Amjad, A.M., Breeze, P., Brillinger, D.R., and Halliday, D.M. (1989). The Fourier approach to the identification of functional coupling between neuronal spike trains. Prog Biophys Mol Biol 53, 1-31.

Sale, A., De Pasquale, R., Bonaccorsi, J., Pietra, G., Olivieri, D., Berardi, N., and Maffei, L. (2011). Visual perceptual learning induces long-term potentiation in the visual cortex. Neuroscience 172, 219-225.

Sasaki, T., Takahashi, N., Matsuki, N., and Ikegaya, Y. (2008). Fast and accurate detection of action potentials from somatic calcium fluctuations. J Neurophysiol 100, 1668-1676.

Sato, T.R., Gray, N.W., Mainen, Z.F., and Svoboda, K. (2007). The Functional Microarchitecture of the Mouse Barrel Cortex. PLoS Biol 5, e189.

Schoups, A., Vogels, R., Qian, N., and Orban, G. (2001). Practising orientation identification improves orientation coding in V1 neurons. Nature 412, 549-553.

Schrader, S., Grun, S., Diesmann, M., and Gerstein, G.L. (2008a). Detecting synfire chain activity using massively parallel spike train recording. J Neurophysiol 100, 2165-2176.

Schrader, S., Grün, S., Diesmann, M., and Gerstein, G.L. (2008b). Detecting synfire chain activity using massively parallel spike train recording. J Neurophysiol 100, 2165-2176.

Schuett, S., Bonhoeffer, T., and Hübener, M. (2001). Pairing-induced changes of orientation maps in cat visual cortex. Neuron 32, 325-337.

Schulz, J.M., Redgrave, P., and Reynolds, J.N. (2010). Cortico-striatal spike-timing dependent plasticity after activation of subcortical pathways. Front Synaptic Neurosci 2, 23.

Shea-Brown, E., Josic, K., de la Rocha, J., and Doiron, B. (2008). Correlation and synchrony transfer in integrate-and-fire neurons: basic properties and consequences for coding. Phys Rev Lett 100, 108102.

Simons, D.J., and Land, P.W. (1987). Early experience of tactile stimulation influences organization of somatic sensory cortex. Nature 326, 694-697.

Sjulson, L., and Miesenböck, G. (2007). Optical recording of action potentials and other discrete physiological events: a perspective from signal detection theory. Physiology (Bethesda) 22, 47-55.

Song, S., Sjöström, P.J., Reigl, M., Nelson, S., and Chklovskii, D.B. (2005). Highly nonrandom features of synaptic connectivity in local cortical circuits. PLoS Biol 3, e68.

Staiger, J.F., Flagmeyer, I., Schubert, D., Zilles, K., Kötter, R., and Luhmann, H.J. (2004). Functional diversity of layer IV spiny neurons in rat somatosensory cortex: quantitative morphology of electrophysiologically characterized and biocytin labeled cells. Cereb Cortex 14, 690-701.

Stosiek, C., Garaschuk, O., Holthoff, K., and Konnerth, A. (2003). In vivo two-photon calcium imaging of neuronal networks. Proc Natl Acad Sci U S A 100, 7319-7324.

Sun, Q.-Q.Q., Huguenard, J.R., and Prince, D.A. (2006). Barrel cortex microcircuits: thalamocortical feedforward inhibition in spiny stellate cells is mediated by a small number of fast-spiking interneurons. J Neurosci 26, 1219-1230.

Tetzlaff, T., Rotter, S., Stark, E., Abeles, M., Aertsen, A., and Diesmann, M. (2008). Dependence of neuronal correlations on filter characteristics and marginal spike train statistics. Neural Comput 20, 2133-2184.

Thomson, D. J., and Chave, A. D. (1991). “Jackknifed error estimates for spectra, coherences, and transfer functions,” in Advances in Spectrum Analysis and Array Processing, ed. S. Haykin (Englewood Cliffs, NJ: Prentice Hall.), 58–113.

Turrigiano, G.G., and Nelson, S.B. (2000). Hebb and homeostasis in neuronal plasticity. Curr Opin Neurobiol 10, 358-364.

Urban-Ciecko, J., Kossut, M., and Hess, G. (2005). Effects of sensory learning on intracortical synaptic transmission in the barrel cortex of mice. Acta Neurobiol Exp (Wars) 65, 195-200.

van Rossum, M.C., Turrigiano, G.G., and Nelson, S.B. (2002). Fast propagation of firing rates through layered networks of noisy neurons. J Neurosci 22, 1956-1966.

Vogel, A., and Ronacher, B. (2007). Neural correlations increase between consecutive processing levels in the auditory system of locusts. J Neurophysiol 97, 3376-3385.

Vogels, T.P., and Abbott, L.F. (2005). Signal propagation and logic gating in networks of integrate-and-fire neurons. J Neurosci 25, 10786-10795.

Vogelstein, J.T., Watson, B.O., Packer, A.M., Yuste, R., Jedynak, B., and Paninski, L. (2009). Spike inference from calcium imaging using sequential Monte Carlo methods. Biophys J 97, 636-655.

Weinberger, N.M., Hopkins, W., and Diamond, D.M. (1984). Physiological plasticity of single neurons in auditory cortex of the cat during acquisition

of the pupillary conditioned response: I. Primary field (AI). Behav Neurosci 98, 171-188.

Wiechert, M.T., Judkewitz, B., Riecke, H., and Friedrich, R.W. (2010). Mechanisms of pattern decorrelation by recurrent neuronal circuits. Nat Neurosci 13, 1003-1010.

Xu, C., Zipfel, W., Shear, J.B., Williams, R.M., and Webb, W.W. (1996). Multiphoton fluorescence excitation: new spectral windows for biological nonlinear microscopy. Proc Natl Acad Sci U S A 93, 10763-10768.

Yaksi, E., and Friedrich, R.W. (2006). Reconstruction of firing rate changes across neuronal populations by temporally deconvolved Ca2+ imaging. Nat Methods 3, 377-383.

Yang, T., and Maunsell, J.H.R. (2004). The effect of perceptual learning on neuronal responses in monkey visual area V4. J Neurosci 24, 1617-1626.

Yoshimura, Y., and Callaway, E.M. (2005). Fine-scale specificity of cortical networks depends on inhibitory cell type and connectivity. Nat Neurosci 8, 1552-1559.

Yuan, Q., Isaacson, J.S., and Scanziani, M. (2011). Linking neuronal ensembles by associative synaptic plasticity. PLoS One 6, e20486.

Zilberter, M., Holmgren, C., Shemer, I., Silberberg, G., Grillner, S., Harkany, T., and Zilberter, Y. (2009). Input specificity and dependence of spike timing-dependent plasticity on preceding postsynaptic activity at unitary connections between neocortical layer 2/3 pyramidal cells. Cereb Cortex 19, 2308-2320.

Zohary, E., Shadlen, M.N., and Newsome, W.T. (1994). Correlated neuronal discharge rate and its implications for psychophysical performance. Nature 370, 140-143.

Vita

Gayathri Nattar Ranganathan was born in Madurai, India in 1983. She graduated from D.A.V. (CBSE) Senior Secondary School in Mogappair, Chennai, in 2001. Thereafter, she enrolled at the Vellore Institute of Technology, Vellore, India, from where she received her undergraduate degree in Biotechnology in 2005. She was admitted to the Institute for Neuroscience at the University of Texas at Austin in August 2005. Since then, she has specialized in optical investigation of computation in neuronal networks under the guidance of Dr. Helmut Koester.

Permanent e-mail address: gayathri@clm.mail.utexas.edu

This dissertation was typed by the author.